

**DEVELOPMENT OF CONTROL AND
OPTIMIZATION METHODS FOR WOOD DRYING**

**PUIDU KUIVATUSE KONTROLLI JA
OPTIMEERIMISE MEETODITE ARENDAMINE**

HANNES TAMME

A Thesis
for applying for the degree of Doctor of Philosophy
in Forestry

Väitekirj
filosoofiadoktori kraadi taotlemiseks
metsanduse erialal

Tartu 2023

Eesti Maaülikooli doktoritööd

**Doctoral Theses of the
Estonian University of Life Sciences**



DEVELOPMENT OF CONTROL AND OPTIMIZATION METHODS FOR WOOD DRYING

PUIDU KUIVATUSE KONTROLLI JA OPTIMEERIMISE
MEETODITE ARENDAMINE

HANNES TAMME

A Thesis
for applying for the degree of Doctor of Philosophy
in Forestry

Väitekirj
filosoofiadoktori kraadi taotlemiseks
metsanduse erialal

Tartu 2023

Institute of Forestry and Engineering
Estonian University of Life Sciences

According to verdict No 6-14/5-1 of June 9, 2023, the Defence Board of PhD theses in Forestry of the Estonian University of Life Sciences has accepted the thesis for the defence of the degree of Doctor of Philosophy in Forestry.

Opponent: **Uldis Spulle**, Dr. sc. ing.
Latvia University of Life Sciences and Technologies

Supervisors: Professor Emeritus **Peeter Muiste**, PhD
Institute of Forestry and Rural Engineering
Estonian University of Life Sciences

Research Scientist **Valdek Tamme**, PhD
Institute of Forestry and Rural Engineering
Estonian University of Life Sciences

Defence of the thesis:
Estonian University of Life Sciences, room 2A1, Kreutzwaldi 5, Tartu
on August 30th, 2023, at 10:00.

The English and the Estonian language in the thesis were revised by
Mrs. Karit Jäärats.

© Hannes Tamme, 2023

ISSN 2382-7076
ISBN 978-9916-719-18-3 (trükis)
ISBN 978-9916-719-19-0 (pdf)

CONTENTS

LIST OF ORIGINAL PUBLICATIONS.....	7
ABBREVIATIONS.....	9
1. INTRODUCTION.....	10
2. REVIEW OF THE LITERATURE.....	13
2.1. Determination of wood moisture content using the electrical resistance method.....	13
2.2. Determination of wood moisture content using the electrical capacitance method.....	15
2.3. Determination of wood moisture content using the electrical impedance method.....	17
2.4. Modelling and optimizing of the wood drying process.....	17
3. AIMS OF THE STUDY.....	19
4. MATERIALS AND METHODS.....	20
4.1. Theoretical background of wood moisture meters (I), (II) and (III).....	20
4.1.1. Resistance-type wood moisture meter.....	20
4.1.2. (Polarization-type) wood moisture meter with electrical charging effect.....	21
4.1.3. Impedance-type wood moisture meter.....	23
4.1.4. Capacitance-type wood moisture meter.....	24
4.2. Methodology for calibration of wood moisture meters (I), (II), (III) and (IV).....	24
4.2.1. Methodology for individual calibration of measuring electrodes.....	26
4.3. Methodology for testing the reliability of the capacitance-type wood moisture meter and impedance-type wood moisture meter in indoor wood kiln conditions (III).....	28
4.4. Adding a monitoring function to the wood moisture meters (I) and (II).....	31
4.5. Theoretical background of the wood drying simulation program TORKSIM.....	33
4.6. Methodology for determining the local diffusion constant in drying pine wood at different depths from the board surface (IV)....	35

4.7. Methodology for applying the timed moistening impulse in the drying process (IV)	36
4.8. Automation of data processing and statistical analyses (I), (II), (III) and (IV).....	36
4.9. Materials (I – IV)	39
5. RESULTS.....	40
5.1. Calibration results of wood moisture meters according to the Rozema criterion (I), (II), (III)	40
5.1.1. Wood electrical charging number	46
5.1.2. Wood moisture meter prototype based on charging number ideology.....	48
5.2. Operational reliability test results of a capacitance-type wood moisture meter and impedance-type wood moisture meter in kiln climate conditions (III).....	51
5.3. Pine wood drying optimization results (IV).....	53
5.3.1. New wood drying monitoring sensors added to the experiment – surface layer displacement sensor and surface layer electrical resistance sensor	53
5.3.2. Critical diffusion constant of wood surface layer and critical drying air humidity	54
5.3.3. Simulation of drying process optimization results with TORKSIM program using critical drying air humidity and moistening impulse	57
5.3.4. Wood drying stress evolution indicator.....	60
6. DISCUSSION.....	63
7. CONCLUSIONS	69
REFERENCES.....	73
SUMMARY IN ESTONIAN	85
ACKNOWLEDGEMENTS	90
ORIGINAL PUBLICATIONS.....	91
CURRICULUM VITAE.....	175
ELULOOKIRJELDUS	177
LIST OF PUBLICATIONS	179

LIST OF ORIGINAL PUBLICATIONS

The thesis is based on the following papers, references to which in the text are given by Roman numerals. The papers are reproduced by the kind permission of the publishers.

- I Patentne leiutis: Niiskusmõõtur ja meetod puidu elektrilise laadumise efektiga puidu küllastuspunktist suurema niiskussisalduse mõõtmiseks; Omanikud: Eesti Maaülikool, Metsanduse- ja Maachituse Instituut, Eesti Maaülikool, Tehnikainstituut, Tartu Ülikool; Autorid: Valdek Tamme, **Hannes Tamme**, Toomas Bernotas, Peeter Muiste, Jüri Olt; Prioriteedi number: EE201800017; Prioriteedi kuupäev:16.07.2018. <https://www.etis.ee/Portal/IndustrialProperties/Display/974edb6b-39df-44ea-b1ba-403cdcaa81aa>
- II Tamme, V., **Tamme, H.**, Miidla, P., Muiste, P., 2021. Novel polarization-type moisture meter for determining moisture content of wood above fibre saturation point. *European Journal of Wood and Wood Products*, 79: 1577–1587.
- III **Tamme, H.**, Kask, R., Muiste, P., Tamme, V. 2021. Comparative testing of two alternating current methods for determining wood moisture content in kiln conditions. *Forestry Studies*, 74: 72–87.
- IV **Tamme, H.**, Muiste, P., Tamme, V. 2021. Optimizing the pine wood drying process using a critical diffusion coefficient and a timed moistening impulse. *Forestry Studies*, 75, 150–165.

The contributions from the authors to the papers in alphabetical order are as follows:

	I	II	III	IV
Original idea	VT	VT	HT	HT
Study design	JO, TB			
Data collection	VT, HT	VT, HT	HT , RK VT	HT VT
Data analysis	VT, HT	VT, PMi	HT	HT
Preparation of manuscript	VT, JO PM	VT, PMi PM	HT HT , PM	HT HT , PM

Peeter Muiste – PM, Regino Kask – RK, Peep Miiidla – PMi, Valdek Tamme – VT, **Hannes Tamme – HT**, Jüri Olt – JO, Toomas Bernotas – TB.

ABBREVIATIONS

Above FSP	Above the Fibre saturation point (>30% MC)
AC	Alternating current
ADC	Analog digital converter
CAM	Capacitance meter
ChN	Wood charging number
CoV	Coefficient of variation
D(S)PST	Double (Single) Pole Single Throw relay
DC	Diffusion coefficient, Direct Current
DECM	Dielectric capacitance method
DOE	Design of experiment
DS	Displacement sensor
EIS	Electric impedance spectrometry
ESCR	Electrical surface core ratio
FSP	Fibre saturation point (~30% MC)
(G)UI	(Graphical) User interface
I2C	Inter-Integrated Circuit
LDC	Local Diffusion coefficient
log	Logarithm
ln	Natural logarithm
MC	Moisture content
MCU	Microcontroller unit
MEC	Measuring capacitor
NDT/NDE	Nondestructive testing and evaluation
PD	Polarization-depolarization
PDM	Polarization-depolarization method
Rcr	Rozema criterion
RH	Relative humidity
RMSE	Root-mean-square error
RSM	Response surface methodology
SE	Standard error

1. INTRODUCTION

The purpose of wood drying is to obtain material with the desired final moisture content. During the process, it is necessary to find a balance between the quality of the wood and the energy and time spent. In order to find an optimal solution, it is important to know the condition of the material to be dried at a specific time. The alternative is a costly trial-and-error method that requires the input of a highly experienced kiln operator.

In widely used chamber-type convective dryers, wood is dried using turbulent drying air. In practice, to monitor wood drying, the electrical resistance method is predominantly used (Tronstad et al., 2001; Onysko et al., 2008; Björngrim et al., 2017; Bes-Bollmann, 2023), less often the capacitance method (Moschler, 2004; Magill, 2010; Lyons Jr. et al., 2004), and the impedance method (Tiiitta et al., 2010).

To determine the moisture content (MC) of wood, in addition to the resistance method and capacitance method, methods with a completely different physical operating principle have been used, for example: neutron activation (Mannes et al., 2009), X-ray absorption and X-ray tomography (Danvind, 2005; Cai, 2008; Vikberg et al., 2012), nuclear magnetic resonance (MR) and nuclear magnetic resonance imaging (MRI) (Lamason et al., 2013), near-infrared (NIR) and near-infrared spectroscopy (NIRS) (Hans et al., 2013), microwave (James et al., 1985; Aicholzer, 2017), time domain reflectometry (TDR), or radio location method (White et al., 2019).

The aim of this PhD thesis is the development of methods for controlling and optimizing the drying of wood, based mainly on the practical or easy-to-add capabilities of the infrastructure that is more widespread in the industry. The focus is on the methods for determining wood moisture above the fibre saturation point and optimizing the drying process to reduce wood stress, energy consumption, and drying time. In the process, various prototypes of practical measuring devices and calibration methods have been developed, which can be used in kiln climate.

Finding the most suitable drying mode starts with reliable measurement data. Reliability can be assessed by matching the results of sensors operating on different physical principles. In order to get a complete picture, this PhD thesis examines the capacitance method for determining the average moisture content of wood, the resistance method for determining the moisture content of wood at different depths of the material, and the deformation of the wood surface. Based on the measurements taken from the surface of the board at different depths, it is possible to create a profile of the moisture content of the material, i.e. the MC distribution of the wood in the radial direction. Water vapour diffusion at different depths of wooden material from the surface describes the process of wood drying. Insufficient accuracy in determining the effective diffusion coefficient in the radial direction, especially above the fibre saturation point, has an adverse effect on either drying time, energy consumption, or material quality.

Often, the standard equipment of an industrial kiln is not enough when implementing a new drying schedule. In addition, there is a need for software that simulates wood drying, providing the initial drying regime, which can then be further optimized using the methodologies and sensors presented in this study. The wood drying simulation program may also be considered as one of the methods of controlling wood drying stresses. The moment and maximum of stress in an actual kiln can be predicted using a drying simulation program. In the practice of wood drying, a well-known method for determining the drying stresses of wood is the so-called case-hardening test (Poljakov, 2013; Mändoja, 2015; E.D.G., 1992; EDG, 2010). Unfortunately, the classic case-hardening test does not allow real-time monitoring of drying stresses. Real-time drying stress monitoring is enabled by a wood drying stress indicator functioning on the acoustic emission (AE) principle (Kawamoto and Williams, 2002). The problem of the AE indicator, however, is distinguishing AE impulses from other sources of acoustic noise occurring in an industrial kiln (fans, motors, etc.) (Tiitta et al., 2010). For this reason, it would be necessary to develop a resistance-type drying stress indicator that is relatively insensitive to disturbances.

In the Articles (I–II), the calibration models of the innovative polarization-type wood moisture meter were studied. Modelling was used to find out how many repeated measurements should be made in a series of measurements in order to fulfill the Rozema quality criterion

(Rozema, 2010). The ability of different calibration models (including focusing models) to satisfy the Rozema quality criterion was explained by means of modelling. The self-compensating phenomenon of random measurement deviations in the focal point of different types of focusing models and in their immediate surroundings was studied. The Article (III) examined wood moisture meters working with alternating current. The calibration models of capacitance-type and impedance-type wood moisture meters were studied. In addition, the reliability of both mentioned wood moisture meter types in the harsh climatic conditions of a kiln was examined. The Article (IV) investigated the possibilities of optimizing the wood drying process using the critical diffusion coefficient of the wood surface layer, and precisely timed moistening impulse. The main attention was paid to the changes in moisture content in the surface layer of wood, and the deformation of the surface layer. With sensors installed at different depths in the surface layer, the effect of changes in the surface layer on the inner layers of wood during drying was monitored in real time.

2. REVIEW OF THE LITERATURE

2.1. Determination of wood moisture content using the electrical resistance method

The idea of determining the moisture content of wood using the electrical resistance of wood was first presented by Stamm (Stamm, 1927) as a relationship between the decimal logarithm of the electrical resistivity of wood and the relative moisture content of wood. The electrical resistance of wood can be determined using direct current (DC) or alternating current (AC). In the latter case, it is possible to avoid the arising effects of electrical polarization. Comparative measurements of DC resistance and AC resistance in wood were carried out in studies by Gao et al., 2018, and Berga et al., 2019. The measurements use either a two- or four-electrode system. In the case of a measuring system consisting of two electrodes, the measured electrical resistance includes, in addition to the resistance of the wood itself, the resistance of the contact between the wood and the electrode (Romann et al., 2014). In geophysics, a four-electrode system is used to determine soil resistivity (Wenner, 1915; Sumner, 1976; Urban et al., 2011; Schuetze et al., 2004), in which the contact resistance is separable from the actual resistance of the soil itself. The four-electrode Wenner method was used to study the spread of fungal infection in a wood environment by Martin, T. (2012). Since most of the moisture content (MC) information is still in the double layer formed around the electrode/wood contact surface (Tamme et al., 2012), this limits the usability of the four-electrode system in practice, because the signal-to-noise ratio decreases approximately eight times (Tamme et al., 2012). Since electrical resistance also depends on temperature, correction formulas were derived for it based on the Arrhenius law (Norberg, P., 1999). A comparison of the method and a comprehensive study of the calibrability based on different handheld measuring instruments was carried out within the framework of the IMCOPCO program (Forsen et al., 2000). In this study, it was found that the electrical resistance method is calibrable at moisture contents below the fibre saturation point (below FSP) from 30% MC to 4% MC based on the moisture standard in the sense of ISO 3534-1:1993. The calibrations of moisture meters from different manufacturers are relatively well comparable. In the transition region of 20–30% MC, it is

recommended to use a slightly different formula than Stamm's formula to calibrate the moisture meter (Onysko et al., 2008; Tamme et al., 2012).

The approximate and widely varying electrical resistance of wood at room temperature is approx. 10 giga-Ohms at 8% MC, approx. 10 mega-Ohms at 18% MC, approx. 100 kilo-Ohms at 47%, and approx. 10 kilo-Ohms at 150% (Tamme et al., 2020). The large variation in electrical resistance is caused by the inhomogeneity of wood as a material, for example density, resin content, water pockets, etc. In general, it can be stated that as the moisture content increases, the measurement uncertainty also increases, as a result of which the determination of wood moisture content below 7% and above 30%, i.e. above the fibre saturation point, has been considered inaccurate and unreliable (Vermaas, 2002). In the articles (Tamme et al., 2013, 2014), the general validity of the Vermaas hypothesis at 95% confidence level was shown by statistical modelling, but the hypothesis has two clearly visible exceptions with the existing calibration function. Therefore, the resistance method above FSP, within the limits of exceptions, is also applicable in practice. To some extent, it is also possible to increase accuracy by using alternating current instead of direct current during measurement (Berga et al., 2019).

Measuring instruments based on electrical resistance, which have been widely used so far, have a high measurement uncertainty in the case of a single measurement and, in practice, show increasing inaccuracy above 30% MC (Tamme et al., 2014). To some extent, it is possible to improve the calibration of existing moisture meters by means of the so-called re-calibration, creating a new calibration function from the actual moisture content (Y-variable) obtained during dry weighing and from the electrical resistance of the moisture meter (X-variable) (Tamme et al., 2014). A comprehensive overview on the use of moisture meters based on direct current electrical resistance was given in the following research (Björngrim et al., 2017; Brischke et al., 2008; Li et al., 2018; Norberg, 2000; Uwizeyimana et al., 2020). Unfortunately, the fundamental problem manifested in the large dispersion of single measurements cannot be solved merely by better calibration of a device. It is necessary to develop an essentially new type of wood moisture meter, where the so-called Edwards trend (Edwards, 1974) is reversed at high wood moisture contents above FSP. Reversing the Edwards trend became possible thanks to the empirical phenomenon of self-compensation of random measurement deviations of electrical resistance and electrical

capacitance found in the electrical charging number of wood (I). The electrical charging number of wood made it possible to hypothesize the existence of so-called focusing (or Edwards trend-reversing) calibration models of types A, B and C (Art. II).

Considering the time-dependent polarization effect of electrodes above FSP (Tamme et al., 2012; 2013), a polarization-depolarization (PD) method based on long and ultra-long relaxation time has been introduced to measure wood moisture content using the charging and discharging of wood at optimal voltage and current (Romann, T. et al., 2014). To give a better idea of the research scope related to the PD method, a series of technical details about the technical implementation and programming of the patented wood moisture meter (I) were added to the PhD thesis. As a continuation of this field of research, this thesis for applying for the PhD research degree has been composed.

2.2. Determination of wood moisture content using the electrical capacitance method

The measurement technology described in the standard (EN 13183-3:2005) and COST E53 (2010) is based on the fact that the dielectric constant (relative permeability) of wood and water contained in wood is 20 times lower in wood than in water. Accordingly, absolute dry ϵ wood ≈ 4 and ϵ water ≈ 80 . It is a dimensionless, complex, frequency-dependent quantity, which is compared to the dielectric constant of a vacuum (ϵ vacuum = 1). If you place a wood specimen between two plates of a measuring capacitor, a dielectric between the plates is formed from a mixture of wood and water. In theory, capacitance-type meters are capable of measuring over a wider area than resistance-type devices. Since the capacitance-type meter measures linearly from the total amount of water, the result also depends on the specific density of the wood. The best measurement result is obtained if there is no air gap between the wood and the plate of the measuring capacitor and there is no excess water on the surface of the wood. It should be borne in mind that the lack of an air gap prevents the wood from drying.

Since the capacitance of a plate capacitor depends on the area of the plate, the distance between the plates and the dielectric used, it is easy to experience a situation with wood where the actual measured capacitance is close to or even lower than the capacitance of the pair of wires used.

Cabling capacitance has been addressed in the capacitance method based on a US patent (Magill, 2010), which should allow the calibration of a capacitance-type moisture meter with electronics up to ~ 300 m away from the measuring capacitor. The proposed method uses a coaxial cable as a transmission medium, which allows more flexible selection of the location of the measuring electronics, while maintaining accurate measurement results. In other words, the measuring electronics can be installed in a separate climate-controlled equipment room, and not in a kiln in an extreme drying air environment. The proposed method should also eliminate interference and electrical losses due to long cabling. The use of the long cable has been limited in the past, because the calibration of a measuring device has proven to be too difficult due to the low signal-to-noise ratio. In order to measure the moisture content of wood, wood is used as an insulator for a plate capacitor. The measured capacitance depends on the moisture content of wood and is calculated either directly in the electronics block or sent for post-processing either in a PC (Personal Computer) or a PLC (Programmable Logic Controller). The hardware and software solution of the proposed meter includes a signal generator that generates a variable electromagnetic field between the plates, and an amplifier that raises the signal to a suitable level for the rest of the electronics (comparators for detection of voltage amplitude and phase, and a demodulator for back-calculation of capacitance). Since in the proposed solution it is not necessary to keep all the electronics as close as possible to the measuring capacitor, it is possible to multiplex the input of several measuring capacitors into a single electronic block (up to 40 channels). It is suggested that eight sensors per dryer are sufficient for reliable moisture content determination. In the selection of the electronics measurement method, three implementations have been proposed, which should be functionally identical from the end user's point of view: using a voltage divider, a bridge circuit or a modular LCR (L: inductance, C: capacitance, R: resistance) block. Three measurement methods have also been proposed for the calibration of electronics: RC circuit method, impedance-based LCR method and short-circuit/open-circuit method. From the above, the circuit required for calibration is selected and switched to the circuit instead of the measuring capacitor.

The problem of insulator leakage is addressed in a US patent (Lyons, Jr. et al., 2004), in which the measuring device with electronics is installed in the drying air environment to reduce the cabling length. The plates of the measuring capacitor are covered with plastic to reduce current

leakage, which occurs when a conductive bridge forms between the two plates, i.e. a short circuit.

In this PhD thesis, there was a need to investigate the reliability of the measuring capacitor due to the fact that the basic design of the measuring capacitor (Tamme, H. et al., 2019), which consisted of only two plates and an insulator, did not work properly in the harsh climatic conditions of the kiln. Similar problems with leakage of electric current between the plates as in the patent (Lyons. Jr. et al., 2004) were encountered.

2.3. Determination of wood moisture content using the electrical impedance method

The electrical impedance method is an alternating current method, as well as the electrical capacitance method described in sub-section 2.2. The impedance method was used for wood drying monitoring by Tiitta (Tiitta et al., 2010). The equivalent scheme of the used impedance method was based on two constant phase elements (CPE), which were connected in parallel with resistors. As the measured electrical variable the impedance modulus was used, which was associated in the calibration model with the average moisture content of wood and the MC gradient (Tiitta et al., 1999).

2.4. Modelling and optimizing of the wood drying process

To determine the optimal drying process, it is useful to mathematically simulate the course of the process. For example, an actual drying process lasting about one week can be simulated on a computer within one second. The one-dimensional simulation program TORKSIM 5.1 has been used (Vikberg, T. et al., 2012), combined with industry best practices. The mathematical model of the previous version TORKSIM ver. 3.1 is not described in detail, but based on Salin's PhD thesis, it can be assumed that it is a perfect isotropic Luikov-type coupled model (Salin 1990; 2007; Tamme, 2016). The coupled model means that a term containing the enthalpy of water vapour has been added to the heat transfer equation (Keey et al., 1999; Younsi et al., 2006; Tsotsas and Mujumdar (eds.), 2014; Tamme, 2016).

In order to keep the cost of experiments for mathematical optimization of wood drying low, drying experiments are performed as little as possible.

To achieve this, the drying experiment must be designed accordingly (DOE). An experiment is defined as a systematic procedure carried out under controlled conditions to discover an unknown effect, to test or establish a hypothesis, or to illustrate a known effect. When analysing the process under consideration, experiments are used to assess which process inputs significantly affect the process output, and what the level of these inputs should be to achieve the desired result. Experiments can be designed in many different ways to collect this information. An experiment is an entire series of tests.

The theoretical foundations of the optimization of technological processes, which were developed in 1951, later became known as the response surface method (RSM, eg. Box-Wilson method). Theory and application examples of multi-reaction process optimization can be found in the Handbook of Statistics (NIST/SEMATECH, 2018). To optimize the constant drying mode for thin material, the statistical software package Design-Expert (DE) developed by the company Stat-Ease Inc. for planning and analysing experiments has been used (Sova et al., 2016). DE enables comparative tests, screening, description, optimization, parameter evaluation, etc. DE allows the use of up to 50 factors and the identification of statistical significance of these factors using analysis of variance (ANOVA). The area of possible factor values within which combinations of factor values of potential interest lie is called the experimental area. It is necessary to be determined before the experiment. If the final results of the analysis are outside the range of the experiment, it must be repeated with a new range.

Constant drying modes of thin material (up to 20 mm) simulated by TORKSIM v. 5.1 were given as an input in DE (Sova et al., 2016). In the case of thicker material, when using a constant drying mode, excessive drying stresses occur, which in turn cause drying cracks and warping of the material, which reduces the final quality of the wood. This fact does not allow the wood drying process to be mathematically optimized without reducing the drying quality (Tamme et al., 2021c). The task of mathematical optimization can also be solved on the basis of the ideology of artificial neuron networks (NN-Tool, 2023), using the system's self-learning algorithm. In this way, the practical goal (i.e. optimization) is achieved, but there is no possibility to get additional information about the statistical modelling of the result (model + ANOVA + p-values, etc.).

3. AIMS OF THE STUDY

The primary aim is the development and optimization of measurement systems used in the environment of an industrial kiln.

Basic hypotheses:

- MC measuring errors can be compensated either by increasing the number of measurements or by choosing a suitable calibration function (I, II).
- The capacitance method causes operating reliability problems in the climatic conditions of the kiln (III).
- If the critical diffusion constant is exceeded, the drying process of the surface layer of the wood will also affect the inner layers of the wood (IV).

Aims:

- Checking the occurrence of theoretically simulated moistening impulse response in experiments based on synchronous surface displacement, temperature and surface moisture sensors (IV).
- Developing specific sensors for monitoring that can be used in kiln climate (I, II, III).
- Developing an electrical indicator of maximum wood drying stresses (IV).
- Enhancing the moisture meter prototype hardware corresponding to the patent description (I, II).

4. MATERIALS AND METHODS

4.1. Theoretical background of wood moisture meters (I), (II) and (III)

4.1.1. Resistance-type wood moisture meter

The classical resistance-type wood moisture meter theory is applicable below FSP (7–30%). The classical theory can be described by Stamm's formula and its various extensions (Tamme et al., 2012; Uwizeyimana et al., 2020). Stamm (1927) presented the equation:

$$\log(\rho) = C + D \log(M) \quad (1)$$

where ρ – resistivity, M – moisture content MC, C and D – constants at constant temperature.

This expression (1) was found to perform satisfactorily in the MC measurement range of 7–30%. In practice, instead of wood resistivity, it is more convenient to use wood electrical resistance R :

$$R = \frac{\rho L}{A} = K\rho \quad (2)$$

where $A(\text{m}^2)$ is the conductor cross-section, L is length, K is the cell constant, or measuring volume constant.

In the calibration model for the non-linear transition range (ca. 23% to 40% MC) and specifically for Douglas Fir wood the double logarithm empirical formula by Straube et al. (2002) was used:

$$\log(MC) = 2.99 - 2.113(\log(\log(R))) \quad (3)$$

where MC is the moisture content (%), R is resistance in ohms (Ω).

The same general formula was presented by several authors (Norberg, 2000; Tamme et al., 2012; Fredriksson et al., 2013) under the constant temperature assumption:

$$\log(R) = a \log(MC) + b \quad (4)$$

where MC (%) is the moisture content, R (Ω) is the corresponding electrical resistance, a is slope.

Considering the dependence of electrical resistance on moisture content and temperature (Skaar, 1988; Li et al., 2018; Uwizeyimana et al., 2020), a linear relationship can be expressed in logarithmic scale:

$$a \log(MC) + b = \log(R_{meas}) + 0.025(T - 35) \quad (5)$$

Formula (5) represents a logarithm equation the solution of which with respect to MC shows a relationship for determining the moisture content on the basis of electrical resistance R_{meas} measured at a given temperature T, that is, the mathematical shape of the calibration curve of the resistance-type wood moisture meter is:

$$MC(R_{meas}, T) = \left(\frac{10^{\log(R_{meas}) + 0.025(T - 35)}}{10^b} \right)^{1/a} \quad (6)$$

4.1.2. (Polarization-type) wood moisture meter with electrical charging effect

The need to accurately determine the moisture content of wood led to the development of a prototype of a novel moisture meter based on the charging number of wood. Knowing the appropriate calibration function, the moisture content of wood can be calculated from the electrical resistance. The result obtained can be verified using the desired reference model (ISO/IEC 2008; Laaneots and Mathiesen, 2006).

The patent ‘EE 05822 B1’, “Moisture Meter and the Method for Measuring the Moisture Content of Wood above the Fibre Saturation Point with the Wood Electrical Charging Effect” has been issued by the Estonian Patent Office with regard to the calibration method applied.

Above the fibre saturation point, wood electrical resistance R(t) depends on time logarithmically and capacitance C(t) linearly (Tamme et al., 2013):

$$R(t) = a \ln(t) + b \quad (7)$$

$$C(t) = c t + d \quad (8)$$

where a, b, c and d are spatial positional constants.

The method is based on the fact that the resistance of wood R and the product of capacitance C are almost constant at each different moisture content, $RC \sim \text{constant}$.

Figure 1 the circuit diagram of the electrometer underlying the technical specification of patent ‘EE 05822 B1’ is provided:

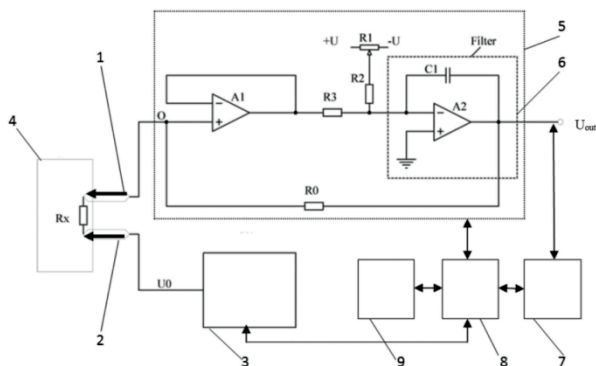


Figure 1. MC block diagram. Where 1 and 2 is measuring electrodes, 3 is reference voltage, 4 is wood, 5 is analogue electronics, 6 is operational amplifier IC, 7 is ADC, 8 is MCU and 9 is user interface.

Wood resistance R_x (9), polarization current I_{pol} (10) and capacitance C_x (11) can be found with the following formulas:

$$R_x = U_{out} \frac{R_0}{U_0} \quad (9)$$

where R_x – wood electrical resistance in ohms, U_0 – reference voltage, R_0 – feedback resistor.

$$I_{pol} = \frac{U_0}{R_x} \quad (10)$$

where I_{pol} – wood charging current in amps, U_0 – reference voltage, R_x – wood electrical resistance in ohms.

$$C_x = \frac{Q}{U_0} \quad (11)$$

where C_x – wood electrical capacitance in farads, Q – wood charge in coulombs (result of I_{pol} numerical integration by MCU).

4.1.3. Impedance-type wood moisture meter

The electrical equivalence of geometrically different sensors can be tested with an impedance spectrometer (EIS). If the measurement results of the DC resistance method are comparable to the AC impedance method, it is indicative of the independence of the results from the measurement method.

The EIS also allows to study the reliability problems of the dielectric sensor in climate chamber conditions and optimize the frequency range used to increase the signal-to-noise ratio.

Impedance spectrometry is an informative measuring technique for analysing multiple electrical processes (Cole-Cole, 1945; Debye, 1945; Bard et al., 1980; Chaumat et al., 1999; Krause, 2003; Zelinka et al., 2007, 2008).

Impedance (12) has a magnitude ($Z_A = \frac{E_A}{I_A}$) and phase angle and is thus a vector quantity:

$$Z = Z_A(\cos\theta + j\sin\theta) = Z' + jZ'' \quad (12)$$

where $j = \sqrt{-1}$, Z' is the real part of impedance, Z_A is the amplitude of impedance and Z'' the imaginary part of impedance.

Impedance magnitude (or so-called modulus) is expressed through the real and imaginary part of the impedance as follows:

$$|Z| = Z_A = \sqrt{(Z')^2 + (Z'')^2} \quad (13)$$

If sinusoidal voltage is applied across a pure capacitor, impedance (14) can be calculated according to the relationship:

$$Z = \frac{1}{j\omega C} = -\frac{j}{\omega C} \quad (14)$$

where C is the capacitance and the phase angle $\varphi = -90^\circ$, that is, impedance depends on frequency and is entirely imaginary (Krause, 2003).

4.1.4. Capacitance-type wood moisture meter

The capacitance method is a non-destructive method used to measure the average moisture content of wood, where wood is not sliced, and needle or screw electrodes are not inserted into wood. The capacitance of the plate capacitor used in the experiments can be found with the formula (15) (Zuleta, 2005).

$$C = \varepsilon \varepsilon_0 \frac{A}{d} \quad (15)$$

where C is the capacity of the parallel plate capacitor, A is single plate area, d is distance between plates, ε is relative dielectric permeability and ε_0 is dielectric permittivity of vacuum.

The dielectric constant ε of absolute dry wood is 4 and of water it is 80. Thus, the theoretical change in capacitance in drying wood is up to 20 times.

4.2. Methodology for calibration of wood moisture meters (I), (II), (III) and (IV)

The measuring instrument is calibrated using the appropriate calibration methodology in accordance with the standard ISO/IEC 17025:1999. Calibration is a set of procedures that, under fixed conditions, determines the relationship between the value reported by the measuring instrument and the corresponding value of the quantity realized by the reference used in the calibration (EVS758:2009).

The result of performing calibration procedures is a measurement model or calibration model within the scope of EVS758:2009. For example, the different stages of the procedure (statistical modelling) for calibrating the moisture content of a resistance-type wood moisture meter above FSP can be described as follows.

The first stage. A description of the starting position for modelling, i.e. a qualitative description of the actual situation, for example, qualitative

assessments of problems with the calibration of resistance-type moisture meters from various sources (Bergmann, 2010; Class et al., 2010; ASTM D4444-08:2008).

The second stage. Getting acquainted with known physical models of resistance-type wood moisture meters (4.1). If possible, examining a resistance-type wood moisture meter using electrical resistance references. In developing the calibration model, proceeding from the corresponding standard on the methods for determining type A and B uncertainties (ISO/IEC, 2008).

The third stage. Calibration experiment. This is the most laborious and responsible part of the calibration procedures. The calibration experiment begins with the preparation of the reference material (Brookhuis, 2009) for carrying out measurements. The reference material is essentially a working standard intended to be used for generating a sample for only one calibration model. A piece of the reference material with specific dimensions (length longitudinal, width tangential, thickness radial) was called a specimen. The main issue in the calibration of wood moisture meters is the establishment of a statistical relationship (or regression model) between a certain level of the average moisture content of wood and the measured electrical variables. Consequently, it is necessary to vary the moisture content of the reference material in a way as to exclude, as much as possible, the occurrence of systematic errors in the calibration procedure (Laaneots and Mathiesen, 2006). The occurrence of random errors during the calibration procedure cannot be avoided. They can, however, be described at certain confidence levels with an adequate calibration model and they form a component of so-called standard uncertainty in general or extended uncertainty (Laaneots and Mathiesen, 2006). In order to vary the moisture content of the wood specimen during the calibration experiment, the wood drying method above FSP (above 30% MC) was applied ((I), (II) and (III)). Below FSP a hygroscopic method (ISO 3130:1975, 1975) was used in article (III) to vary the moisture content of the specimen. The differences in moisture content in the specimen are called moisture gradients that can, to some extent, be adjusted by the dimensions of the specimens and the drying plan. In the paper (Tamme et al., 2014) specimens of relatively small dimensions (60x60x100mm, up to 60 pieces) were used, all of which were simultaneously dried according to a special drying plan. The result was a three-dimensional moisture gradient in each specimen

and relatively high variability in the average moisture content of the specimens. The articles (I, II and III) used a single massive specimen (wood board), where vapour barriers prevented moisture diffusion from wood longitudinally and tangentially, the moisture could leave the wood only in the radial direction. The result was a one-dimensional moisture gradient in the reference material which was symmetrical to the centre of the board. The specimen thickness (36 mm was selected) and a special drying plan (Tamme et al., 2013) ensured that, in accordance with the standard (EN13183-2), the average moisture content level was numerically equal to the actual moisture content of wood determined at a depth of 1/3 of the surface of the specimen. Electrical quantities were also measured at a depth of 1/3 thickness (i.e. 12 mm from the surface). This avoided the potential for systematic errors in the average wood moisture content to be transferred to the calibration model. The specimen was weighed just before measuring each electrical quantity (electrical resistance, electrical capacitance, impedance modulus, etc.). Repeat experiments for one calibration model were performed from N = 60 to 70. At one average moisture content level of the specimen, 20 to 25 repeat measurements were done. 25 repeat measurements took approximately 2 to 2.5 hours to complete. During this time, the massive specimen only managed to dry by 2% to 2.5% MC. Weighing of the specimen was performed at random time moments, so all measurement data on the actual (gravimetric) moisture content of the specimen obtained by weighing were also independent random quantities, but with relatively low variability (see (II) Results, Table 3). The measurement data of electrical quantities also represented independent random quantities of certain variability (see Results, Table 2).

4.2.1. Methodology for individual calibration of measuring electrodes

The need for individual calibration of measuring electrodes arises when it is important to monitor the moisture content of wood in specimen drying at different depths from the specimen surface as well as at different time moments at all depths simultaneously. For this purpose, an eight-channel electrical resistance meter (Scantronik, 2023) is used to determine the electrical resistance of wood at a certain time moment and depth. At the same control depths, the actual moisture content of wood is also determined in the immediate vicinity of the measuring electrodes where electrical resistance was measured. The control depths, or degrees

of depth, were selected as follows: 1 mm, 4 mm, 8 mm, 12 mm and 18 mm from the surface of the wood specimen (Figure 4). Of these, a depth of 12 mm (1/3 of thickness) should, in accordance with the standard EN 13183-2:2005, represent the average moisture content of the wood specimen. Determining the actual MC of wood in different layers is done by the so-called slicing method (Tremblay et al., 2000; Hukka, A., 1999) by which the actual MC profile of wood (moisture distribution curve) is found at a specific point in time (IV). Monitoring of the electrical resistance of wood during drying takes place at a one-hour interval. It is understandable that determining the actual MC of wood every hour would be too laborious and would interfere with the main experiment (i.e. wood drying) too much because the specimens were located in the same drying chamber. If it is known before the drying experiment that the calibration function of wood moisture meters is linear within the MC range of 150% and 30% (Tamme et al., 2012, 2014), then two values of the actual wood MC at the selected depth, plus two values of the electrical resistance of wood at the same depth, are sufficient for individual calibration of this MC range above FSP. If it is known before the drying experiment that the calibration function of wood moisture meters is linear within the MC range of 24% and 7% (Uwizeyimana et al., 2020; Tamme et al., 2012, 2014), then two values of the actual MC of wood at the selected depth, plus two values of the electrical resistance of wood at the same depth, are sufficient for individual calibration of this MC range below FSP. The question is how to calibrate the measuring electrodes individually in the MC range of 24% to 30%, where the relationship between the decimal logarithm of the electrical resistance of wood and the actual MC of wood is no longer linear. The article (IV) presented a solution where the nonlinear region was roughly imitated by different linear sections. Thus, the result of the individual calibration procedure was a so-called sectionally linear calibration function at a selected depth from the surface of the wood specimen. That included the surface layer where the electrical resistance sensors were calibrated according to the same methodology as needle sensors located at different depths in wood. The coordinates of the endpoints of the sections were common for the two intersecting calibration lines, so the projected wood MC was also of the same value for the two calibration lines at the intersecting point. In summary, individual calibration of measuring electrodes allows wood electrical resistance monitoring at different depths in wood to be replaced by wood MC monitoring at different depths. MC monitoring at different depths is a key source of information for the experimental determination of the local diffusion coefficient in wood (see Section 5.3.2).

The sectional linear method (16) was used for individual calibration of the resistance sensor at different depths of the specimen (board), which provided us with one calibration function for each actual MC range of wood.

$$\frac{y-y_1}{y_2-y_1} = \frac{x-x_1}{x_2-x_1} \quad (16)$$

where $(x_1; y_1)$ is the coordinate of endpoint A of the section and $(x_2; y_2)$ is the coordinate of endpoint B of the section (Art. IV, figure 2).

4.3. Methodology for testing the reliability of the capacitance-type wood moisture meter and impedance-type wood moisture meter in indoor wood kiln conditions (III)

In the case of the capacitance method, measurement errors due to water vapour condensation and triboelectric charge must be observed.

In a more humid environment, the predominant problem is the resulting condensation of water vapour, against which additional heating of the capacitor plates and insulators helps. In a dry environment, however, triboelectric charges are a problem, which trigger an additional component, the so-called parasite capacitance, to the useful capacitance of the measured wood.

The cross-section of the measuring capacitor (MEC) used to examine the reliability of the capacitance method is given in Figure 2.

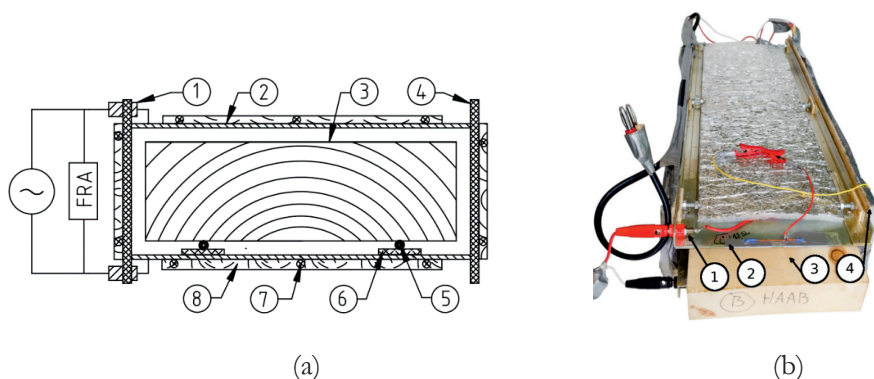


Figure 2. Cross-section of the measuring capacitor (MEC) (a) and specimen placement in MEC (b). Where 1 is signal connector, 2 is capacitor plate, 3 is wood specimen, 4 is capacitor insulator, FRA is frequency response analyser, 5 is triboelectric charge collector, 6 is film insulator, 7 is heating cable and 8 is heat insulator.

A specially developed design was used to study the operational reliability of the MEC (Figure 2, a). It can be seen from the design of the MEC that it has the capacity to selectively prevent triboelectric charges and condensation, while also creating prerequisites for studying the fundamental aspects that affect reliability. Testing was carried out in the climate chamber (Feutron GmbH, 2023) at 50°C and 98% RH and 60% RH to simulate the environmental conditions in the wood kiln.

The methodology for studying the reliability of the MEC can be described in stages. The first two stages examined the effects of water vapour condensation on the measurement results and the third stage examined the effects of triboelectric static charges on the measurement results. The third stage studies were switched to when, during the re-testing, a tendency was seen that the confounding effect of condensation on the research results reached a safe level. In physics terms, this meant that the dew point situation, which was a prerequisite for condensation of water vapour on the surface, no longer occurred.

The first stage of MEC reliability investigation. The MEC was empty to investigate reliability, i.e. without a wooden specimen placed between the plates. Thus, between the MEC plates, instead of wood, there was air, the relative dielectric permeability of which is approximately equal to one (15). The MEC was placed directly from the cold environment (i.e. refrigerated to +5 degrees Celsius) in the hot and high humidity (50 degrees and 95% RH) environment of the climate chamber. This induced intense condensation of water vapour on all the details of the MEC design (Figure 2) in the climate chamber. The heating (element 7) of the MEC plates (element 2) was turned on, at the same time the heating of the insulators (element 4) was turned off. With this method of heating, condensation was allowed on insulators, but excluded on plates. The first stage was completed by picking up the impedance beam spectrum in a situation of intense water vapour condensation.

The second stage of MEC reliability investigation. At the second stage, the heating of the insulators was turned on, but at the same time the heating of the plates was turned off. With this method of heating, condensation was allowed on insulators, but excluded on plates. At the second stage with this type of heating, the effect of condensation only on the plates was studied. The second stage was completed by picking up the impedance beam spectrum in a situation of intense water vapour condensation.

The MEC impedance spectrum caused by parasitic capacitance was studied using 20 frequencies with a frequency range of 1 MHz to 10 Hz and an amplitude of 50 mV. The direct current component was not added to the alternating current (i.e. the potential was set to zero before the measurements). For the quantitative determination of parasitic capacitance and parallel resistance, the impedance spectrum was modelled using a simple “circle fit” analysis methodology – a tool integrated into the composition of the Autolab measurement program NOVA 1.8 (Eco Chemie, MetrOhm Autolab B. V., 2023).

The third stage of MEC reliability investigation. If humidity in the climate chamber was less than 60%, then the risk of condensation of water vapour on the MEC plates and insulators was low even without heating. This humidity corresponded to approximately 12% equilibrium moisture content of wood (Higgins, 1957). The experiment showed that the drier the surface of the wood, the more the triboelectric charge generated by friction between the MEC plates, and the surface of the wood will interfere with the measurement of electrical capacitance. Friction between the wooden specimen and the MEC plates inevitably occurs when the specimen is placed between the MEC plates for measuring electrical capacitance, as well as when the specimen is removed between the plates. Despite the presence of triboelectric charge neutralization contour in the MEC design (Figure 2, element 5), some triboelectric charges remain on the surface of relatively dry wood (less than 12% equilibrium moisture). The potential generated by triboelectric charges was measured with a high (10^{12} ohms) input electrometer (Keithley 6517B) (Keithley, 2023). Measuring the potential did not allow determining the magnitude of the triboelectric charge generated in coulombs, but nevertheless proved to be a sensitive indicator showing the presence of these charges.

The reliability of the wood impedance method was visually examined using the method of random deviations (point scattering) on the Nyquist graph. It should be mentioned that both the capacitance method and the impedance method are characterized by very small operating currents of 2–10 nano-amperes according to the readings of the Autolab display. Therefore, the impedance method was also assumed to be relatively interference-sensitive due to its weak operating current, especially to the various electromagnetic disturbances propagating in the surrounding environment, as well as to the interference coming in via Autolab power.

It cannot be ruled out that interference can also occur through the grounding circuit of the experiment.

Wood impedance measurements were carried out on stainless steel insulated electrodes nailed to the specimen at $\frac{1}{3}$ depth at the Bode phase angle minimum (Tomppo et al., 2011). If the Bode phase angle is minimal, then the impedance modulus differs minimally from the resistance of the real part of the impedance. The frequency range of 1 MHz to 10 Hz with 50 mV amplitude was used. The direct current component was not added to the alternating current (i.e. the potential was set to zero before the measurements).

4.4. Adding a monitoring function to the wood moisture meters (I) and (II)

A philosophy widely used in software development of Unix-like operating systems is: „Make each program do one thing well and expect the output of every program to become the input to another” (McIlroy et al., 1978). If the source code of the wood moisture meter software is available and licencing permits, then necessary functionality can be added directly to the source code (or hardware). That was the case with the developed MC meter. The data format was well-defined and human-readable, and any necessary modification could be done directly in the source code. Also, the data file or output stream can be easily further processed with widely used command line tools (sed, awk, grep, etc.) and transmitted over an SSH tunnel. For the moisture meter prototype, the data format for log files and output stream was:

“<timestamp> <value> <unit>”.

The situation becomes more complicated regarding closed-source code. In this case, you have to find a way to get the output of the program to favour further data processing. User interfaces can generally be divided into graphical and text-based.

Suppose it is a device with a text interface. Then the solution is to filter the input to some extent and forward it to another program. For the Ahlborn system, data is transmitted via the rs232 protocol. On the receiving side in Linux, it is accessible via the device file `‘/dev/USB0’`. The data filtering snippet is shown in Figure 3, c.

However, if a device has a graphical user interface and it is not capable of outputting text, then the only usable solution is to manipulate the same GUI in some automated form. In other words, the functions described in the program for replacing the keystrokes of the human user. Such functionality is available in SikuliX software package. It is possible to identify screen regions, generate keystroke events and input-output text defined in code in Figure 3, a.

A Linux-based virtual machine coming from Qemu or Virtualbox is well suited to fulfil the role of a central monitoring component. To connect the system, you need at least one Ethernet switch and a number of ports sufficient to connect all devices.

The architecture (Tamme H., 2013) shown in Figure 3 was used to expand and aggregate the functionality of the closed-source programs.

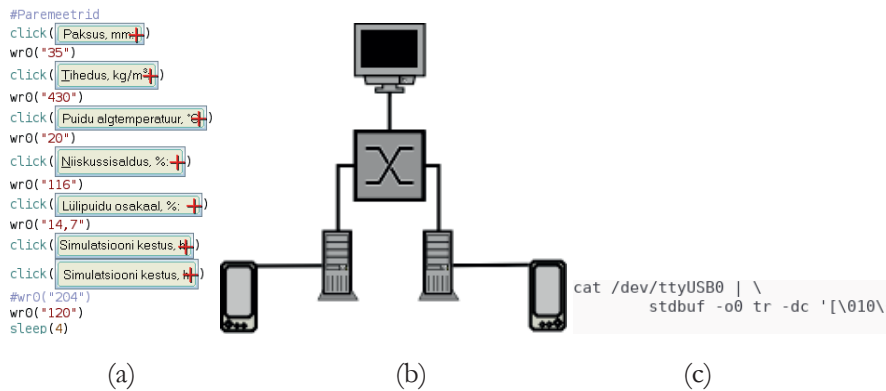


Figure 3. Graphical user interface automation (a), system architecture (b) and text-based interface automation (c).

The measurement data issued by various devices were collected in the central monitoring system in the form of text in Figure 3, b. This collection method requires that the used devices are connected to a computer with its own driver program, which in turn can be accessed over the Ethernet network with either the RDP or SSH protocol.

The workflow for this architecture is as follows. First, a connection is established to the computer for controlling a particular device from the central machine. Second, the device driver is manipulated until the desired output is obtained. Third, the result is returned to the central machine for post-processing. Post-processing is necessary to uniform

data formats issued by different devices and to correct the time marker of data points (Tamme, H., 2013).

4.5. Theoretical background of the wood drying simulation program TORKSIM

The first part of the heat transfer equation (17) describes thermal processes and the second part describes the amount of heat flux transmitted by water vapour in a one-dimensional case (Siau, 1984):

$$\rho c_p \frac{\partial T}{\partial t} = \frac{\partial}{\partial x} \left(\lambda \frac{\partial T}{\partial x} \right) + \frac{\partial u}{\partial t} \rho_w G_m H_m \quad \text{I} \quad (17)$$

where x is distance along the flow direction (m), t is time (s), ρ is wood density (kg m^{-3}), u is a moisture content (kg kg^{-1}), c_p is the specific heat capacity of wood ($\text{J kg}^{-1} \text{K}^{-1}$) as a function of temperature and moisture content u (kg kg^{-1}), T is temperature (Kelvin), λ is wood thermal conductivity ($\text{W m}^{-1} \text{K}^{-1}$) expressed as a function of temperature and moisture content u , ρ_w is water density (kg m^{-3}), G_m is wood specific gravity ($\text{kg} \cdot \text{kg}^{-1}$) and H_m is latent heat of moisture in wood ($\text{J} \cdot \text{kg}^{-1}$).

The specific gravity of wood G_m is the ratio of wood density to water density for the same comparable volume. The moisture content of wood is expressed as the mass of water divided by the mass of absolute dry wood.

For a simplified diffusion-based model, it is experimentally possible to determine the diffusion coefficient of moisture in wood based on Fick's first law (Fick, 1855; Salin, 1990; Tamme et al., 2011; 2016) which falls within the range of 10^{-8} up to $10^{-10} \frac{\text{m}^2}{\text{s}}$ (Keey et al., 1999; Kretchetov, 1972; Tamme et al., 2011; 2016):

$$F = -D \frac{\partial u}{\partial x} \quad (18)$$

where F is mass flux ($\frac{\text{kg}}{\text{m}^2}$), D is diffusion coefficient ($\frac{\text{m}^2}{\text{s}}$), u is mass concentration ($\frac{\text{kg}}{\text{m}^3}$) and x is coordinate (m).

The fundamental equation of diffusion for non-stationary isothermal moisture transfer through the wooden specimen represents Fick's second law in the one-dimensional case (Crank, 1956):

$$\frac{\partial u}{\partial t} = \frac{\partial}{\partial x} \left(D_t(T, u) \frac{\partial u}{\partial x} \right) \quad (19)$$

where D_t is diffusion coefficient perpendicular to wood ($m^2 \cdot s^{-1}$).

When wood drying is done in a narrow temperature range of 50–60 °C, that is, in a special isothermal case, then the simplified Fick's second law can be used:

$$D_t \frac{\partial^2 u}{\partial x^2} = \text{const} \quad (20)$$

The solution to such a differential equation is a polynomial of the second degree. A drying plan, which considers the dynamics of moisture content and temperature, gives a parabolic distribution of moisture content perpendicular to the surface of a material and was called by Luikov the quasi-stationary drying regime (Luikov, 1966; Tamme et al., 2011).

To ensure the quality of wood drying, it is necessary to find tensile stress in wood caused by the differences in the moisture profile at various depths of the material. The model for calculating tensile stress in the one-dimensional isotropic case (Salin, 1990):

$$\sigma = \alpha E \left(\frac{\int_0^{l/2} E \rho_b dx}{\int_0^{l/2} E dx} - \rho_b \right) \quad (21)$$

where σ is tensile stress (Pa), α is unrestricted shrinkage coefficient, ρ_b is content of bound water ($kg \cdot m^{-3}$), E is modulus of elasticity (Pa), l is board thickness (m), x is coordinate from the surface of the board (m).

Basic equation for wood deformation calculation in the drying process:

$$\frac{\partial \epsilon}{\partial t} = \frac{1}{E} \frac{\partial \sigma}{\partial t} + \frac{\partial \epsilon_v}{\partial t} + (\alpha + m\sigma) \frac{\partial \rho_b}{\partial t} \quad (22)$$

where ϵ is total strain, σ is tensile stress (Pa), E is modulus of elasticity (Pa), ϵ_v is viscoelastic strain, α is unrestricted shrinkage coefficient ($m^3 kg^{-1}$), m is mechano-sorptive creep coefficient ($m^3 kg^{-1} Pa$), ρ_b is content of bound water ($kg \cdot m^3$), t is time (s).

It should be kept in mind that the modulus of elasticity is not constant, but depends on the wood moisture content and temperature (Salin, 1990).

In the numerical solution of Luikov's system of differential equations, E is set as a constant only in a provided layer of calculation.

4.6. Methodology for determining the local diffusion constant in drying pine wood at different depths from the board surface (IV)

The placement of the sensors on the specimen in the climate chamber is shown in Figure 4, a. The measuring electronics are separate from the drying air via the outlet on the left. The reference specimen and the specimen for slicing are placed to the right of the specimen measured in the experiment under the same environmental conditions. The schematic of the experiment is shown in Figure 4, b.

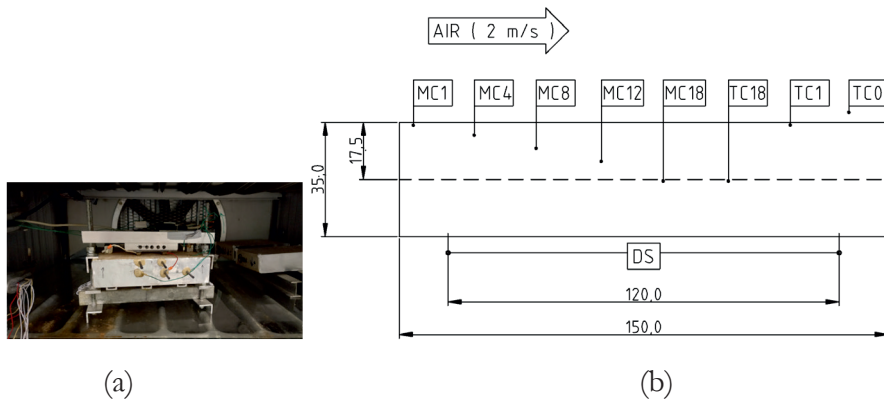


Figure 4. Climate chamber internal view (a) and sensor placement schematic (b).

The experiments made use of three specimens of pine sapwood cut from the same material, with a thickness of 35 mm, width of 150 mm and length of 100 mm along the grain. The first specimen was accordingly equipped with moisture sensors MC, temperature sensors TC and displacement sensor DS (Figure 4).

The second specimen was there to collect drying curve data using the dry weight method. The third specimen was used for individual calibration of electrodes and for determining the diffusion constant at different depths. As one of the objectives was the development of sensors used in an actual wood drying chamber, the experiment was carried out at a constant air velocity of 2 m/s at 50–80°C and 95–100% RH. The moisture gradient was found using five resistance sensors at different depths, which were compared to the simulation program based on the produced maximum voltage, using the industry-developed drying

program as a basis for optimization. The electrical quantities recorded in the sensor data logger together with automated simulations were recorded at 1 h resolution at the same time.

4.7. Methodology for applying the timed moistening impulse in the drying process (IV)

The moistening impulse is a short-term increase in moisture in the drying process. Accurate measurement data and simulations based on these with TORKSIM allow the timing of a suitable moistening impulse to suppress the drying stress, which does not significantly increase the drying time. The moistening impulse represented an increase in the RH of the drying chamber from 65% to 95% over the period of 116 h to 119 h, leaving the other parameters specified in the drying plan unchanged.

4.8. Automation of data processing and statistical analyses (I), (II), (III) and (IV)

The equipment used in the laboratory gives its output mainly in a format that requires some pre-processing. Since, in most cases, when creating the user interface, it is assumed that a person is in the role of information processor, it is incredibly time-consuming to direct the output of a device in one format to the input of another device waiting for a different format. To some extent, National Instruments has offered a solution to the problem, for example, with its software package called LabVIEW, which supports devices that can communicate with each other using the appropriate driver. Unfortunately, such an approach is ecosystem limited. In other words, if the device driver is not available, compatibility will not succeed. As an alternative, a software package called Sikulix has been offered, which allows for building a program-controlled modular automation layer on top of the graphical management interface. Then it is not necessary to modify the closed-source software. It is also possible to aggregate devices or programs attached to different physical computers into a single workflow. Computer network interconnect must be functional for tasks like this.

When automating the graphical user interface, the appropriate area on the screen that needs to be manipulated is identified. For example, if you need to press a button with the left mouse button, the first step is to determine the coordinates of the button's location, and the second step

is to generate the button press event. Or, if it is necessary to read some part of the screen, after finding a suitable region and reading data into a buffer, the data can be copied to a machine with appropriate software for post-processing. In most cases, a Linux-based device is used for post-processing. It is so mainly because the ideology of UNIX-like system philosophy encourages that the output of every program can become the input of another.

The prerequisite for data processing was the temporal overlap of data points recorded by different data loggers. However, the latter was difficult because the measuring devices were not synchronized against the same time server or did not issue a time marker. The initial data of the experiment were pre-processed with different bash scripts, and the definition of time markers was based on the handwritten test protocol. The result was a comma-separated value file, easily importable to Excel, R or Python language libraries.

Carrying out large-scale simulations of the simulation program TORKSIM became a different problem due to the graphical user interface, which wanted to receive a large amount of input data to run each simulation. The solution to the problem was to provide the initial parameters as an array (Figure 5, a) and export the results as text (Figure 5, b) using the SikuliX software package and shell scripts. This approach made it possible to eliminate several hours of error-prone human work for text entry.

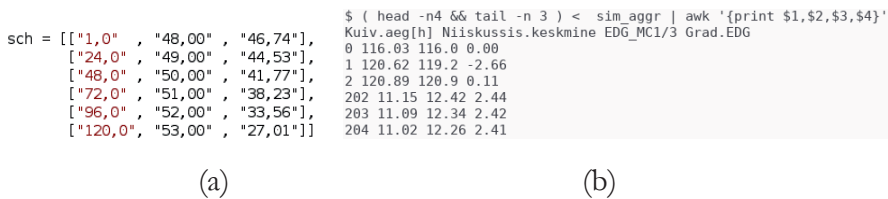


Figure 5. Input array (a) and post-processing (b).

Statistical analysis and visualization, in addition to Excel, LibreOffice, mainly python NumPy, Pandas, lmfit and matplotlib libraries, were used in the Jupyter Notebook environment. The latter allows different code segments, e.g. cells to be run in a freely chosen sequence. This approach ensures the repeatability of the procedures used in the analysis and visualization in a self-documenting way (Figure 6).

```
In [46]: m, b = np.polyfit(df_t_trimmed['telg'], df_t_trimmed['keskosa_temperatuur(°C)'], 1)
plt.plot(df_t_trimmed['keskosa_temperatuur(°C)'],
plt.plot(df_t_trimmed['telg'], m*df_t_trimmed['telg'] + b)
```

Figure 6. Jupyter Notebook cell.

(III) Statistical processing of the test results was based on the principles of a metrology standard ISO 1993 and carried out with software R (2010), MS Excel and NOVA 1.8. In the case of Student t-distribution and linear regression for the single measurement, the upper and lower tolerance lines (confidence limits) of the regression line are presented in MS Excel at 95% confidence level as follows (Kiviste, 1999):

$$\text{Intercept } b_{0\text{lower}} = b_0 - TINV(\alpha; n - 2)S_{b_0} \quad (23)$$

$$\text{Intercept } b_{0\text{upper}} = b_0 + TINV(\alpha; n - 2)S_{b_0} \quad (24)$$

$$\text{Slope } b_{1\text{lower}} = b_1 - TINV(\alpha; n - 2)S_{b_1} \quad (25)$$

$$\text{Slope } b_{1\text{upper}} = b_1 + TINV(\alpha; n - 2)S_{b_1} \quad (26)$$

where S_{b_0} and S_{b_1} are the standard errors of the regression line intercept and slope (Kiviste, 1999).

The following formulas were used to estimate the standard error (SE) and the root-mean-square error (RMSE) of the regression model:

$$SE = \sqrt{\frac{1}{n-2} \sum_{i=1}^n (y_i - \hat{y})^2} \quad (27)$$

$$RMSE = \sqrt{\frac{1}{n} \sum_{i=1}^n (y_i - \hat{y})^2} \quad (28)$$

where y_i is the estimated values and \hat{y} is the actual values.

The non-parametric Kolmogorov-Smirnov test and the Shapiro-Wilk test (Tamme et al., 2014) were used in the R software environment to check the normality assumption of residuals of regression models.

4.9. Materials (I – IV)

Calibration experiments (I–III) used black alder and birch boards with a thickness of 35 mm, width of 150 mm and length of 470 mm.

The drying experiments made use of three specimens of pine sapwood cut from the same material, with a thickness of 35 mm, width of 150 mm and length of 100 mm along the grain. The electrodes shown in the figure were placed on the first specimen.

In the drying experiments, the second specimen was intended for collecting drying curve data using the dry weight method. The third specimen was used for individual calibration of electrodes and for determining the diffusion constant at different depths. In all the specimens listed, the moisture distribution was carefully obstructed in the longitudinal and tangential direction by special vapour barriers. Moisture could only leave the specimens in the radial direction. In this way, a one-dimensional moisture gradient in the specimens was guaranteed.

5. RESULTS

5.1. Calibration results of wood moisture meters according to the Rozema criterion (I), (II), (III)

Figure 7 represents time-dependent electrical resistance (a) and electrical capacitance (b) raw files in a polarization-type wood moisture meter. Time dependencies are described by formulas (7) and (8). Electrical capacitance C was determined according to the formula (11) with numerical integration of the polarization current I_{pol} . By simultaneously analysing the R and C variances obtained at different electrode insertion points at a given average wood MC, the comparison of the coefficient of variation (CoV) showed that electrical resistance has the lowest CoV in the first second and electrical capacitance also has the lowest CoV in the first second. CoV is the largest in the 20th second. Consequently, it would be advisable to select R_{1n} and C_{1n} as independent variables in the calibration model. Index n is the index of the insertion location of the measuring electrodes into wood. Opting for this, the initial variability of the independent variables was kept as low as possible. From Figure 7 it may be concluded that even arithmetic averaging of temporal changes would increase variability. It is therefore not feasible to select the arithmetic averages of time-dependent $R_n(t)$ and $C_n(t)$ as independent variables. Further exploration of the independent variables R and C in the reference model types in Table 1 is done without subscripts, since the meaning of the indices has been defined. Article (II) provides definitions of the calibration model and the corresponding reference model. Calibration functions are given in Article (II, Table 2).

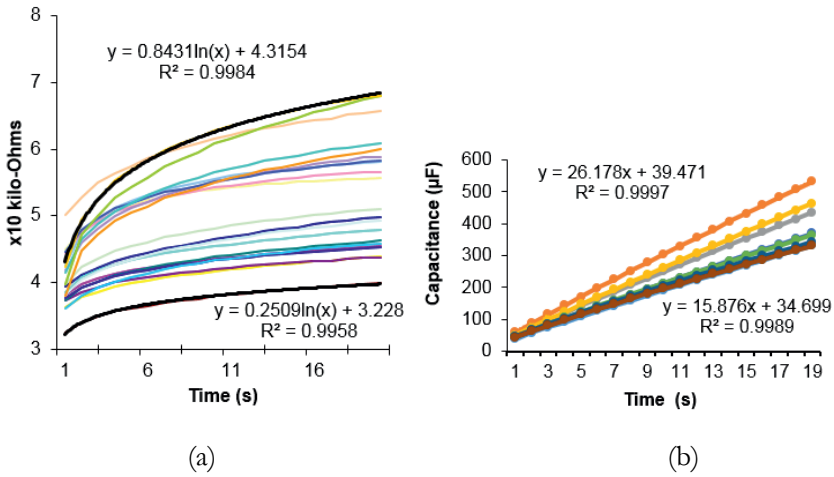


Figure 7. Electrical resistance (a) and electrical capacitance (b).

Rozema (2010) criterion (Rcr) have been developed to assess the goodness of fit of the calibration model of resistance-type wood moisture meters. The criterion are for generalizing, comparing, and delimiting the results of the calibration experiment of the moisture meters. Essentially, this is a calibration model tolerance interval (TI) width with a 95% confidence level for a single measurement, presuming the theoretical Student distribution (Sachs, 1982). The Rozema criterion states that the tolerance interval for a single measurement should not be wider than 3.5% MC. The Rozema criterion is suitable not only for assessing the calibration models of resistance-type wood moisture meters, but also for comparing the calibration models of wood moisture meters with various operating principles (capacitance-type, polarization-type, impedance-type, etc.). The Rozema criterion is rather strict. In moisture levels above FSP, it is quite difficult to fulfil it for a single measurement. The exception was the polarization-type wood moisture meter in which the criterion for a single measurement was managed to be met in a relatively limited MC range (Table 1.). Therefore, sample-based measuring series were used in modelling to meet the Rozema criterion. The arithmetic averages of a series of measurements drawn from 16 single measurements were used as measuring series, whereas for further modelling the averages thus formed were treated as single measurements. This model was called a multiple model with a period of $k=16$. Table 1. shows the most important reference models for the polarization-type wood moisture meter. These include:

- Type A:** $R + C; R+f(C)$
- Type B:** $R_{1n} + R_{20n}; f(R_1 + R_{20})$
- Type C:** $f(R) + f(C)$

The reference models in Table 1. were obtained for alder wood at a temperature of 50 degrees Celsius. If the values of electrical capacitance C were ignored in the sample of measurement data, then the calibration model (and the corresponding reference model in Table 1. RM2) of the traditional resistance-type wood moisture meter could be obtained. The use of RM2 for comparison with a focusing model RM5 is shown in Figure 9, b. In Table 1. the location of the RM5 focal point is at 151% MC and the wood MC range (142%–160%) corresponding to the Rozema criterion has been highlighted in bold. Logarithming of electrical resistance measurement results (Table 1. , RM3 and RM2) compared to the original measurement results model (RM2) allows some compression of the so-called Edwards trend (I) (i.e., tolerance interval progressive expansion as wood MC increases). However, logarithming does not completely eliminate the said trend, nor does it reverse it, as can be seen in Table 1. , RM5 and Figure 9, a. As Table 1. also indicates the lower and upper line equations of the tolerance interval for each model type, substituting the 151% value of the moisture content into the equations for example to generate numerical examples results in comparative tolerance intervals for different models. At MC 151%, the predicted single measurement tolerance interval of RM2 is $TI = 178 - 124 = 53\%$ MC; for RM3 it is 26% MC and for RM5 it is 0.8% <3.5%.

A peculiar focusing model (with the focal point at MC=120%) is RM7. Namely, this analysed model lacks electrical capacitance C – the characteristic component of the focusing model. Covertly, the last element of the electrical resistance time series Rn20 plays the role of capacitance C. Visually, the result is the same as for the other model types containing the electrical capacitance C. RM7 can also be called the model based on the raw data of the electrical resistance time series (Art. II, figure 12).

The fundamentals of metrology provide that random measurement deviations can be smoothed out by arithmetic averaging of measurement results. The well-known moving average is used to smooth time series. Table 1. gives the so-called multiple models where new single

measurements have been generated on the basis of the arithmetic averages of a series of 16 measurements. The use of measuring series allows for a significant shrinkage of the tolerance interval of the arithmetic averages of the measuring series representing a single measurement in the model. It is interesting to compare the effect of using measuring series and the focusing model on the tolerance interval. In model RM8, the Rozema criterion was met after 16 measurements, but in model RM9 the same result was achieved with only a single measurement. The difference in the labour intensity of the measurements is impressive, that is, 16-fold.

Table 1. Relevant reference models (RM) with the statistical characteristics for above FSP wood moisture content. The independent x variable in all RMs is the actual wood moisture content, the dependent y variable in all RMs is the predicted wood moisture content.

Mod. No. Obs. No	Model type	Equations for calculating single measurement tolerance intervals (T. I.)	R2	p-value	*Focal point on MC%	Calculated MC range where T. I. <3.5% MC (acc. Rozema (2010) criterion)
RM2 N=63	R-mod.	$y_{upper} = 1.2075x - 4.888$ $y_{lower} = 0.796x + 3.897$	0.96	<0.01	30	> 3.5%
RM3 N=63	logR	$y_{upper} = 1.0071x + 7.6164$ $y_{lower} = 0.8924x - 1.14$	0.99	<0.01	30	> 3.5%
RM4 N=63	(R+C) (Type A)	$y_{upper} = -0.0015x^2 + 1.14x + 4.01$ $y_{lower} = 0.0052x^2 + 0.2717x + 14.2$	0.99	<0.01	117	110 - 120
RM5 N=63	R+f(C) (Type A)	$y_{upper} = -0.0009x^2 + 1.12x + 1.07$ $y_{lower} = 0.0033x^2 + 0.407x + 13.8$	0.98	<0.01	151	142 - 160
RM6 N=63	R1n+R20n (Type B)	$y_{upper} = -0.0012x^2 + 1.09x + 11.2$ $y_{lower} = 0.0061x^2 - 0.022x + 31.5$	0.97	<0.01	129	123 - 133
RM7 N=63	f(R1+R20) (Type B)	$y_{upper} = -0.0042x^2 + 1.549x - 5.47$ $y_{lower} = 0.0072x^2 - 0.1469x + 32.7$	0.97	<0.01	120	116 - 124
RM8 N=18 k=16	k*R (Multiple model)	$y_{upper} = 0.998x + 1.3446$ $y_{lower} = 0.9852x + 0.3413$	0.99	<0.01	30	30 - 151
RM9 N=63	f(R)+f(C) (Type C)	$y_{upper} = 1.03767x - 2.0483$ $y_{lower} = 1.01872x - 3.5253$	0.99	<0.01	78	30 - 105

*) the model focal point has been defined as the specific value of actual wood moisture content, when the calculated tolerance interval reaches the minimal value.

Comparison results for two alternating current methods namely DECM and EIS for determining wood moisture content in kiln conditions are given in Table 2. In regression models, the independent x-variable is the actual MC (%), and the dependent y-variable is the predicted MC (%). The predicted single measurement tolerance bands on the 95% confidence level, y_{upper} and y_{lower} , are calculated using formulas (23), (24), (25) and (26). The SE is calculated according to formula (27). The tolerance interval (TI) is calculated using the formula $TI = y_{upper} - y_{lower}$. In Table 2 N is the number of measurements repeated under the same test conditions and k is the number of measurements averaged per series of measurements (i.e., the averaging period). For models with a series of measurements (k), the identification type shall be „multiple”.

Table 2. Modeling results of the dielectric capacitance method (DECM) and electric impedance spectrometry (EIS) method.

N obs., k-period	Method type, Fig. no.	Equations for predicting single measurement tolerance bands and TI	R2	p- value and tests*	SE
N = 63	DECM (above FSP), Fig. 8	$y_{upper} = 1.0131x + 5.9063$ $y_{lower} = 0.9406x + 0.8399$ $TI = 0.0728x + 5.075$	0.97	<0.01 K-S	4.88
N = 42	DECM (below FSP)	$y_{upper} = 1.0135x + 0.2792$ $y_{lower} = 0.9788x - 0.1954$ $TI = 0.0348x + 0.4746$	0.99	<0.01 K-S S-W	0.61
N = 63 k = 16	DECM (above FSP) (multiple), Fig. 8	$y_{upper} = 1.006x + 0.44$ $y_{lower} = 0.9929x - 0.4163$ $TI = 0.0124x + 0.8775$	0.99	<0.01 K-S S-W	0.46
N = 63	EIS (above FSP), Fig. 8	$y_{upper} = 0.9448x + 11.196$ $y_{lower} = 0.787x + 2.41$ $TI = 0.1622x + 8.135$	0.87	<0.01 K-S	5.01
N = 63 k = 16	EIS (above FSP) (multiple), Fig. 8	$y_{upper} = 1.0134x + 1.728$ $y_{lower} = 0.968x - 0.84$ $TI = 0.0365x + 2.836$	0.99	<0.01 K-S	0.867

* Kolmogorov-Smirnov (K-S) test and Shapiro-Wilk normality (S-W) test

Results for meeting the Rozema criterion in AC-powered capacitance-type and impedance-type wood moisture meters with reference models are given in Table 2 and Figure 8. As can be seen in Table 2 and Figure 8, for these two types of moisture meters, the Rozema criterion for single measurements above FSP cannot be met in any cases. When using measuring series in models where the period k=16, the situation is better. According to Figure 8 the Rozema criterion (the red line parallel

to the x-axis in the figure) can only be met with a capacitance-type wood moisture meter (DECM). The EIS-multiple model is on the borderline, and it would probably require some increase in k – the number of repeat measurements – in the measuring series to fulfil the Rcr. The residual standard deviation of the EIS model ($SE = 0.867$) would, in fact, allow for such an approach.

In Table 2, the second row, the only exception is the model DECM, below FSP (Article III, Figure 7), where the Rozema criterion can also be met for a single measurement without the need to use measuring series. By substituting in the TI equation of the said model the 30% MC value of the agreed maximum limit of below FSP, we get $TI = 0.0348 \cdot (30\% MC) + 0.4746 = 1.58\% < 3.5\% MC$. In this context, it should be noted that the EIS method does not function properly at below FSP ($< 30\% MC$) moisture levels due to its low sensitivity. This method was therefore not modelled in Article (III) at moisture levels below FSP.

(III) “In Moschler’s paper (2004) it was found that the actual MC point of 28.60% of the high frequency capacitance method (4.5 to 6.0 GHz) is estimated to have a predicted extended uncertainty of $\pm 3.62\%$, thus, the corresponding tolerance interval for this point is 7.24% MC. In comparison, a tolerance interval of 7.26% MC calculated for the same actual MC point of 28.60% was found in this study for the low-frequency capacitance method (DECM) (Table 2, second row), using the relevant formulas: $TI = 0.0348x + 0.4746$; $TI = 0.0348(28.60\% MC) + 0.4746 = 7.26\% MC$ ”

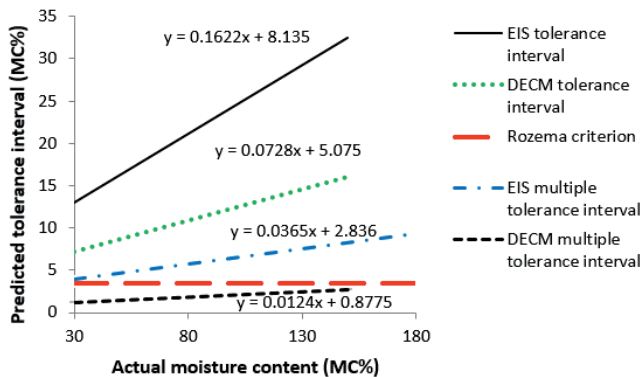


Figure 8. TI models above FSP.

5.1.1. Wood electrical charging number

The electrical charging number for wood was first defined in patent (I). It represents an empirical constant with very little variability, with the same numerical value at all levels of the average MC of wood. The product of wood capacitance and resistance is practically constant (or of minimal variability) at any moisture content above 30% FSP. We call the product of the aforementioned the wood charging number. Since the wood charging number itself does not depend on the moisture content of the wood, it is not suitable as a variable in the calibration model, the purpose of which is to predict the moisture content of the wood at a level of more than 30%. At the same time, the function $f(R,C)$ chosen by the variables R and C is used in the regression model to compress measurement deviations, improve the signal-to-noise ratio, and increase the accuracy of the calibration model at the desired focal points of the model, at preferred moisture contents.

The following hypothesis was put forward in Article (II): “Random deviations of electrical resistance R and electrical capacitance C at a given measuring point are inversely proportional and may cause the tolerance interval convergence predicted for a single measurement at high moisture levels of wood, if used with an appropriately selected calibration function of two variables $f(R, C)$.”

In Article (II) it was established that a sample corresponding to the definition of the electrical charging number can be used to define certain two-variable function types A, B, and C (Table 1, second column (II)), which, however, depend on wood moisture content. These function types lead to the concentration of random measurement deviations in a two-variable (the variables are R and C) calibration model at a certain characteristic point, the so-called focal point. The function types A, B, and C are given in Table 1. As shown in the previous chapter, these function types can be used to meet the Rozema criterion for above FSP moisture levels even in the case of a single measurement. Definition of the charging number (II):

“We found that $R \cdot C$ proved nearly constant for every actual moisture content value used in the calibration model, thus showing that the obtained empirical constant is independent of the wood moisture content. The consistency of $R \cdot C$ means that in any wood moisture

content above the FSP, wood electrical resistance and electrical capacitance are in an inversely proportional and non-linear dependence. This empirical constant, thus found to be independent of the moisture content, was called the wood empirical charging number, or for short, the wood charging number”

$$RC = 1994.993 (k\Omega * \mu F) = 1.995 \text{ sec} = \text{const} = ChN \quad (29)$$

where ChN is the charging number.

For a better graphical representation of the wood charging number and its association with Figure 9 (a) and (b), formula (29) can be given in a logarithmic form:

$$\log(R) + \log(C) = \log(ChN) \quad (30)$$

The value of the variation coefficient characterizing the dispersion of the empirical charging number is 0.597%. When we compare the charging number variation coefficient and the variation coefficients of electrical resistance R and electrical capacitance C (vt. (II), Table 3, columns 9 and 13), we can conclude that the variation coefficient of the charging number is considerably (about 16 times) smaller than for the electrical variables (0.597% for R x C versus 9.85% for electrical resistance R and 9.47% for electrical capacitance C).

The definition of wood charging number was first presented in a patent application (Tamme et al., 2020). For this research, the definition of wood charging number is the basis for our hypothesis:

“Random deviations of electrical resistance R and electrical capacitance C at a given measuring point are inversely proportional and may cause the tolerance interval convergence predicted for a single measurement at high moisture levels of wood, if used with an appropriately selected calibration function of two variables f (R, C)”.

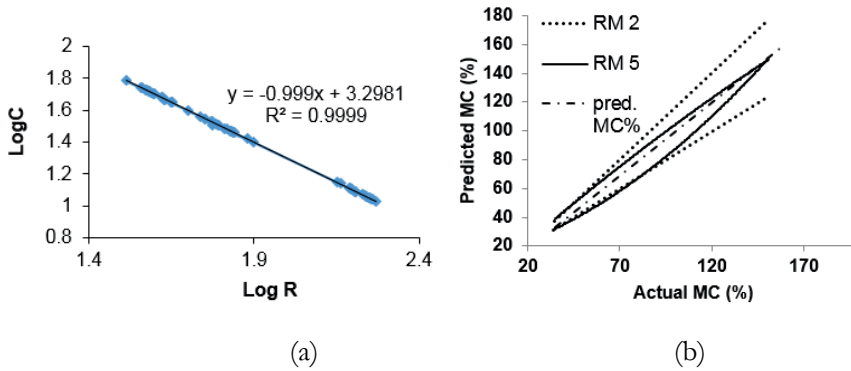


Figure 9. Wood charging number (a) and $R + f(C)$, R model TI (b).

5.1.2. Wood moisture meter prototype based on charging number ideology

The prototype consists of three modules connected by coaxial cables. The first module is the so-called switching block for implementing the PD cycle according to the logic of the MCU program. The second module is the so-called analogue block which is essentially an electrometer based on operational amplifiers. The third module, the so-called digital block, contains the computing technology necessary for controlling the switching component, digitizing, processing and transmitting the output of the analogue part.

At the beginning of the polarization cycle, the measuring electrodes of the electrometer (sense and non-sense) are connected to the input of the analogue component. The output of the analogue part is connected to the input of the digital component (ADC). At the beginning of depolarization, the measuring electrodes are connected directly to the digital block and the electrometer, i.e. the analogue part, is removed from the circuit. After recording the measurement results of the depolarization cycle, the sense and non-sense electrodes are short-circuited for the final discharge of the wood.

Sense and non-sense switching to the input of the analogue part is made with the DPST-CO reed relay. Sense and non-sense switching between the output of the analogue part and the input of the digital part are made with a DPST-NO reed relay. Sense and non-sense shorting are made with the SPST-NO reed relay. The maximum switching duration for different combinations is 3 ms.

The output of the electrometer is digitized by a two-channel 16-bit 860 SPS sigma-delta differential analogue-to-digital converter (ADC). The conversion frequency of 128 measurements per second is chosen based on the optimal signal-to-noise ratio, the switching speed of the reed relay and the performance of the microcomputer. In this case, less than one measurement is lost during the PD cycle transition. The results of the ADC conversion are transmitted over the i2c bus to a microcomputer (Raspberry Pi) for digital processing and need-based data transmission over the ethernet (wireless) network with the ssh protocol or using the built-in serial port rs-232. Between the electrometer and the ADC is a buffering (unity gain and common-mode level shifting) differential amplifier followed by a pre-amplifier containing integrated RFI and EMI rejection filters. The fixed gain stages of the pre-amplifiers (programmable gain amplifier, PGA) are selected so that one channel has a maximum allowable differential input voltage of 0–5 V and the other channel has 0–250 mV. One channel is used at a time, which is selected depending on whether a narrow or wide humidity range is under investigation. It is optimal if the precision feedback resistor selected with the tumbler switch in the feedback circuit is of the same magnitude as the measured resistance of the wood. The situation where only a narrow range of the wide measurement range is used means a loss of resolution that could be avoided by choosing a more sensitive channel.

The current consumption of the system is in the order of 40 mA for the analogue component and 100 mA (160 mA with Wi-Fi) at a supply voltage of 5.2 V, which means the ability to power the prototype from a battery bank, i.e. an autonomous device.

Since the prototype is a real device in real space, it is necessary to adjust the cumulative errors of the components e.g. zero correction.

The correction of the digital part is done with numerical correction in the program code, and the correction of the analogue part is realized with a potentiometer in the feedback circuit of the operational amplifier.

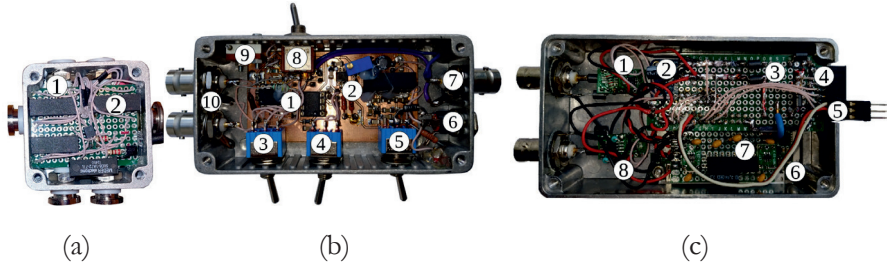


Figure 10. PD moisture meter prototype modules. Switching (a), analogue (b) and digital module (c).

where a1 is BNC connector, a2 is reed relay, b1 is precision rail-to-rail operational amplifier, b2 is high precision low noise low dropout voltage reference, b3 is Conductance or Resistance mode selector, b4 is reference voltage selector, b5 is power switch, b6 is +5V supply connector, b7 is voltage output 0–5 V, b8 is feedback resistor selector, b9 is zero voltage corrector, b10 is sense and non-sense input, c1/c8 is unity gain, differential amplifier, ADC driver and rail-to-rail operational pre-amplifier, c2 is differential ADC, c3 is voltage filters area, c4 is switch (reed relays) block output, c5 is rs232 communication channel, c6 is microcomputer with peripherals and c7 is dual supply DC-DC converters.

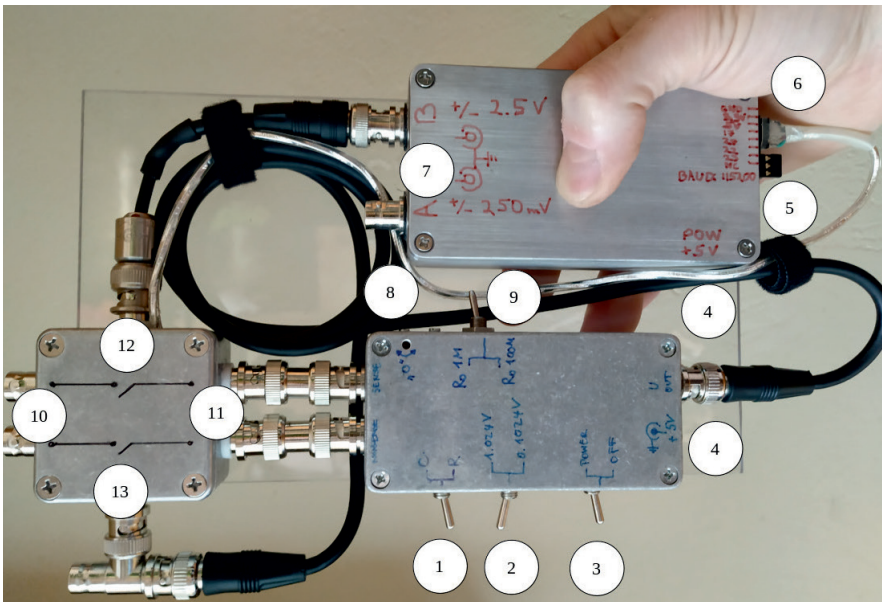


Figure 11. PD moisture meter prototype assembly where 1 is mode selector, 2 is feedback voltage selector, 3 is power switch, 4 is power input, 5 is rs232 port, 6 is GPIO output, 7 is voltage input, 8 is zero adjustment, 9 is feedback resistor selector, 10/11 is sense and non-sense input, 12 is ADC input and 13 is MC meter analogue output.

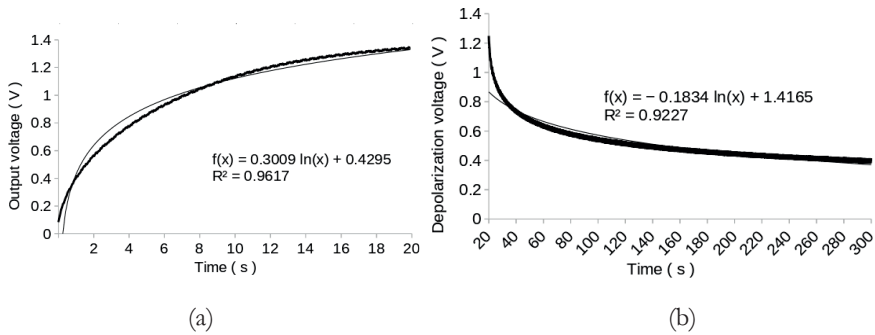


Figure 12. Typical wood polarization (a) and depolarization (b) cycles.

During the polarization phase wood is charged up and analogue part voltage output is sampled by ADC and recorded in the microcomputer local memory. Depolarization phase voltage is measured directly from electrodes with a low-impedance electronic circuit.

5.2. Operational reliability test results of a capacitance-type wood moisture meter and impedance-type wood moisture meter in kiln climate conditions (III)

The purpose of the reliability tests was to identify ranges of reliable useful capacitance for which wood MC calibration models for both below FSP and above FSP moisture levels could be generated. As a capacitance meter (CAM), the Meterman LCR capacitance meter (Wavetek Meterman, 2023) and the MetrOhm Autolab impedance spectrometer (Eco Chemie, 2023, 2023a) were used in the tests. The range of reliable useful capacitance cannot be found until all risks to the reliability of the MEC design have been mitigated. The main MEC reliability characteristics found in reliability testing are presented in the following Table 3.

Table 3. The main physical reliability characteristics of the dielectric capacitance method (DECM) in a kiln climate and the corresponding capacitance meter (CAM) response.

Effect, parameter, figure no.	Effect range	CAM response
Condensation of water vapor on MEC plates	$C_{\text{parasite}} = 340 \text{ to } 845 \text{ pF}$ $C_{\text{parasite}} = 681 \text{ pF}$, determined using EIS method	CAM reading recorded ca. 5x and moderately increasing**
Leakage of MEC insulators	$C_{\text{parasite}} = 163 \text{ to } 681 \text{ pF}$ $R_{\text{parallel}} = 61 \text{ to } 0.778$ kOhm	Floating of CAM reading
Triboelectric charges on MEC plates	$U_{\text{static}} = - 10.5 \text{ to } 4.29 \text{ V}$	Floating of CAM reading, CAM spoilage risk
Useful MEC capacitance,* below FSP (0.% to 30%)	$C_{\text{useful}} = 121 \text{ to } 205 \text{ pF}$ MC = 0.% to 30%	CAM reading stable and reliable
Useful MEC capacitance, above FSP (30% to 105%)	$C_{\text{useful}} = 205 \text{ to } 231 \text{ pF}$ MC = 30% to 105%	

* Useful MEC capacitance depends on the moisture content of wood and the thickness of the wood material according to the MEC, formula (15). Wood moisture content is related to the dielectric constant ϵ in formula (15).

** „Moderately increasing” means that it is possible to manually retrieve a CAM numerical reading, but it slowly increases as the water vapor condensation progresses.

For example, water vapour condensation on plates can cause up to 5 times the measured capacitance, a drop in resistance from 10 giga-Ohms to 61 kilo-Ohms when insulators leak, and a potential of triboelectric charges of up to 10 V.

In summary, the various reliability disruptive effects are selectively and quantitatively outlined in Table 3. The ranges of parasite capacitance and parallel resistance associated with insulator leakage are given in Table 3 in the first and second row.

On the last row in Table 3 it was found as a result of reliability testing that the useful capacitance range for below FSP 0–30% MC is 121–205 picofarads, and for above FSP 30–105% MC is 205–231 picofarads. By dividing the useful capacitance range by the corresponding MC range, we get DECM sensitivity of 2.8 pF/MC% for below FSP, and 0.35 pF/MC% for above FSP. Therefore, the difference in sensitivity between below FSP and above FSP MC ranges is 8-fold, that is, in favour of the below FSP range.

Triboelectric charges only begin to form at below 60% RH, which corresponds to the wood surface equilibrium moisture content (EMC)

of 12%. Triboelectric charges, otherwise known as static charges, cause an electrostatic field potential on the surface of the wood in volts, which was recorded in real time with a high input impedance ($10^{12} \Omega$) electrometer. Since the charges affect the electrical capacitance of an electrostatic system, in principle, as in the case of insulator leakage, we are dealing with parasitic capacitance, only the formation mechanism is different.

With the impedance method, the risk to operating reliability does not lie in the leakage of pin insulators under kiln (dryer) conditions, but in insufficient grounding and shielding of the measuring device. This type of disturbance can easily be eliminated and does not require special examination.

5.3. Pine wood drying optimization results (IV)

5.3.1. New wood drying monitoring sensors added to the experiment – surface layer displacement sensor and surface layer electrical resistance sensor

In addition to the new sensors and insulated pin electrodes, the monitoring of the drying process dynamics is also complemented by thermocouple sensors, which are, according to the layout of the placement of sensors on the specimen (Figure 4, b), arranged as follows: 10 mm of the surface is the drying air temperature sensor, 0.5 mm of the surface is the wood surface layer temperature sensor, and finally, at a depth of 18 mm, there is the specimen centre temperature sensor.

A modified Ahlborn (Ahlborn, 2023) displacement sensor (Type FWA 025-T) (Figure 13, b) was used to detect surface layer displacement in the kiln. Since the sensor does not operate on electronics, it can be stored in the drying medium without cooling. This sensor measures displacements only in the surface layer of wood. As the surface layer electrical resistance sensor, a sensor electrically equivalent to a pin sensor was used (Figure 13, a)

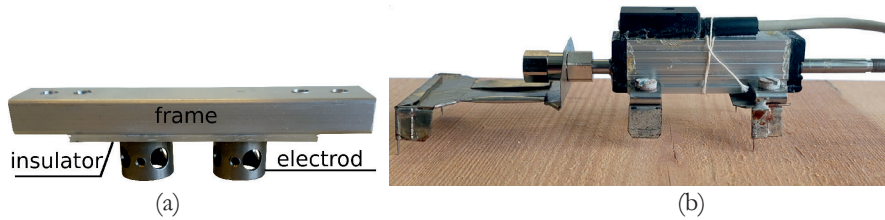


Figure 13. Wood surface layer resistance sensor (a) and displacement sensor (b).

According to Figure 17 the distinction between the first and second drying phases is most easily made on the basis of monitoring temperature differences.

The drying experiment in Article (IV) allowed monitoring two temperature differences. First, the difference between drying air temperature and wood surface temperatures and second, the difference between the wood surface temperature and the specimen centre temperatures.

The temperature monitoring revealed that the temperature sensors practically fail to respond to the moistening impulse. However, the displacement sensor and electrical resistance sensors react vigorously to the moistening impulse.

5.3.2. Critical diffusion constant of wood surface layer and critical drying air humidity

The situation preceding a sharp drop in wood layer diffusion is characterised by the critical diffusion coefficient. This is a borderline where the drying speed of the wood changes significantly, moving into a slow drying phase. The timed moistening impulse suppresses the maximum strain. The goal is to keep the strain below the 0.33 limit (Salin, J. G. 2007), because exceeding it creates a risk of drying cracks.

From Article (IV): “The maximum value of the diffusion coefficient immediately before entering into the second drying phase was named the critical diffusion coefficient. Mass flux, gradient, and critical DC are values which are difficult to determine under industrial wood drying conditions. Therefore, based on the separating line of the first and second drying phase, it makes more sense to determine the critical relative humidity (RH) of the drying air on the basis of the laboratory test, below which the drying process enters the second drying phase. Monitoring

the critical RH value is not a problem in industrial conditions, as wood kilns are usually standard-equipped with a corresponding sensor and a logging option. The determination of critical RH is shown schematically in Figure 4”

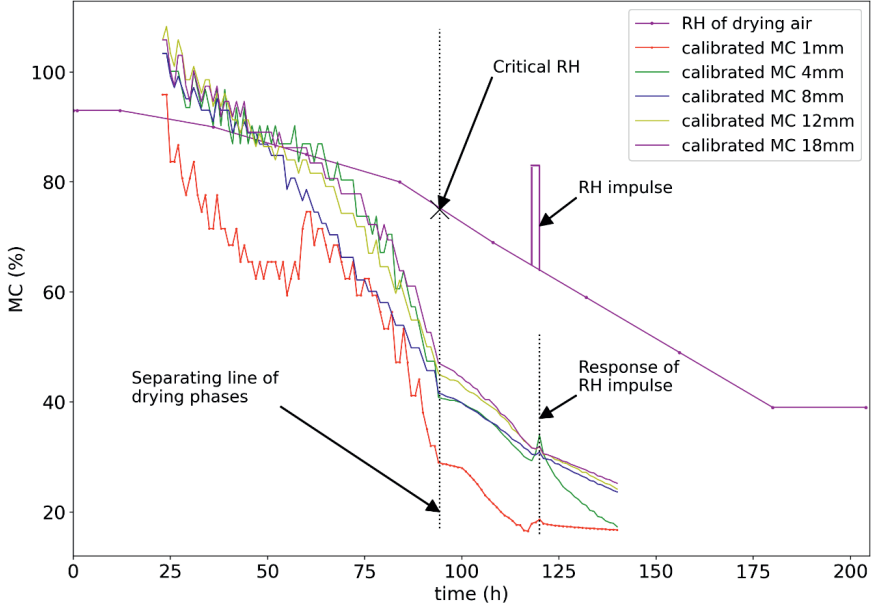


Figure 14. Identification of the critical RH of the drying air according to the separating line of the first and second drying phase.

Figure 15 shows the schematic for determining the critical diffusion constant in the surface layer of wood (at a depth of 2.5 mm from the surface) using the four-point method. This is based on formula (16) in finite increments.

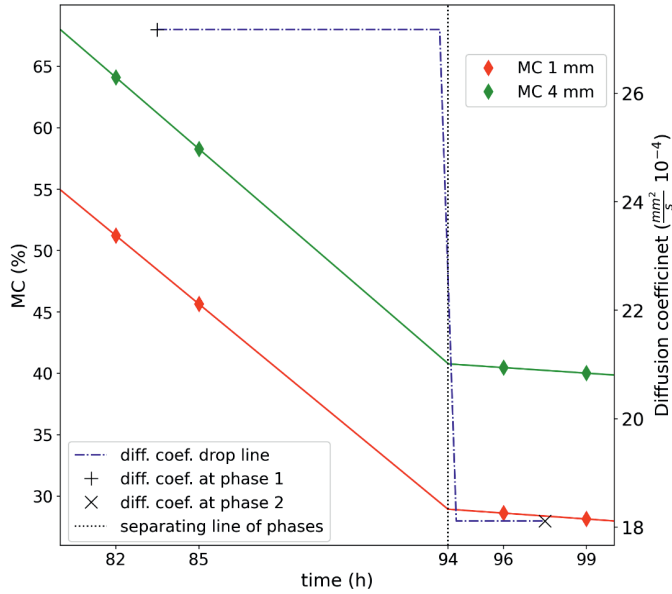


Figure 15. A schematic for calculating the diffusion coefficients in the first and second drying phases, using the four-point method based on experimental data.

In principle, the diffusion coefficient DC can be given according to Formula (18) as the ratio of the mass flux to the gradient:

$$D = -\frac{\text{Massflux}}{\text{Gradient}} \quad (31)$$

$$\text{Massflux} = -\Delta(\text{MC} \%) \frac{m_{\text{dry}}}{\Delta t S} \quad (32)$$

$$\text{Gradient} = \Delta(\text{MC}\%) \frac{\rho_{\text{wood,dry}}}{\Delta x} \quad (33)$$

where D is diffusion coefficient (DC) (m²/s); $\Delta(\text{MC}\%)$ is the finite increment of the wood's MC% on the time axis for the mass flux and in the material thickness (x-axis) for the gradient (MC%); m_{dry} is the wood's dry mass (kg); S is the specimen's surface area (m²); Δt is the time increment (s); $\rho_{\text{wood,dry}}$ is the wood's dry density (kg/m³); Δx is the x coordinate's increment (m).

The calculation schematic with formulas (31), (32), and (33) allows for the determination of the local diffusion coefficient at different depths of the wood surface in a non-equilibrium state (i.e., both the mass flux and gradient change over time). A prerequisite for this is the presence of individually calibrated resistance-type measuring electrodes that enable

monitoring wood MC at different depths from the specimen surface (Figure 4). Repeating the critical diffusion coefficient determination in the next drying test is a rather laborious operation. For this reason, Figure 14 also makes it feasible to determine the relative humidity of the drying air corresponding to the critical diffusion coefficient. The relative humidity of the drying air thus determined can be used in the search for and simulations of optimal drying modes. Tables 4, 5, and 6 show drying schedules designed according to the recommended critical drying air humidity and to the precisely timed moistening impulse. When constructing the moistening impulse using the TORKSIM simulation program, it should be borne in mind that all the moisture used to raise the surface MC of wood with the moistening impulse must also be dried out later. This, in turn, increases the drying time. However, the relaxation of surface strain below the critical breakage limit outweighs the increase in drying time due to the moistening impulse. The time frames of the simulated moistening impulse always appear in the second, variable-speed drying phase.

From Article (IV): “After carrying out these calculations, the values of the experimental DC were the following: DC1ph. = $27 * 10^{-4}$ mm²/s in the first drying phase and DC2ph. = $18 * 10^{-4}$ mm²/s in the second drying phase (Tamme et al., 2021). At the end of the first drying phase and at the beginning of the second drying phase, the simulated DC has an almost equal value (i.e. $11.8 * 10^{-4}$ mm²/s).”

5.3.3. Simulation of drying process optimization results with TORKSIM program using critical drying air humidity and moistening impulse

In the case of a simulation, a mathematical model of the drying process is created on a computer. During the simulation, information is obtained about the state of wood when the drying mode is completed. The simulation provides, in the form of graphs and tables, the moisture curve generally 100% for sapwood and 100% for heartwood. Based on the results received, it can be decided whether the drying mode meets the requirements or whether it needs to be changed. Simulation is an important tool for companies who want to check what happens to wood before starting a new drying operation. Table 4 shows the optimizable mode used in an industrial kiln.

Table 4. Industrial drying schedule.

Time (h)	Air temp. (°C)	Air RH (%)
0	20	93
1	47	93
12	47	93
36	50	90
60	52	85
84	52	80
108	52	69
132	52	59
156	52	49
180	52	39
204	52	39

Table 5. Optimized drying schedule.

Time (h)	Air temp. (°C)	Air RH (%)
0	20	60
1	47	83
113	52	81 (crit. RH)
132	52	59
156	52	49
180	52	39
204	52	39

Table 6. Optimized drying schedule with moistening impulse, RH decrease 16% 24h, strain below 0.33.

Time (h)	Air temp. (°C)	Air RH (%)
0	20	93
1	47	93
24	47	77
48	50	61
72	52	45
(90)	(52)	(40)
96	52	29
120	52	13

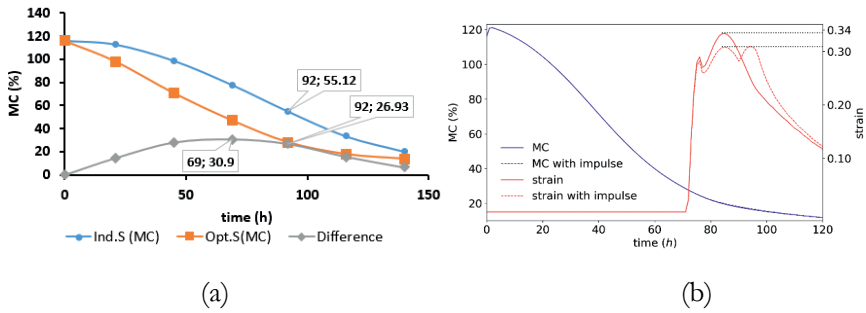


Figure 16. Optimized and unoptimized drying schedule (a) and optimized simulation schedule with and without the moistening impulse (b).

Figure 16, a shows the results of optimizing the drying process using the critical diffusion coefficient. In Figure 16, a the upper drying curve was simulated based on a typical industrial drying schedule, and the lower curve was simulated while considering the critical diffusion coefficient. The comparison is based on a typical industrial wood drying schedule (see Table 4 and the upper curve). The result of the comparison is illustrated with the third curve representing the difference.

With markers, the numerical effect of optimization is indicated in the figure. The drying of a 36 mm thick pine board was optimized. The results were compared by drying time and strain. In the preparation of an optimized drying schedule that considers the critical diffusion coefficient, the drying time of a typical industrial drying schedule was reduced from 140 hours to 92 hours, i.e. 48 hours or two days. The final moisture content was 26% in the optimized mode and 27% in the industrial mode, i.e. essentially the same. The optimized mode was characterized by somewhat higher relative strains instead of the promised 0.33 (Salin, J.G, 2007; Sova et al., 2016), which were relieved by a timed moistening impulse.

Figure 16, b represents the result of optimization using a timed moistening impulse. The figure shows that the dangerous maximum drying strain is levelled by a rather imperceptible moistening impulse in the drying schedule (Table 6, the row in brackets). A minimum MC increase is traded for a significant strain decrease. So, to achieve a positive result, the moistening impulse does not need to be of very large amplitude or long duration. This fact, in turn, saves drying time, because the moisture added to the wood by the moistening impulse must still be dried out later.

5.3.4. Wood drying stress evolution indicator

Resistance sensors located at five different depths in wood, when taken together, could also provide additional information on the drying stress of the wood, in addition to the moisture content. Feedback on the validity of such possible information can be obtained by using the drying process simulation program TORKSIM. In the case of a tree species for which there is no simulation program, one way to get feedback is by the rate of shrinkage of the displacement sensor base on Figure 17. According to the feedback received, the mathematical shape (34) of the electrical indicator of drying stresses can be corrected, where, for clarity, the log scale has been replaced by the measurement channel name U1 – U5:

$$ESCR = \frac{10\log R_{1mm} + 10\log R_{4mm}}{10\log R_{8mm} + 10\log R_{12mm} + 10\log R_{18mm}} = \frac{(U1+U2)}{(U3 + U4 + U5)} \quad (34)$$

Visualization of the temperature and displacement sensor measurement results provides an overview of the temporal sequence of processes occurring in different drying phases.

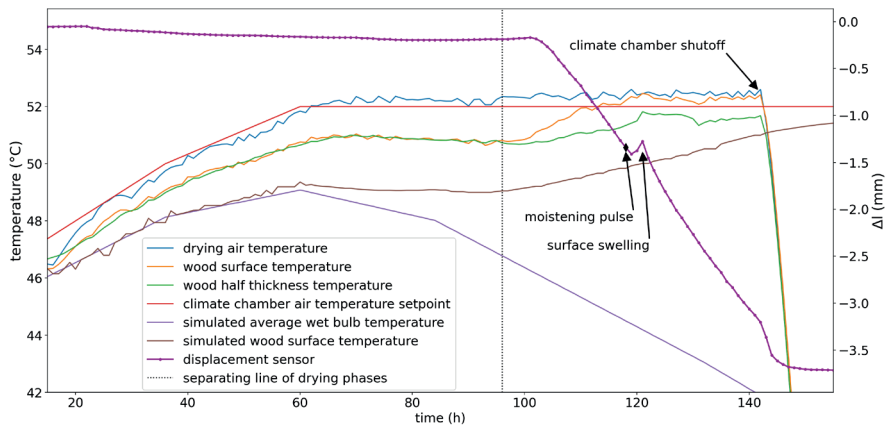


Figure 17. A distinction between the first and the second drying phases based on the log files of three thermocouples and an displacement sensor.

The moistening impulse was used to check the accuracy of the indicator timeline. The goal was to bring the indicator maximum together with the simulated stress maximum by drying according to the same drying schedule. So, the indicator ideology is based on the usual comparison of the result of the experiment and the result of the simulation. Also helpful in the development of the drying stress indicator was the influence of the moistening impulse on the resistance sensors. The result of the use

of the indicator for the detection of the maximum stress in the drying process is depicted on Figure 18.

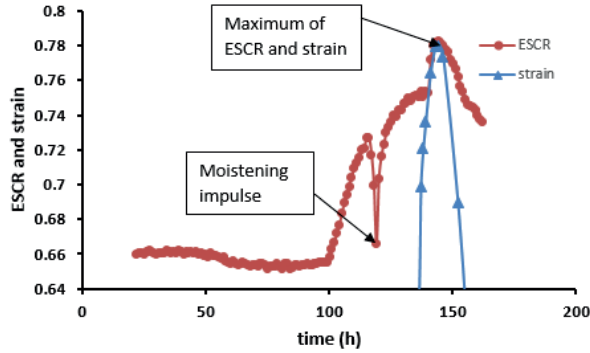


Figure 18. Dependencies of the ESCR value and the TORKSIM v5.11 simulated relative drying stresses on drying time. For a better visual comparison, the simulated relative stresses are multiplied by a factor of 3.12.

With the use of the displacement sensor in the experiment to monitor deformations in the surface layer, it was found that the drying shrinkage of wood in the surface layer begins significantly earlier than throughout the entire cross-section of the wood. The shrinkage of the surface layer begins already when the average MC of the wood is just 60%, but the total maximum drying stress occurs only after the average MC of the wood is below FSP, i.e. less than 27% MC. This result is confirmed in addition to the displacement sensor (Figure 17) and humidity profile graph at the 92nd hour (Figure 19) also by the drying stress indicator graph (Figure 18). Indeed, at the 92nd hour, a rise can be witnessed also on the indicator graph. Of course, the proportions of the indicator graph may not exactly correspond to the actual drying stress profile. That is why this is merely an indication.

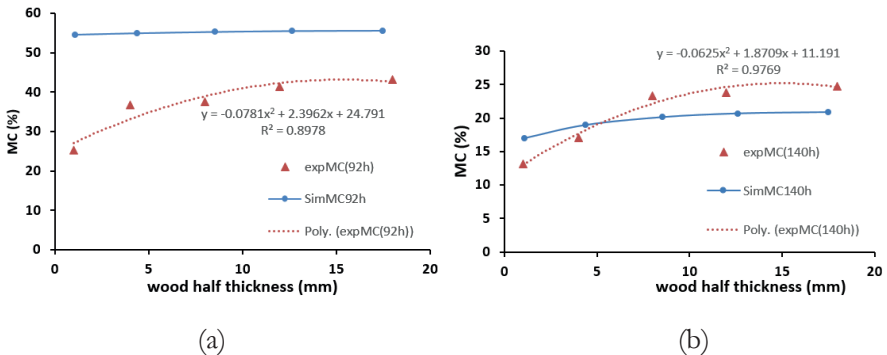


Figure 19. Comparison of experimental and simulated moisture profiles in pine wood: after 92 hours (a) and after 142 hours (b).

A comparison of experimental and simulated moisture profiles also supports the conclusions of the ESCR indicator. Figure 19, a shows the simulated and experimentally determined humidity profile at the 92nd hour, and Figure 19, b indicates the corresponding simulated and experimental moisture profile at the 140th hour. It can be seen that at the 92nd hour, according to the simulation, no drying occurs in the surface layer yet, but in the experiment, the surface layer has dried below FSP, i.e. wood MC is less than 27%. Thus, the surface layer begins to shrink, which is also indicated by the displacement sensor (Figure 17). Compared to the 92nd hour, both the simulated and experimental moisture profile are below FSP at the 140th hour, suggesting maximum simulated and experimental stresses.

6. DISCUSSION

Monitoring methods and calibration of wood moisture meters

Before preparing the calibration model, it is expedient to perform some simpler pre-processing on the sample of the collected test data. First of all, a solution to the problem of asymmetry in the number of measurement data should be found. The problem of asymmetry in the number of measurement data means that more than one value of the electrical variable may correspond to a value of the actual wood moisture content found by weighing. The reason is that electrical measurements are very fast, and thus a large number of high-quality (i.e. low-dispersed) electrical quantity measurements are generated for a single measurement of actual wood moisture content. A few examples of numerical asymmetry can be given.

E1. *Capacitance method for measuring the moisture content of wood* (Art. III). One measurement of actual moisture content of the wood corresponds to one measurement of the electrical capacitance of wood, so there is no asymmetry in the number of measurements.

E2. *Electrical polarization method for measuring the moisture content of wood* (Art. I and II). With this method, 200 measurement points correspond to one value of the actual moisture content of wood during a 20-second measurement period and a 0.1-second measuring interval, and additionally 200 measurement points of electric capacitance, so a total of 400 measurement points.

E3. *Impedance method for determining the moisture content of wood* (Art. III). With this method, 80 high-quality electrical quantities (i.e. 20 x real part of impedance + imaginary part of impedance + Bode phase angle + modulus or magnitude of impedance) correspond to one real value of wood moisture content at 20 selected frequencies in the impedance spectrum (Tomppo et al., 2011).

To smooth out the asymmetry of the measurement data, the arithmetic averaging of the measurement data of electrical quantities (Scantronik, 2023), selection of one variable in the model and ignoring the rest, defining an auxiliary variable, parametrization by modelling (Art. I and

II) may be used, and finally, one of the options is the use of rather clumsy multivariate statistical methods (Crawley, 2023) to deal with a large number of independent X variables. The pre-processing stage should necessarily include a descriptive statistics procedure for obtaining point estimates in each moisture group before the final calibration model for interval estimation is created. The pre-processing stage can turn out to be quite extensive. Therefore, it would be feasible to use data processing automation (see chapter 4.8).

This is followed by the creation of the final calibration model with the corresponding reliability bands using the linear or non-linear regression method. Finally, the reliability of the obtained regression method itself should be tested with visual methods (Q-Q plot and histogram) applied to the regression residuals, and also with non-parametric tests to quantitatively check the normal distribution hypothesis of the forecasted residuals (see chapter 4.8).

The calibration model is then validated. The most common is validation under repeatability conditions. Validation is less often used under reproduction conditions (Laaneots and Mathiesen, 2006). In repeatability conditions, the conditions of the calibration experiment are repeated 100%, but in reproduction conditions only partially. A common technique is to leave some test points out of the calibration model in order to later use these points to check the calibration function (Hans et al., 2013; Johansson et al., 2003). Another common technique is to recalculate experimental data using the calibration function or measuring function found using the calibration model. The result is a scatter plot with the actual wood moisture content values on the x-axis and the wood moisture content values predicted using the calibration function on the y-axis. Such a model was called a reference model in Articles (I) and (II), i.e. an application model of the calibration function. It should be mentioned that it is not possible to actually calibrate any measuring device using the reference model, but it is possible to evaluate the quality of the calibration procedure under repeatability conditions.

Using the individually calibrated pin electrodes, it is possible to monitor changes in wood moisture content at different depths from the surface, as well as temporal changes in the average wood moisture content. Moreover, the signal-to-noise ratio (SNR) achieved in previous studies is very good in the case of individual calibration, i.e. reaching over 10.

Unfortunately, a pin electrode calibrated using the dry weighing method of the resistance method loses its calibration when it is nailed to a new location in wood. The pin electrodes can be individually calibrated only after knowing the dry weighing data. Since in practice it is necessary to obtain accurate measurement results in real time during drying, the need for subsequent calibration should be waived in the future. The symmetrical properties of the wood charging number enable the creation of focusing calibration models, which significantly reduce the variability of the measurement results around the selected focus point. The novel calibration models with two independent variables based on the electrical wood charging number obtained by the PD method would require further research due to their great potential. In principle, the application of the obtained research results to the monitoring of the moisture content of growing trees is not prevented either (Yang et al., 2023).

The quality of the calibration model under repeatability conditions was assessed in this thesis using the Rozema criterion (Rcr). Alternatively, the quality of the calibration model can be evaluated based on the signal-to-noise ratio (SNR). The following qualitative discussion can be presented to compare the two assessment methods.

Rcr is a constant quantity, merely a numerical limit value beyond which the TI (tolerance interval) of a single measurement should not exceed at 95% reliability level. If, for example, it turns out that the total useful signal range is smaller above FSP (fibre saturation point) than at moisture contents below FSP, the signal-to-noise ratio will naturally deteriorate. This, in turn, also affects the predicted MC tolerance interval at moisture contents above FSP. When it comes to the numerical values of SNR, according to the data (Tamme, 2016), $SNR = 1.5$ means that the useful signal is 1.5 times greater than the noise. Such a situation may be statistically modelled, but the Rozema criterion cannot be fulfilled for a single measurement with such an SNR. However, it may turn out to be met in the case of measuring series consisting of 16 elements. Of course, if the standard error limit of the model does not occur. If $SNR \geq 10$, i.e. the useful signal exceeds the noise signal by ten or more times, then we can consider the Rcr fulfilled even by a single measurement without the need for repetitions. This fact is the reason why DECM needed a series of repeated measurements at moisture contents above FSP, but not below FSP (Table 2).

From Article (III): “In another paper (Johansson et al., 2003), an RMSEE of 12.52% MC was found for the high-frequency (9.375 GHz) capacitance method for above FSP, and of 0.74% MC for below FSP. This study found SE values that were very close to the RMSEE, as is shown in Table 2, formulas (27) and (28). Above FSP, the SE was 4.88% MC and below FSP the SE was 0.61% MC. Thus, below FSP the numerical data are comparable, but above the FSP range, the low-frequency capacitance method used in this study provides results that are twice as good as those achieved with the model residual error.”

The physical reason for the difference could be assumed to be the better homogeneity of the alternating electrical field in the parallel plate capacitor compared to the slot capacitor. A parallel plate capacitor was used in this thesis, but a slot capacitor was used in the study by Johansson et al., 2003.

In Table 1 (II, RM9), an auxiliary variable of the $f(R)+f(C)$ type was modelled as an example, which enabled a series of 16 repeated measurements to be replaced by a single measurement to fulfil the Rcr, and thus significantly save on the labour intensity of the measurements. It may be added as a comment that determining the functions $f(R)$ and $f(C)$ in turn requires six trial-and-error parameters, which are very labour-intensive (or even impossible) to determine manually. Solving such a task requires the presence of a special computer program.

As part of the discussion, firstly, operating reliability, and secondly, the calibration results should be analysed in connection with the impedance-type wood moisture meter. In the DECM and impedance measurement system, the alternating current strengths are of the same order of magnitude, about 2 nanoamps. One may ask why DECM is very sensitive to parasitic capacitance, and EIS is not. One possible explanation lies in the different surface area of the electrodes and its effect on parasitic capacitance. For EIS and other contact methods studied in this thesis, the area of one pin electrode was 47 square millimetres. The area of one plate for DECM was $150 \times 500 \text{ mm} = 75,000 \text{ mm}^2$, so the difference was 1,600 times. The parasitic capacitance of DECM determined by circle fit modelling was 680 pF. Therefore, when adjusting to pin electrodes, the parasitic capacitance of a pin electrode was about 0.4 pF. In the paper (Tamme et al., 2022), the capacitance of the pin electrode and the double layer of wood was found to be about 20 microfarads by means of modelling. This is $20 \times 10^6 \text{ pF}$. It is clear that the parasitic capacitance, which

is about a million times smaller, cannot affect the electrical capacitance of the double layer determined by the impedance method. Secondly, when calibrating the impedance meter as a wood moisture meter, the wood impedance modulus (13) was used as an electrical variable. In the comparison of the success of fulfilling the Rozema criterion, the results were to the detriment of the impedance method. The electrical variable impedance modulus was chosen according to an authoritative literature source (Tomppo et al., 2011). The result of the calibration of the impedance method leads to the thought that, in the future, it would not be practical to use some other electrical variable as an independent variable in the calibration model. The impedance spectrum provides a wide range of options for this.

Optimization of the wood drying process.

Traditionally, the drying process is divided on the basis of the drying curve into the first or constant-speed drying stage and the second, variable-speed drying stage (Lazarescu et al., 2010; Remond et al., 2007).

In this thesis, the drying process is also divided into the first and second stages according to the effective local diffusion coefficient, where the transition between the stages is clearly identifiable. The difference with the traditional division into stages is that special attention is paid to the surface layer of the wood, which makes up about 10% of the thickness of the material (EDG, 2010).

Paying special attention to the state of the surface layer of wood in drying experiments may cause some apparent contradiction between the experimental data and the TORKSIM simulation. In the subsection of the results, it was found that the surface layer begins to show all the signs of the transition from the first drying stage to the second drying stage. Firstly, the length of the base of the displacement sensor ($l = 120$ mm) begins to decrease, which indicates the beginning of shrinkage of the surface layer. Secondly, the difference between the temperature of the surface layer and the temperature of the middle part begins to increase (Figure 17). Thirdly, the moisture profile determined in the experiment at the 92nd hour does not match the simulated moisture profile (Figure 19). The simulated moisture profile shows a constant average MC (moisture content) of 60%, but the experiment shows the beginning of drying of the surface layer and the development of a parabolic moisture

profile in the cross section of the material. However, at the 140th hour, the simulation and the experiment both show the same average wood MC of 27%, and maximum drying stress in the wood. The displacement sensor shows an increase in the rate of base shrinkage at the 140th hour. In order to eliminate contradictions between the simulation and experiment, it should be assumed in the discussion that although the formation of stress in the surface layer starts indeed earlier (i.e. at the 92nd hour), numerically this so-called preliminary stress probably makes up a negligible part (estimated 5–10%) of the maximum stress at the 140th hour. After exceeding the maximum at the 140th hour, the stress starts to drop again (Figure 18).

In the course of discussion, it could be asked whether the moistening impulse applied in the second drying stage could return the surface layer of the wood to the first, constant-speed drying stage. Probably not. The physical reason is that the transition from the first stage of drying to the second stage is an irreversible process, i.e. the microstructure of the surface layer of the wood being dried has already been irreversibly changed, and the associated moisture transfer has irreversibly decreased. (Younsi et al., 2006; Kretschmann, 2010; Bergman, 2010).

“Input data generated by another mathematical model, such as the simulation program TORKSIM, may be used as an input for the commercial process optimization program StatEase Expert Composite Design v. 11. Thus, solving the task of optimizing the wood drying process would be done purely on the basis of theory, without using experimental data.” (Tamme et al., 2021c). In this thesis, however, such a solution to the wood drying optimization task was abandoned for the following reasons.

Firstly, the StatEase program requires constant drying modes in its input. Constant drying modes create unnecessarily high stress in the material to be dried in the initial phase of drying, and later waste drying time unnecessarily. Reasonable results from the point of view of stress were obtained only for thin (thickness up to 20 mm) spruce and pine material (Tamme et al., 2021c).

Secondly, if any simulation of the TORKSIM program turns out to be inconsistent with the drying experiment, StatEase takes it as a true result, and the result may be a false conclusion about the optimal region of the factors.

7. CONCLUSIONS

The hypotheses established in this thesis were confirmed.

The first hypothesis of measuring error compensability was confirmed. Indeed, it turned out that the random measuring errors in the wood moisture meter can be reduced either by increasing the number of measurements in the measurement series or by compensating for them in the composition of the two-variable function, using a special auxiliary variable. The result best modelled for the polarization-type moisture meter was characterized by achieving the same measurement accuracy in the model compensating for random measuring errors with a single measurement as with a series of 16 measurements in a traditional resistance-type moisture meter.

The second, operating reliability hypothesis was also confirmed. Indeed, the capacitance-type wood moisture meter had reliability problems in the climatic conditions of the wood kiln. Special experiments were used to find out the sources of the effects disturbing the reliability. These turned out to be the parallel electrical conductance channel formed on the main insulator of the measuring capacitor, and the parasitic capacitances formed on the plates of the capacitor, the origin of which could be either condensation of water vapour or triboelectric charges.

The third hypothesis about the critical diffusion coefficient was also confirmed. Indeed, when the limit of the critical diffusion constant is exceeded, changes in the moisture content of the surface layer spread from the surface layer of the wood to the inner layers. It was found that the advance-paced transition of the surface layer to the second stage of drying causes a decrease in the speed of the diffusion process in the inner layers of the wood as well. A peculiar semi-permeable moisture barrier is formed in the surface layer, which practitioners – kiln operators – also call ‘crust’. Without the semi-permeable moisture barrier in the surface layer, the potentially possible diffusion of water vapour in the inner layers would be many times faster.

The objectives set in the thesis were achieved.

The first objective of the moistening impulse response check was accomplished. Initially found only in simulated form, the response of the moistening impulse to the stress of the surface layer of wood was confirmed in further tests. The exception was the temperature sensors, which were practically insensitive to the moistening impulse.

The second objective for the development of specific sensors has been achieved. New wood surface moisture and wood surface displacement sensors have been developed and tested in the experiment, which withstand the climatic conditions of the wood kiln. Valuable work experience has been acquired in the installation and operation of sensors.

The third objective for the development of the maximum stress indicator has been achieved. An electrical indicator of wood stress has been developed in cooperation with five electrical resistance sensors placed at different depths. On the one hand, the resistance sensors were individually calibrated to monitor the moisture content of wood at different depths, and on the other hand, as an added value, the signal from the resistance sensors was used as an indicator of the maximum drying stress in the wood. It was found that feedback from the wood drying simulation program TORKSIM can be used to refine the indicator's mathematical formula (34) when it comes to pine or spruce wood. If it is a tree species for which there is no simulation program, the contraction rate of the base of the displacement sensor can be used as feedback. A sudden increase in this rate indicates maximum drying stress.

The fourth objective for the development of the moisture meter prototype has been achieved. The hardware capabilities of the moisture meter prototype corresponding to the patent description for collecting measurement information were improved. In the patent description, the moisture meter had only a potentiostatic (i.e. at constant voltage) charging mode. In addition, a constant current generator was added to the moisture meter and, in connection with it, also a galvanostatic (i.e. at constant current) charging mode. In the potentiostatic charging mode, charging voltages of 1.024 V and 0.124 V were used. In the galvanostatic charging mode, a constant charging current of 0.1 microamps was used. Secondly, a multiplexer switching block was added, with which it became possible to monitor the depolarization voltage as well. The possibility of depolarization voltage monitoring was not included in the patent description. With the addition of these two improvements, the collection

of high-quality measurement data was expanded by about four hundred measurement points in one location of the installation of measuring electrodes on wood.

In the study (Tamme et al., 2022), the theoretical background of the patented wood moisture meter prototype was expanded using ZView modelling. In the mentioned study, the focus was on modeling the effect of electrical charging of wood in the time domain and in the frequency domain, which occurs when measuring with a moisture meter.

The wood moisture meter developed in this PhD thesis for monitoring wood drying is basically also usable for monitoring the MC of growing trees (Yang et al., 2023). The moisture meter is small in size, battery-powered and connected to the Internet, enabling data storage, pre-processing and downloading via the Internet. In the future, it would be expedient to study the possibilities of using the polarization-type wood moisture meter developed in this PhD thesis for monitoring the MC of growing trees.

Recommendations for practical wood drying.

In this thesis, the relative humidity value of the critical drying air corresponding to the critical diffusion constant for pine wood was found. It is easy for a timber company to use this information to modify its drying schedules on site.

Technology companies producing control automatics for wood kilns could be recommended for prototyping the sensors monitoring surface moisture and surface deformation developed as part of this PhD thesis, as well as the dielectric capacitance-type sensor (DECM) for the average moisture content of wood.

A significant number of licenses for the wood drying simulation program TORKSIM have been sold in three Baltic countries. This PhD thesis allows a timber company using TORKSIM to navigate the complex mathematical model of the program, as well as to receive practical feedback on the strengths and weaknesses of the program.

A still unsolved problem in practical wood drying is the quick, non-destructive and reliable determination of the average moisture content

of a wood batch immediately before starting the kiln for the wood drying simulation program, as well as for checking the readings of the screw sensors of the kiln itself when drying is started. A dielectric capacitance-type sensor for the average moisture content of wood developed during the project would be suitable for this task. Probably, the DECM reliability issues discussed in this PhD thesis will not be so acutely apparent before the drying is started, i.e. when making measurements at normal room temperature and humidity.

In summary, it can be said that the hypotheses raised in this thesis were confirmed. All the objectives set out in the thesis were fulfilled.

REFERENCES

- Ahlborn Mess- und Regelungstechnik GmbH.
https://www.ahlborn.com/de_DE/produkte/materialfeuchtegeber,
(Accessed: 06.03.2023).
- Aicholzer, A., Schuberth, C., Mayer, H., Arthaber, H. 2018. Microwave testing of moist and oven-dry wood to evaluate grain angle, density, moisture content and the dielectric constant of spruce from 8 GHz to 12 GHz. *Eur. J. Wood Prod.* 76, pp. 89–103.
- Bard, A. J., Faulkner, L. R. 1980. *Electrochemical methods: Fundamentals and applications*, 1st ed.; John Wiley & Sons: New York, 1980, 864 pp.
- ASTM D4444-08. 2008. Standard Test Method for Laboratory Standardization and Calibration of Hand-Held Moisture Meters, *Annual Book of ASTM Standards*, ASTM International, West Conshohocken, PA, 10 pp.
- Bes Bollmann® Drying and Control Systems, <https://www.bes-bollmann.com>, (Accessed: 06.03.2023).
- Berga S. C., Gil R. G., Anton A. E. N., Muñoz A. R. (2019) Novel Wood Resistance Measurement Method Reducing the Initial Transient Instabilities Arising in DC Methods Due to Polarization Effects. *Electronics*, 8:1253 <https://www.mdpi.com/2079-9292/8/11/1253/htm>, (Accessed 25.04. 2023).
- Bergman, R. 2010. *Drying and Control of Moisture Content and Dimensional Changes*. Wood Handbook, General Technical Report No. FPL-GTR-190, Forest Service, Forest Products Laboratory, U. S. Dept. of Agriculture, Madison, WI, 2010, 20 pp. http://www.fpl.fs.fed.us/documnts/fplgtr/fplgtr190/chapter_13.pdf, (Accessed 13.04.2023).
- Björngrim, N., Fjellström, P.-A., Hagman, O. 2017. Resistance measurements to find high moisture content inclusions adapted for large timber bridge cross-sections. *BioResources* 2017 12:3570–3582.
- Brischke, C., Rapp, A. O. 2008. Influence of wood moisture content and wood temperature on fungal decay in the field: observations in different micro-climates. *Wood Sci Technol* 2008 42:663–677.

- Boardman, C. R., Glass S. V., Carll, C. G. 2011. Moisture Meter Calibrations for Untreated and ACQ- Treated Southern Yellow Pine Lumber and Plywood. *Journal of Testing and Evaluation* 40(1): 1–10.
- Brookhuis Micro- Electronics BV. 2009. Moisture measuring manual Version 1.4, 27 pp.
- Cai, Z., 2008. A new method of determining moisture gradient in wood. *Forest Products Journal* 58, 41–45.
- Chaumat G., Vedel E., Diard J. P., Le Correc P. 1999 Interest of Electrical Impedance Measurement for Monitoring the Controlled Air-drying of Waterlogged Archaeological Wooden Wrecks. 6th. International Conference on „non-Destructive Testing and Microanalysis for the Cultural and Environmental Heritage“ Rome, May 17–20, 1999, pp. 1387–1398.
- Class, S.V., Zelinka, S. L. 2010. Wood Handbook, Chapter 04. Moisture Relations and Physical Properties of Wood. General Technical Report FPL-GTR-190. Madison, WI: U.S. Department of Agriculture, Forest Service, Forest Products Laboratory, Madison, WI, USA, 19 pp.
- Cole K. S. and R. H. Cole. 1941 Dispersion and absorption in dielectrics I: Alternating current characteristics. *J. Chem. Phys.* 9: 341–351.
- Crank, J., 1956. *The Mathematics of Diffusion*, Clarendon Press, Oxford, 347 pp.
- Crawley, M.J. *The R Book*. John Wiley and Sons Ltd. 942 pp.
- Danvind, J. 2005. Analysis of drying wood based on non-destructive measurements and numerical tools. Doctoral thesis. Luleå University of Technology, 124 pp.
- Debye P. 1945 *Polar Molecules*. Dover Publications, New York, 172 pp.
- Eco Chemie, Metrohm Autolab B. V. 2019, <https://www.metrohm.com>, (Accessed 27.04.2023).
- Eco Chemie, Metrohm Autolab B. V. 2019a., <https://www.metrohm.com/en/applications/>, (Accessed 13.04.2023).
- E.D.G., 1992. Recommendation on Assessment of Drying Quality of Timber, European Drying Group, Hamburg-Germany.
- EDG. 2010. Dried Timber- how to specify correctly. Editor: Johannes Welling, European Drying Group (EDG) and COST E53 2010, 38 pp.

- Edwards, N. C. 1974. Procedure for the Determination of Species Correction Data for Electrical Resistance Type Moisture Meters. CSIRO Div. Forest Products. (Unpublished divisional report), 10 pp.
- EN 13183-2:2005. 2005. Moisture content of a piece of sawn timber – Part 2: Estimation by electrical resistance method, 6 pp.
- EN 13183-3:2005. 2005. Moisture content of a piece of sawn timber – Part 3: Estimation by capacitance method, 10 pp.
- EVS 758:2009. Metroloogia. Terminid ja määratlused. Tallinn: Eesti Standardiamet 2009, 14 pp.
- Feutron Klimasimulation GmbH. 2021, <https://www.feutron.de/en/weathering-chamber/>, (Accessed 13.04.2021).
- Fick, A., 1855. Ueber Diffusion. Ann. Physik. Chemie, 94, 59–91
- Fredriksson, M., Vadso, L., Johansson, P. 2013. Small resistive wood moisture sensors: a method for moisture content determination in wood structures. Eur. J. Wood Prod. 71: 515–524
- Forsén, H., Tarvainen, V. 2000. Accuracy and functionality of hand-held wood moisture content meters. VTT (Espoo 2000), VTT Publications 420: 102 pp. <http://www.vtt.fi/inf/pdf/publications/2000/P420.pdf>, (Accessed 13.04.2023).
- Gann Mess-u Regeltechnik GmbH. <http://www.gann.de>, (Accessed 13.04.2023).
- Gao, S., Bao, Z., Wang, L., Yue, X. 2018. Comparison of Voltammetry and Digital Bridge Methods for Electrical Resistance Measurements in Wood. Computers and Electronics in Agriculture, 145: 161–168.
- Hans G., Leblon B., Stirling R., Nader J., Cooper, P. Larocque A. 2013. Use of a portable near infrared spectrometer for Populus Sp. log moisture content and basic specific gravity prediction and log sorting. Proceedings 18 th. International Nondestructive testing and Evaluation of Wood Symposium. Madison, Wisconsin, USA, september 24–27 2013, pp. 163–170.
- Higgins, N. C. 1957. The EMC of selected native and foreign woods. Forest Product Journal 7(10): 371–377.
- Hukka, A. 1999. The effective diffusion coefficient and mass transfer coefficient of Nordic softwoods as calculated from direct drying experiments. Holzforschung, 53, 534–540 <https://doi.org/10.1002/andp.18551700105>.

- ISO 3130:1975. 1975. Wood – Determination of moisture content for physical and mechanical tests. International Organization for Standardization, Switzerland, 2 pp.
- ISO 3534-1:1993. 1993. Statistics – Vocabulary and symbols – Part 1: Probability and general statistical terms. Geneva: International organisation for standardization. 105 pp.
- ISO/IEC 17025:1999 General requirements for the competence of testing and calibration laboratories, Geneva:ISO/IEC 1999. 26 pp.
- ISO/IEC, 2008 GUIDE 98-3:2008(E) uncertainty of measurement-part 3: guide to the expression of uncertainty in measurement (GUM:1995). International Organisation for Standardization, Geneva, 120 pp.
- James, W. L. 1975. Dielectric properties of wood and hard-board: Variation with temperature, frequency, moisture content, and grain orientation.- Research Paper FPL 245. USDA Forest Prod. Lab. Madison, WI, 35 pp.
- James, W. L. 1988. Electric moisture meters for wood, General Technical Report No. FPL-GTR-6, U. S. Dept. of Agriculture, Forest Service, Forest Products Laboratory, Madison, WI: 19 pp. <http://www.fpl.fs.fed.us/documnts/fplgtr/fplgtr06.pdf>, (Accessed 13.04.2023).
- James, W. L., Yen Y.-H., King R. J. 1985 A Microwave Method for Measuring Moisture Content, Density and Grain Angle of Wood. United States Department of Agriculture 1985, <http://www.treesearch.fs.fed.us/pubs/5792>, (Accessed 13.04.2023).
- James, W. L. 1993. In: Fundamentals of hand held moisture metes: An outline.- Proceedings. ASTM Hand Held Moisture Meter Workshop, Madison, WJ, Forest Product Society, 5 May1993, 13–16.
- Johansson, J., Hagman, O., Oja, J. 2003. Predicting moisture content and density of Scots pine by microwave scanning of sawn timber. Computers and Electronics in Agriculture, 41, 85–90.
- Kawamoto S. and Williams R. S. 2002. Acoustic Emission and Acousto-ultrasonic Techniques for Wood and Wood-based Composites, review. USDA Gen. Tech. Rep. FPL- GTR-134. 16 pp. <http://www.treesearch.fs.fed.us/pubs/9730>, (Accessed 13.04.2023).
- Krause, S. 2003. In: A. J. Bard, M. Stratmann (Eds.), Encyclopedia of Electrochemistry, vol. 3, Wiley, New York, 196 – 229.

- Keey R. B., Langrich T. A., Walker J. C. F., 1999. Kiln Drying of Lumber. Springer, 331 pp.
- Keithley Instruments & Products.2023, <https://www.tek.com/en/products/keithley>, (Accessed 13.04.2023).
- Keithley 2004. Low Level Measurements Handbook 6th Edition, 239 pp. <http://web.mit.edu/8.13/8.13d/manuals/LowLevMsHandbk.pdf>, (Accessed: 13.04.2023).
- Kiviste, A. 1999. Matemaatiline statistika MS Excel keskkonnas (Mathematical Statistics in MS Excel Environments). Tallinn, GT tarkvara OÜ, 86 pp.
- Kretchetov, I. V. 1972. Kiln Drying. Moscow, 440 pp. (in Russian).
- Kretschmann, D. E. 2010. Wood Handbook, Chapter 05. Mechanical Properties of Wood. General Technical Report FPL-GTR-190. Madison, WI: U.S. Department of Agriculture, Forest Service, Forest Products Laboratory, Madison, WI, USA. 41 pp.
- Laaneots R, Mathiesen O 2006 An introduction to metrology. TUT Press, Tallinn, 271 pp.
- Lamason C., MacMillan B., Balcom B., Leblon B. Pirouz Z. 2013. Log moisture content determination with quantitative magnetic resonance and magnetic resonance imaging. Proceedings 18 th. International Nondestructive testing and Evaluation of Wood Symposium. Madison, Wisconsin, USA, september 24–27, 2013, pp. 186–195.
- Lazarescu, C., Avramidis, S., Oliveira, L.2010. Shrinkage response to tensile stress during hemlock (*Tsuga heterophylla*) drying.- In: 11th International IUFRO Wood Drying Conference, Skellefteå, Sweden, 2010.- Proceedings: International IUFRO Wood Drying Conference, 2010, 122–130.
- Li, H., Perrin, M., Eyma, F., Jacob, X., Gibiat, V. 2018. Moisture content monitoring in glulam structures by embedded sensors via electrical methods. Wood Sci Technol 2018 52:733–752.
- Luikov, A. V., 1966. Heat and mass transfer in capillary-porous bodies. Pergamon Press, 523 pp.
- Lyons Jr. W.F., Riffles La., Hudson M. A., Lessard R. 2004. Dielectric wood moisture meter. Patent No.: US 6,708,551 B1 Mar. 23, 2004, 9 pp.

- Magill, R. 2010. Calibration and metering methods for wood kiln moisture measurement. Patent No.: US 7,676,953 B2 Mar. 16, 2010, 49 pp.
- Mannes D., Sonderegger W., Hering S., Lehmann E., Niemz P. 2009
Non-destructive determination and quantification of diffusion processes in wood by means of neutron imaging. *Holzforschung* 63: 5, 589–596.
- Martin, T. 2012. Complex resistivity measurements on oak. *Eur. J. Wood Prod.* 2012 70: 45-53.
- MatLab™ (MathWorks, Natic, MA). 2023, <https://se.mathworks.com/products/matlab.html>, (Accessed 13.04.2023).
- McIlroy, M. D., et al. “Unix Time-Sharing System: Foreword.” *Bell System Technical Journal*, vol. 57, no. 6, 1978, pp. 1899–1904., <https://doi.org/10.1002/j.1538-7305.1978.tb02135.x>
- Moschler, W. W. 2004. Wireless Microwave Wood Moisture Measurement System for Wood Drying Kilns. Final Technical Report, University of Tennessee, 18 pp.
- Mändoja, M. 2015. Wood drying simulation „TORKSIM“ adjusting to actual industrial drying curve in order to improve the reliability of tension calculations and electrical humidity sensors. Bachelor thesis. Estonian University of Life Sciences. Tartu, 51 pp.
- Norberg, P. 1999. Monitoring wood moisture content using the WETCORR method. *Holz als Roh- und Werkstoff*, V. 57: 448 – 453 http://c.ymcdn.com/sites/www.nibs.org/resource/resmgr/BEST/BEST1_005.pdf
- Norberg. P. 2000. Monitoring wood moisture content using the WETCORR method part 2: calibration and validation. *Holz Roh Werkst* 2000 58:129–134
- NIST/SEMATECH e-Handbook of statistical methods, 2018, 898 pp.
- NN-Tool - Neural Network Simulator for Process Industries and Chemical Engineering, http://www.nntool.de/Englisch/index_engl.html, (Accessed 13.04.2023).
- Onysko, D. M., Schumacher, C., Garrahan, P. 2008. Field Measurement of Moisture in Building Materials and Assemblies: Pitfalls and Error Assessment.- Best 1 Conference – Building Enclosure Science& Technology, Minneapolis, June 10–12, 2008.

- Poljakov, A. 2013. Wood material comparison of actual moisture content monitoring data in wood dryer „Mühlböck“ and „Hekotek“. Master Thesis. Estonian University of Life Sciences. Tartu, 125 pp.
- Ressel, J. B. 2006. Fundamentals of Wood Moisture Content Measurement. Cost E53, Training School, 17. 10 pp. http://www.coste53.net/downloads/TrainingSchool/1stTraining_School/1st_COST_E53_Training_School-all.pdf, (Accessed 13.04.2023).
- Rémond, R., Passard, J., Perré, P. 2007. The effect of temperature and moisture content on the mechanical behaviour of wood: a comprehensive model applied to drying and bending. *European Journal of Mechanics A/ Solids* 26, 558–572
- R-projekt. The R Project for Statistical Computing, <http://www.r-project.org>, (Accessed 13.04.2023).
- Romann, T., Oll, O., Pikma, P., Tamme, H., Lust, E. (2014).s Surface Chemistry of Carbon Electrodes in 1-Ethyl-3-methylimidazolium Tetrafluoroborate Ionic Liquid: An In situ Infrared Study. *Electrochimica Acta* 125: 183–190.
- Rozema, P. 2010. Do's and don'ts in respect to moisture measurement. In: „The Future of Quality Control for Wood&Wood Products“, 4 – 7th May 2010, Edinburgh. The Final Conference of COST Action E 53: 9 pp. <http://www.coste53.net/downloads/Edinburgh/Edinburgh-Presentation/72.pdf>, (Accessed 13.04.2023)
- Sachs, L. 1982 *Applied Statistics: A Handbook of Techniques*. New York, 706 pp.
- Scantronik Mugrauer GmbH. www.scantronik.de, (Accessed 13.04.2023).
- Salin, J. G. 1990. Simulation of the timber drying process. Prediction of moisture and quality changes. Doctoral thesis. EKONO Oy, Helsinki, Finland, 103 pp.
- Salin, J. G. 2007. Lectures. Riga, 2007, <http://www.coste53.net/downloads/WG2/WG2-Riga/Lectures/Riga2007-Salin.pdf>, (Accessed 22.04.2023).
- Siau, J. F. 1984. *Transport processes in wood*. Springer Verlag, 245 pp.
- Skaar, C. 1964 Some Factors Involved in the Electrical Determination of Moisture Gradients in Wood. *Forest Products Journal*. 14(6): 239–244.

- Skaar, C. 1988. Electrical properties of wood. In: Skaar C (ed) Wood–water relations. Springer, Berlin 1988.
- Stamm, A.J. 1927. The Electrical Resistance of Wood as a Measure of Its Moisture Content. *Industrial & Engineering Chemistry* 19, 1021–1025. <https://doi.org/10.1021/ie50213a022>
- Siau, J. F. 1984. Transport processes in wood. Springer Verlag, 245 pp.
- Schuetze A. P., Lewis W., Brown C., Geerts W. J. 2004. A laboratory on the four – point probe technique. *Americal Journal of Physics*, Vol. 72, No 2, p. 149–153.
- Sova, D., Bedeleian, B. and Sandu, V. 2016. Application of Response Surface Methodology to Optimization of Wood Drying. *Baltic Forestry*, 22(2): 348-356.
- Straube, J., Onysko, D., Schumacher, C. 2002. Methodology and Design of Field Experiments for Monitoring the Hydrothermal Performance of Wood Frame Enclosures.- *Journal of Thermal Envelope and Building Science*, V. 26, No. 2, 123–151.
- Sumner J. S. 1976. Principles of induced polarization for geophysical exploration. Elsevier Scientific Publishing Company, Amsterdam, 277 pp.
- Tamme, V., Muiste, P., Polyachenko, R., Tamme, H. 2010. Determination of Dynamics of Moisture content, Temperature and Mechanical Stress of Pine Wood During Convective Drying. *Proceedings of 11th International IUFRO Wood Drying Conference*, Skellefteå, Sweden, 2010: 147–154.
- Tamme, V., Muiste, P., Mitt, R., Tamme, H. 2011. Determination of Effective Diffusion Coefficient and Mechanical Stress of Pine Wood During Convective Drying.- *Baltic Forestry*, V. 17, 110–118.
- Tamme, V., Muiste, P., Kask, R., Padari, A., Tamme, H. 2012. Experimental study of electrode effects of resistance type electrodes for monitoring wood drying process above fibre saturation point. *Forestry Studies*, 56, 42–55. DOI: 10.2478/v10132-012-0004-6.
- Tamme, V., Kask, R., Muiste, P., Tamme, H. 2012a. Comparison of wood moisture meters in extended measuring range. *Proceedings of 14th Conference “Investigation and Usage of Renewable Energy Sources”*, Tartu, Estonia, 2012: 98–108.

- Tamme, H. 2013. Process management framework on the example of convective drying of wood and spectroelectrochemistry. MSc. Thesis, University of Tartu, Tartu, 25 pp.
- Tamme, V., Muiste, P., Tamme, H., 2013. Experimental study of resistance type wood moisture sensors for monitoring wood drying process above fibre saturation point / Takistus-tüüpi puidu niiskuse andurite eksperimentaalne uurimine puidu kuivatamise monitooringul niiskussisaldustel üle kiu küllastuspunkti. *Forestry Studies* 59, 28–44. <https://doi.org/10.2478/fsmu-2013-0009>.
- Tamme, V., Muiste, P., Padari, A., Tamme, H. 2014. Modelling of Resistance-Type Wood Moisture Meters for Three Deciduous Tree Species (Black Alder, Birch, Aspen) in Moisture Contents Above Fibre Saturation Point. *Baltic Forestry*, 20 (1): 157–166
- Tamme, V. Development of resistance-type control methods for wood drying. PhD thesis, 2016, 135 pp.
- Tamme, H., Tamme, V., Kask, R., Muiste, P. 2019. Non-destructive dielectric method for determining the moisture content of newly sawn timber for moisture content above FSP. *Proceedings: 21st International Nondestructive Testing and Evaluation of Wood Symposium.: 21st International Nondestructive Testing and Evaluation of Wood Symposium, Freiburg, Germany, 2019*. Ed. Wang, Xiping, Sauter, Udo H., Ross, Robert J. Forest Research Institute Baden-Württemberg, pp. 213–224.
- Tamme V, Tamme H, Bernotas T, Muiste P, Olt J 2020 Moisture meter and method for measuring the moisture content of wood above the fibre saturation point of a wood with the electric charging effect. Patent No EE 05822B1 Priority: 16. 07. 2018.
- Tamme, V., Tamme, H., Miidla, P., Muiste, P., 2021. Novel polarization-type moisture meter for determining moisture content of wood above fibre saturation point. *European Journal of Wood and Wood Products* 79, 1577–1587. <https://doi.org/10.1007/s00107-021-01682-6>.
- Tamme, H., Kask, R., Muiste, P., Tamme, V., 2021a. Comparative testing of two alternating current methods for determining wood moisture content in kiln conditions. *Forestry Studies* 74, 72–87. <https://doi.org/10.2478/fsmu-2021-0005>.

- Tamme, H., Muiste, P., Tamme, V. 2021b. Optimizing the pine wood drying process using a critical diffusion coefficient and a timed moistening impulse. *Forestry Studies*, 75, 150–165.
- Tamme, V., Tamme, H., Muiste, P. 2021c. Puidu konvektiivkuivatuse (kamberkuivatus ja tunnelkuivatus) kvaliteedi ja energiakulu optimeerimise eksperimentaalse ja teoreetilise meetodika välja töötamine. KIK metsanduse programmi projekt nr. 16200 lõpparuanne. (in Estonian), 44 pp. <https://mi.emu.ee/userfiles/instituudid/mi/MI/Projektid/Projekt1620.pdf>, (Accessed 22.04.2023).
- Tamme, V., Jänes, A., Romann, T., Tamme, H., Muiste, P., Kangur, A. 2022. Investigation and modeling of the electrical charging effect in birch wood above the fiber saturation point (FSP). *Forestry Studies* 77, 21–37. DOI: 10.2478/ismu-2022-0010.
- Tiitta, M., Savolainen, T., Olkonen, H., Kanko, T. 1999. Wood Moisture Gradient Analysis by Electrical Impedance Spectroscopy. *Holzforschung* 53: 68 d–76.
- Tiitta, M., Tomppo, L., Lappalainen, R. 2010. Combined method for monitoring wood drying process. In: *Proceedings of 11th International IUFRO Wood Drying Conference*, 18 th – 22 January, Skellefteå, Sweden, pp. 76–80.
- Tomppo, L., Tiitta, M., Laakso, T., Harju, H., Venäläinen, M., Lappalainen, R. 2011. Study of stilbene and resin acid content of Scots pine heartwood by electrical impedance spectroscopy (EIS). *Holzforschung*, 65, 643–649.
- Tsotsas, E. and Mujumdar, A. S. (eds.) 2014. *Modern Drying Technology*. Vol. 1 – 5, WILEY-VCH Verlag GmbH & Co.
- Tremblay, C., Cloutier, A., Fortin, Y. 2000. Experimental determination of the convective heat and mass transfer coefficients of wood drying. *Wood Science and Technology*, 34, 253–276.
- Tronstad, S., Sandland, K., Toverød, M. & H. 2001. Drying quality of softwood based on 140 industrial tests in Norwegian sawmills and actions to improve the quality.- In: *Paper 3rd Workshop on softwood drying to specific end-uses,- COST Action E15, Advances in the drying of wood (1999-2003)*. VTT Building and Transport, Espoo, Finland, 11.-13. June 2001. 13 pp.

- Urban J., Bequet R., Mainiero R. 2011 Assessing the applicability of the earth impedance method for in situ studies of tree root systems. *Journal of Experimental Botany*, 62(6): 1857–69, <http://www.ncbi.nlm.nih.gov/pubmed/21273337>, (Accessed 28.04.2023).
- Uwizeyimana, P., Perrin, M., Eyma, F. 2020. Moisture monitoring in glulam timber structures with embedded resistive sensors: study of influence parameters. *Wood Science and Technology*, 54, 1463–1478.
- Vermaas, H. F. 1975. Experimental variables affecting the measurement of the DC resistance of wood. *Holzforschung. Int J Biol Chem Phys Technol Wood* 1975 29:140–144
- Vermaas, H. F. 2002. State of the Art and Latest Technological Advances in the Drying of Fast- grown Eucalyptus.- In: 4th COST E 15 Workshop „Methods for Improving Drying Quality of Wood“ 30-31 May 2002, Santiago de Compostela, Spain, 17 pp.
- Vikberg, T., Oja J., Antti, L. 2012. Moisture content measurement in scotts pine by microwave and X- rays. *Wood and fiber science*, vol.44, issue:3, 280-285
- Vikberg, T., Hansson, L., Schajer, L., Gary, S. et al. 2012a. Effect of microwave measurements and simulations when collecting data close to edges of wooden boards. *Measurement*, 45:(3), 525–528
- Wavetek Meterman. 2021, <https://www.tequipment.net/WavetekMetermanLCR55.html>, (Accessed 13.08.2021)
- Wenner F. 1915. A method of measuring earth resistivity. *Bur. Stand. (U.S.) Bull.* 12, 469 – 478.
- White R. B., Schimleck L. R., Anthony F., Daniels R. F. 2019. Exploration of Seasonal Moisture Variation in Standing Loblolly and Slash Pine using Time domain Reflectometry. *European Journal of Wood and Wood Products*. 77: 1045–1052.
- Yang, Z., Wu, Y., Liu, Y. A. Wireless Acoustic Emission Sensor System with ACMD-IGV-XGBoost Algorithm for Living Tree Moisture Content Diagnosis. *Plants* 2023, 12, 601. <https://doi.org/10.3390/plants12030601>
- Younsi, R., Kocaeffe, D., Poncsak, S., Kocaeffe, Y., 2006. A diffusion-based model for transient high temperature treatment of wood. *Journal of Building Physics*. 30, 113-134

- Zelinka, S. L., Stone, D. S., Rammer, D. L. 2007. Equivalent circuit modeling of wood at 12% moisture content.- *Wood and Fiber Science*, V. 39(4), 556–565.
- Zelinka, S.L., Rammer, D.R., Stone, D.S. 2008. Impedance spectroscopy and circuit modelling of Southern pine above 20 % moisture content. *Holzforschung*, 2008 62, 737–744.
- Zuleta, M. 2005. Electrochemical and ion transport characterisation of nanoporous carbon derived from SiC. – Doctoral thesis. Stockholm, KTH-Royal Institute of Technology, Department of Chemical Engineering and Technology. 85 pp. <http://www.diva-portal.org/smash/record.jsf?pid=diva2%3A7694&dswid=-1261>, (Accessed 13.04.2023).

SUMMARY IN ESTONIAN

PUIDU KUIVATUSE KONTROLLI JA OPTIMEERIMISE MEETODITE ARENDAMINE

Sissejuhatus

Puidu kuivatamise eesmärgiks on saada soovitud lõppniiskusega materjali. Protsessi käigus on vaja leida tasakaal puidu kvaliteedi, kulutatud energia ning aja vahel. Optimaalse lahenduse leidmiseks on oluline teada millises seisus on konkreetsel ajahetkel kuivatatav materjal. Laialdaselt kasutusel olevates kamber-tüüpi konvektiivkuivatites toimub puidu kuivatamine turbulentsel kuivatusõhu vahendusel. Puidukuivatuse monitooringuks kasutatakse praktikas valdavalt elektrilist takistusmeetodit (Tronstad et al., 2001; Onysko et al., 2008; Björngrim et al., 2017; Bes-Bollmann 2023), vähem mahtvusmeetodit (Moschler 2004; Magill 2010; Lyons Jr. et al., 2004) ja impedantsi meetodit (Tiitta et al., 2010).

Uurimuse peamised hüpoteesid olid järgmised:

- Puidu niiskussisalduse mõõtevead on kompenseeritavad mõõtmiste arvu suurendamise või sobiva kalibreerimise funktsiooni valikuga (I, II).
- Mahtvusmeetodil tekivad töökindluse probleemid puidukuivati kliima tingimustes (III).
- Kriitilise difusioonikonstandi ületamisel hakkab puidu pinnakihi kuivamisprotsess mõjutama ka puidu sisemisi kihte (IV).

Väitekirja eesmärgid olid järgmised:

- Kontrollida kas teoreetiliselt simuleeritud niisutusimpulsi reaktsioon ilmneb ka katses, tuginedes sünkroonselt pinna nihke-, temperatuuri-, ja pinnaniiskuse andurile (IV).
- Töötada välja monitooringuks spetsiifilised andureid mis on kasutatavad puidukuivati kliimas (I, II, III).
- Töötada välja puidukuivatuse pingete maksimumi elektriline indikaator (IV).
- Täiustada patendikirjeldusele vastava niiskusmõõtuuri prototüübi riistvara (I, II).

Sageli ei piisa tööstusliku puidukuivati standardvarustusest uue kuivatusplaani juurutamisel. Lisaks on vaja puidu kuivatamist simuleerivat tarkvara, mis annab esialgse kuivatusrežiimi, mida saab edasi optimeerida, kasutades käesolevas töös toodud meetodikaid ja andureid. Puidu kuivatuse simulatsiooni programmi TORKSIM võib pidada samuti üheks puidu kuivamise pingete kontrolli meetodiks.

Materjal ja meetodika

Nõuetekohaselt ette valmistatud puitmaterjalist katsekehad on vajalikud nii laboratoorsete kuivatuskatsete läbiviimiseks (IV) kui ka erineva tööpõhimõttega puidu niiskussisalduse andurite kalibreerimiseks (I–III).

(IV) Laboratoorse kuivatuse katsetes kasutati kolme samast materjalist lõigatud männi maltspuidu katsekeha paksusega 35 mm, laiusel 150 mm ja pikkusega 100 mm puidu kiudude sihis. Esimesele katsekehale olid paigutatud joonisel kujutatud elektroodid.

(I–III) Erinevat tüüpi puidu niiskuse mõõtmise katsetes kasutati katsekehadena kaselauda ja lepalauda paksusega 35 mm, laiusel 150 ja pikkusega 470 mm.

Puidu niiskuse mõõtmise kalibreerimise meetodika oli alljärgnev.

Kalibreerimise katsekeha keskmist niiskussisaldust (NS) varieeriti spetsiaalse kuivamisplaaniga kuivatamise meetodil. Ühemõõtmelise niiskusgradiendi saamiseks katsekehas radiaalsuunas oli niiskuslevi katsekehas pikikiudu hoolikalt tõkestatud. Igal katsekeha keskmise NS tasemel tehti 21–26 kordsmõõtmist mõõte-elektroodide erinevas juhuslikult valitud asukohas katsekehal. Mõõte-elektroodide naelutamise sügavus valiti vastavalt standardile (EN 13183-2) 1/3 materjali paksusest.

(IV) Puidukuivatuse protsessis puidu NS registreerimiseks kuivatatava laua pinnast erinevatel sügavustel kasutati individuaalselt kalibreeritud süsinikkiud nõel-elektroode. Süsinikkiud valiti elektroodide materjaliks korrosioonikindluse tõttu.

Kalibreerimismudelite koostamiseks vajalik statistiline analüüs viidi läbi vastavalt metroloogia standardile (ISO/IEC GUIDE 98-3:2008(E), 2008).

Statistiline modelleerimine viidi läbi programmide R (R-project), MATLAB (MathWorks, Natic, MA) ja MS Excel (Kiviste, A., 1999) keskkonnas. Modelleerimise tulemuste hindamiseks kasutati Studenti teoreetilisel jaotusel (Sachs, 1982) põhinevat tolerantsi intervalli üksikmõõtmise jaoks ja selle põhjal defineeritud Rozema kriteeriumi. Lisaks kasutati modelleerimise tulemuste hindamiseks determinatsioonikordajat R^2 ja olulisustõenäosust $p < 0.01$. Regressioonimudelite jääkide normaaljaotuse hindamiseks kasutati visuaalseid meetodeid, nagu Q-Q plot ja histogram. Täpsemaks jääkide normaaljaotuse hindamiseks kasutati Kolmogorov-Smirnovi ja Shapiro Wilki mitteparameetrilisi teste.

Tulemused ja arutelu

Rozema (2010) kriteeriumid (I–III) on välja töötatud takistus-tüüpi puidu niiskusemõõtjate kalibreerimise mudeli headuse hindamiseks. Kriteeriumid on niiskusemõõtjate kalibreerimise eksperimendi tulemuste üldistamiseks, võrdlemiseks ja piiritlemiseks. Sisuliselt on tegemist kalibreerimismudeli tolerantsi intervalli (II) laiusega üksikmõõtmise jaoks 95% usaldusnivool, teoreetilise Studenti jaotuse eeldusel. Rozema kriteerium (Rcr) sätestab, et üksikmõõtmise tolerantsi intervall ei tohiks olla laiem kui 3.5% NS. Rozema kriteerium sobib mitte ainult takistus-tüüpi puidu niiskusemõõtjate kalibreerimise mudelite hindamiseks, vaid ka erinevatel tööprintsüüpidel (mahtuvus-tüüpi, polarisatsioon-tüüpi, impedants-tüüpi jne) töötavate puidu niiskusemõõtjate kalibreerimismudelite võrdlemiseks. Rozema kriteerium on küllaltki range. Üle kuu küllastuspunkti (above FSP) niiskussisaldustel on seda üksikmõõtmise jaoks küllalt keeruline täita. Erandiks osutus polarisatsioon-tüüpi puidu niiskusemõõtja, kus kriteeriumi üksikmõõtmise jaoks õnnestus täita suhteliselt piiratud NS vahemikus (Table 1.). Sellepärast võeti Rozema kriteeriumi täitmiseks modelleerimisel appi valimi baasil mõõteseriaate moodustamine. Mõõteseriaatena kasutati 16 üksikmõõtmisest koostatud mõõteseria aritmeetilisi keskmisi, kusjuures edasisel modelleerimisel käsitleti sel viisil moodustatud keskmisi üksikmõõtmistena. Sellist mudelit nimetati mitmeseks mudeliks (*multiple model*) perioodiga $k=16$ (Table 1. , Table 2).

Rcr üksikmõõtmise jaoks täideti DECM alla kuu küllastuspunkti niiskussisaldustel ja üle kuu küllastuspunkti niiskussisaldustel pol-tüüpi niiskusemõõtja $f(R)+f(C)$ mudeli korral. Arvutuslik NS vahemik kus $TI < 3.5\%$ NS piirkonnas täideti Rcr järgmiste fokuseerivate mudelite tüüpide jaoks:

A: $R + C; R + f(C)$

B: $R_{1n} + R_{20n}; f(R_1 + R_{20})$

C: $f(R) + f(C)$

Mõõteseriade jaoks perioodiga $k=16$ täideti Rcr dielektrilise mahtuvusmeetodi DECM ja elektrilise impedantsi meetodi EIS jaoks. Rcr täidetuse kontrollimiseks tuletati vastavad valemid sõltuvana puidu niiskussisaldusest.

Vahelduvvooluga töötavate DECM ja EIS töökindluse uurimisel selgitati välja kasuliku mahtuvuse vahemik alla ning üle kiu küllastuspunkti. Vastavalt saadi DECM kasuliku mahtuvuse piirkonnaks 0–30% NS jaoks 121–205 pikofaradit, ja 30–105% NS jaoks 205–231 pikofaradit. Jagades kasuliku mahtuvuse piirkonna vastava NS piirkonnaga saame DECM tundlikkuseks 2.8 pF/NS% *alla FSP* piirkonnas, ja 0.35 pF/NS% *üle FSP* NS piirkonnas. Niisiis on erinevus tundlikkuses 8-kordne.

Lisaks modifitseeriti patendikirjeldusele vastava polarisatsioon-tüüpi puidu niiskusemõõtja aparatuurseid võimalusi. Lisati galvanostaatilise laadumise režiim ja depolarisatsiooni pinge monitooringu võimalus (I–II).

Puidu kuivatuse optimeerimise tulemused (IV).

Uuriti puidu pinnakihi üleminekut kuivatuse esimesest faasist teise kuivatuse faasi. Leiti, et pinnakihi (ca 2.5 mm sügavusel pinnast) üleminek teise kuivatuse faasi aeglustab difusiooni kiirust ka puidu sisekihtides, mis muidu oma NS-i poolest võiksid veel olla kuivatuse esimeses faasis. Pinnakihi difusiooni konstandi (DK) mõju iseloomustamiseks sisekihtidele defineeriti kriitilise difusiooni konstandi mõiste. Simulatsiooni programm TORKSIM kriitilise difusiooni konstandi olemasolu ei näidanud. Arvuliselt leiti puidu pinnakihi jaoks järgmised difusiooni konstandi väärtused.

Pärast arvutuste tegemist olid eksperimentaalse lokaalse difusiooni konstandi väärtused 2,5 mm sügavusel katsekeha pinnast järgmised: DK1.-faas = $27 * 10^{-4}$ mm²/s esimeses kuivatusfaasis ja DK2.-faas. = $18 * 10^{-4}$ mm²/s teises kuivatusfaasis (Tamme, H. et al., 2021). Esimese kuivatusfaasi lõpus ja teise kuivatusfaasi alguses on simuleeritud DK(sim) väärtus peaaegu võrdne (s.o. $11.8 * 10^{-4}$ mm²/s).

Leiti ka kriitilisele difusioonikonstandile ($27 * 10^{-4} \text{ mm}^2/\text{s}$) vastav kuivatusõhu kriitiline suhteline niiskus $RH = 81\%$.

Kriitilise difusioonikonstandi arvesse võtmisega optimeeritud kuivatusplaani koostamisel õnnestus tüüpilise tööstusliku kuivatamise plaani kuivatuse aega lühendada 140 tunnilt 92 tunnini, st 48 tunni ehk kahe ööpäeva võrra. Lõppniiskus oli optimeeritud režiimil 26% ja tööstuslikul režiimil 27%, ehk praktiliselt sama. Optimeeritud režiimi iseloomustasid mõnevõrra suuremad suhtelised pinged lubatud 0,33 asemel (Salin, J.G., 2007; Sova et al., 2016), mis tasandati ajastatud niisutusimpulsiga.

Kokkuvõte

Käesolevas väitekirjas leiti männipuidu jaoks kriitilisele difusiooni konstandile vastav kriitilise kuivatusõhu suhtelise niiskuse väärtus. Seda infot on puiduettevõtetel lihtne kuivatusplaanide modifitseerimiseks kasutada.

Puidukuivatitele kontrollautomaatikat tootvatele tehnoloogiafirmadele võiks prototüüpimiseks soovitada selle doktoritöö raames välja töötatud puidu pinna seisukorda monitoorivaid pinnaniiskuse ja pinna deformatsiooni andureid, samuti ka puidu keskmise niiskussisalduse dielektrilist mahtuvus-tüüpi andurit (DECM).

Kolmes Balti riigis on müüdnud märkimisväärset koguses puidukuivatuse simulatsiooniprogrammide TORKSIM-i litsentse. See doktoritöö võimaldab TORKSIM kasutaval puiduettevõttel orienteeruda programmi keerukas matemaatilises mudelis, samuti saada praktilist tagasisidet programmi tugevustele ja nõrkustele.

Põhimõtteliselt on puidukuivatuse monitooringu ühe meetodina välja töötatud uudne polarisatsioon-tüüpi puidu niiskuse mõõtur rakendatav ka kasvavate puude niiskussisalduse monitooringuks (Yang et al., 2023).

Kokkuvõtvalt võib öelda, et selles väitekirjas püstitatud hüpoteesid leidsid kinnitust. Kõik väitekirjas püstitatud eesmärgid täideti.

ACKNOWLEDGEMENTS

I would like to thank my supervisor Professor Peeter Muiste and co-supervisor Valdek Tamme, PhD whose deep professional knowledge and determination kept my research on track. It is like wood drying – a good start is a key to success, and well-timed guidance will lead to a finished product. The supervisors' help with planning, carrying out, and writing the thesis made this journey much more manageable.

I want to express my gratitude to Engineer Toomas Bernotas from the University of Tartu for in-depth electronics advice in electrometry. So many hurdles were avoided. I also want to thank Madis Noppel, PhD from the Laboratory of Environmental Physics at the University of Tartu.

I am very grateful to Tavo Romann, PhD from the Institute of Chemistry at the University of Tartu, for his expert advice in electrochemistry and his lab for system automation test ground.

I am thankful to my colleagues at the Institute of Forestry and Engineering for the excellent study environment. Also, I would like to thank my colleagues at the high performance computing centre from the University of Tartu, led by Ivar Koppel, for encouraging my studies.

I also want to thank all the co-authors for contributing to the papers. And I hope that joint effort will continue in the future.

I want to thank Mrs. Karit Jäärats for her linguistic revision.

I am grateful for previous students whose work provided excellent datasets for preliminary analysis. It was so much easier to build on top of already existing knowledge.

And finally the support from my family pulled all the previously mentioned aspects together.

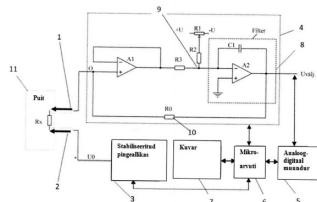
Patentne leiutis: Niiskusmõõtur ja meetod puidu elektrilise laadumise efektiga puidu küllastuspunkti suurema niiskussisalduse mõõtmiseks;
Omanikud: Eesti Maaülikool, Metsanduse- ja Maachituse Instituut, Eesti Maaülikool, Tehnikainstituut, Tartu Ülikool; Autorid: Valdek Tamme, **Hannes Tamme**, Toomas Bernotas, Peeter Muiste, Jüri Olt;
Prioriteedi number: EE201800017; Prioriteedi kuupäev: 16.07.2018.
<https://www.etis.ee/Portal/IndustrialProperties/Display/974edb6b-39df-44ea-b1ba-403cdcaa81aa>

(11) **EE 05822 B1**(51) Int.Cl.
G01R 27/00 (2006.01)
G01N 27/00 (2018.01)(12) **PATENDIKIRJELDUS**

(21) Patenditaotluse number: P201800017	(73) Patendiomanik: Eesti Maaülikool Fr. R. Kreutzvaldi 1a, 51014 Tartu, EE
(22) Patenditaotluse esitamise kuupäev: 16.07.2018	(72) Leiutise autorid: Valdek Tamme
(24) Patendi kehtivuse alguse kuupäev: 16.07.2018	Hannes Tamme
(43) Patenditaotluse avaldamise kuupäev: 17.02.2020	Toomas Bernotas
(45) Patendikirjelduse avaldamise kuupäev: 15.06.2020	Peeter Muiste
	Jüri Olt

(54) **Niiskusemõõtur ja meetod puidu elektrilise laadumise efektiivsuse suurendamiseks**

(57) Leiutus kuulub materjalide uurimise ja analüüsivõime valdkonda, täpsemalt puidu niiskussisalduse määramise elektriliste meetodite hulka, ja on kasutatav puidu kiu küllastuspunkti suurema niiskussisalduse korral. Niiskusemõõtur puidu elektrilise laadumise efektiivsuse suurendamiseks sisaldab kahte mõõteelektroodi, stabiilset tugipingeallikat, elektromeetrilise sisendiga eelvõimendit, analoog-digitaalmuundurit, täppistakistit elektromeetrilise sisendiga eelvõimendi tagasisideahelas, elektroonilise aktiivfiltrite plokki, mis sisaldab filtreid madalsageduslike ning kõrgsageduslike mõõtemärade filtreerimiseks operatsioonivõimendi ja kondensaatori abil, mikroarvuti mõõtmisprotsessi juhtimiseks ning LCD-displeid, kusjuures mikroarvutisse on mõõtmisprotsessi täieliku automatiseerimise eesmärgil sisestatud matemaatilised algoritmid. Meetod puidu elektrilise laadumise efektiivsuse suurendamiseks sisaldab niiskussisalduse mõõtmiseks, mille kohaselt mõõdetakse puidu puidu elektritakistust, mõõdetud laadimisvoolu ajalise käigu alusel leitakse reaalselt puidu elektrimahtuvus eri ajamomentidel ning määratakse puidu laadumisarv kalibreerimismudeli koostamiseks ja valideerimiseks, kusjuures mõõtmisprotsessi juhitakse digitaalselt.



(57) The invention belongs to the area of material research and analysis, specifically among electrical methods for determining wood moisture content, and can be used in moisture contents above the fibre saturation point. Moisture meter with the electric loading effect above the fibre saturation point of wood enables on-line registration of temporal patterns of wood electrical resistance and electrical capacitance as well as saving these in the memory of a microcomputer in the course of the wood electrical charging cycle at a previously set measuring speed. After the measurements have been carried out, the file containing calibration model and a prognosis of wood moisture content is presented along with the estimated statistical error. The distinctive characteristic of the method of calibration of the moisture meter with the electric loading effect above the fibre saturation point of wood is the occurrence of a significant decrease in the uncertainty of measurement as wood moisture content increases when moisture levels above the fibre saturation point are measured. The decrease in the uncertainty of measurement, especially in high wood moisture contents of 100% and above, is achieved by the original application of the wood charging number and consideration thereof in the compilation of the calibration model.

EE 05822 B1

Niiskumõõtur ja meetod puidu elektrilise laadumise efektiga puidu küllastuspunkti suurema niiskussisalduse mõõtmiseks

TEHNIKAVALDKOND

5 Käesolev leiutus kuulub materjalide omaduste uurimise ja analüüsimise valdkonda, puidu niiskuse määramise meetodite ja seadmete, täpsemalt elektriliste juhtivus- ja impedantsmeetodite ja seadmete hulka.

TEHNIKA TASE

Puidu niiskussisalduse määramise idee puidu elektrijuhtivuse mõõtmise alusel esitas esmakordselt Stamm 1927. aastal. Sellest ajast peale on puidu elektritakistuse või 10 elektrijuhtivuse (mis on elektritakistuse pöördväärtus) põhimõttel töötavaid puiduniiskumõõtureid tööstuslikult seeriaviisiliselt toodetud ja neid kasutatakse laialdaselt praktikas ka tänapäeval. Praktikas kasutusel olevate tuntud takistus-tüüpi puiduniiskumõõturite jaoks probleemne mõõtepiirkond algab 30% puidu niiskussisaldusest (kuivkaalu suhtes) ja sellest edasi niiskussisalduse suurenedes kuni ca 150% 15 niiskussisalduseni. Seda niiskussisalduste piirkonda nimetatakse puidu kiu küllastuspunkti kõrgemaks piirkonnaks, sest siis hakkab puidu kapillaaridesse kogunema vaba vesi.

Puidu elektritakistus varieerub väga laiades piirides, sõltuvalt puidu niiskussisaldusest, temperatuurist, ja mingil määral ka puidu liigist. Puidu elektritakistuse laborimõõtmised kinnitasid jämedat hinnangut, et näiteks toatemperatuuril 20 kraadi Celsiuse järgi on 8% 20 niiskussisaldusega puidu elektritakistus ca 10 giga-oomi, 18% niiskussisaldusega umbes 10 mega-oomi, 47% niiskussisaldusega umbes 100 kilo-oomi, 150% niiskussisaldusega umbes 10 kilo-oomi. Sellest tulenevalt on usaldusväärse mõõtetulemuse saamiseks vajalik niiskumõõturit kalibreerida.

25 Kirjanduse (Tamme, V., Muiste, P., Padari, A., Tamme, H. 2014. Modelling of Resistance-Type Wood Moisture Meters for Three Deciduous Tree Species (Black Alder, Birch, Aspen) in Moisture Contents Above Fibre Saturation Point. *Baltic Forestry*, 20 (1): 157-166) andmetel läbi viidud ulatusliku uuringu põhjal kolme praktilises kasutuses ja tootmises olevate puidu niiskumõõturite usaldusväärse küsimuse selgitamiseks puidu kiu

küllastuspunkti suuremal ehk puidu üle 30% varieeritavatel niiskussisaldustel. Uuringu tulemusena leiti, et 95% usaldusnivool oli tuntud niiskumõõturi ja kolme puuliigi korral võimalik varustada uued kalibreerimismudelid, mille alusel on võimalik kõrvaldada algselt leitud suured süstemaatilised vead (kuni 75% niiskussisaldust (NS)) mõõtetulemustes.

- 5 Puidu elektritakistus on tuntud leiutistes mõõdetud kas alalisvoolu või vahelduvvoolu meetodil. Mõlemad variandid on kasutusel.

Patendi US4408128 (A) järgi on tuntud meetod puidu niiskussisalduse määramiseks oma olemuselt puidu vahelduvvoolu elektritakistuse määramine. Tuntud tehnilise lahenduse puhul on puidu niiskussisalduste mõõtepiirkonnaks leiutiskirjelduses toodud 10% kuni 40% niiskussisaldust. Selle niiskussisalduste vahemiku jaoks on patendikirjelduses ära toodud ka kalibreerimiskõver, mis seob omavahel puidu tegelikku niiskussisaldust ja vahelduvvoolu elektritakistust.

Vastavalt patendile ES2566775 B2 (A1) on tuntud meetod puidu niiskussisalduse määramiseks oma olemuselt puidu vahelduvvoolu elektritakistuse määramine. Tuntud tehnilises lahenduses on puidu niiskussisalduse mõõtepiirkonnaks on toodud 7% kuni 20% niiskussisaldust. Nimetatud mõõtepiirkonna kohta on patendikirjelduses ära toodud ka kalibreerimiskõver, mis seob mõõdetud puidu vahelduvvoolu elektritakistuse vastava puidu tegeliku niiskussisaldusega. Kalibreerimiskõverad on antud kahe puuliigi jaoks.

Vastavalt patendile US4259633 (A) on tuntud meetod puidu niiskussisalduse määramiseks oma olemuselt puidu alalisvoolu elektritakistuse määramine. Elektritakistuse ajaline muutumine ehk triiv kompenseeritakse toitepinge analoogkorrigeerimisega, et saada püsivat näitu. Tuntud tehnilise lahenduse kirjelduses kalibreerimismudeli kohta avalikult kättesaadavad andmed puuduvad. Tuntud tehnilise lahenduse üldiseks mõõtepiirkonnaks on patendikirjelduses deklareeritud 10% kuni 90% niiskussisaldust.

25 Vastavalt patendile US67008555 (A) on tuntud kalibreerimise meetod, mille iseloomulikuks tunnuseks on see, et mõõdetavat suurust, puidu elektrimahtuvust C, seostatakse kalibreerimise meetodis puidu niiskussisaldusega.

Kõige lähemaks tehniliseks lahenduseks on vastavalt patendile US4621229 (A) tuntud puidu niiskussisalduse määramine alalisvoolu elektritakistuse meetodiga. Tuntud niiskumõõturi lugem on sisuliselt niiskumõõturi sisemise andmetöötluse algoritmi ehk kalibreerimisfunktsiooni abil arvatud ehk prognoositud puidu niiskussisaldus. Tuntud
 5 tehnilise lahenduse iseloomuliks tunnuseks on see, et mõõdetavat suurust puidu elektritakistust R seostatakse kalibreerimise meetodid puidu niiskusesisaldusega. Tuntud meetodi puuduseks on see, et mõõdetav suurus, puidu elektritakistus, seostatakse kalibreerimise meetodis puidu niiskussisaldusega, mis ei võimalda anda usaldusväärsuset mõõtmistulemust puidu kiu küllastuspunkti suuremal ehk puidu üle 30% varieeritavatel
 10 niiskussisaldustel.

Tuntud meetodi peamiseks puuduseks on see, et üle kiu küllastuspunkti puidu niiskussisaldustel elektritakistuse mõõtmisandmete dispersioon kasvab progresseeruvalt puidu niiskuse kasvades, põhjustades tõsiseid probleeme takistustüüpi puidu niiskumõõturite kalibreerimisel, mis omakorda on puidu niiskussisalduse määramise
 15 ebapiisava täpsuse põhjuseks puidu üle 30% niiskussisaldustel.

Kõige lähemaks tehniliseks lahenduseks on vastavalt patendile US4621229 (A) on tuntud niiskumõõtur puidu elektrilise laadumise efektiga puidu küllastuspunkti suurema niiskussisalduse mõõtmiseks, mis sisaldab mõõteelektroode, tugipingegaallikat, elektromeetrilise sisendiga eelvõimendit ning analoog-digitaalmuunduri niiskumõõturiga
 20 ning mille konstruktsiooni illustreerib patendi US4621229 (A) joonis fig. 1.

Tuntud niiskumõõturi puududeks on puidu niiskussisalduse määramise ebapiisav täpsus, kuna mõõdetavat suurust, puidu elektritakistust, seostatakse selles puidu niiskussisaldusega.

Kirjanduses (V. Tamme. Elektriliste takistus-tüüpi kontrollmeetodite arendamine puidukuivatites. Väitekiri filosoofiadoktori kraadi taotlemiseks. Tartu, 2016, 135 lk) on
 25 analüüsitud puidu niiskussisalduse määramisel mõõteelektroodide nn individuaalse kalibreerimise võimalust puidu kiu üle 30% niiskussisalduse määramisel. On välja selgitatud, et mõõteelektroodide individuaalse kalibreerimise abil on praktiliselt võimalik välistada juhuslike mõõtmisvigade tekkimine puidu kius üle 30% niiskussisalduse määramisel.

Individaalse kalibreerimise puuduseks on see, et elektrootidde jaoks konkreetses asukohas läbi viidud individaalne kalibreerimine kaotab oma kehtivuse, kui mõõteelektrootid (nõel- või kruvielektrootid) paigaldada puidus järgmisesse juhuslikult valitud asukohta. Seega on individaalse kalibreerimise näol tegemist tegelikult ühekordseks kasutamiseks mõeldud protseduuriga, mis õigustab ennast vaid laboritingimustes.

Mõõteelektrootidde individaalse kalibreerimise kogemusest võib teha ühe olulise järelduse: puidu kiu üle 30% niiskussisalduse määramisel tekkivate suurte juhuslike mõõtmisvigade tegelikuks põhjuseks on kõige tõenäosemalt puidu/mõõteelektrooti elektrilise kontakti takistus, mille väärtus on igas mõõteelektrootidde puitu sisestamise kohas individaalne ja unikaalne puidu heterogeensete ja varieeruvate looduslike omaduste (tihedus, niiskussisaldus, nn veetaskud, vaigusisaldus jne) tõttu.

Tuntud tehnilistes lahendustes on puiduniiskusmõõturid tegelikult puidu elektrilise takistuse mõõturid, mis on kalibreeritud kuivkaalu meetodil (näit standard ISO 3130:1975) puidu niiskussisalduse mõõtjateks. Vastavad kalibreerimismudelid koostatakse tavaliselt lineaarse regressiooni mudelitena.

Kirjanduse (vt V. Tamme. Elektriliste takistus-tüüpi kontrollmeetodite arendamine puidukuivatuses. Väitekiri filosoofiadoktori kraadi taotlemiseks. Tartu 2016, 135 lk) põhjal on teada, et puidu kiu üle 30% niiskussisaldustel kaasneb mõõteelektroot-puit kontakti elektritakistusega ka elektroot-/puitkontakti elektrimahtuvuse teke, kusjuures mõlemad – nii elektritakistus kui ka elektrimahtuvus – on ajast sõltuvad suurused.

Praktika on näidanud, et tuntud leiutist omava firma Gann (www.gann.de) originaalsete metallist valmistatud mõõteelektrootidde (tüüp M19) korrosioon võib olulisel määral häirida elektritakistuse ja elektrimahtuvuste ajaliste sõltuvuste ülesvõtmist.

Leiutise eesmärgiks oli välja töötada uue põlvkonna puiduniiskusmõõtur ja meetod selle kalibreerimiseks, puidu kiu küllastuspunkti suurema, täpsemalt üle 30% puidu niiskussisalduse usaldusväärseks määramiseks,

LEIUTISE OLEMUS

Käesoleva leiutise olemus seisneb selles, et luua senituntud tehnilisest lahendusest erinev niiskusemõõtur puidu niiskussisalduse määramiseks puidu kiu küllastuspunktist suurema, täpsemalt üle 30% puidu niiskussisalduste korral, ja meetod niiskusemõõturi kalibreerimiseks.

Niiskusemõõtur puidu elektrilise laadumise efektiga puidu kiu küllastuspunktist suurema niiskussisalduse mõõtmiseks sisaldab kahte mõõteelektroodi, stabiilset tugipingeaallikat, elektromeetrilise sisendiga eelvõimendit, analoog-digitaalmuundurit, täppistakistit elektromeetrilise sisendiga eelvõimendi tagasisideahelas, elektrooniliste aktiivfiltrite plokki, mis sisaldab filtreid madalsageduslike ning kõrgsageduslike mõõtemürade filtreerimiseks operatsioonivõimendi ja kondensaatori abil, mikroarvutit mõõtmisprotsessi juhtimiseks ning LCD-displeid, kusjuures mikroarvutisse on mõõtmisprotsessi täieliku automatiseerimise eesmärgil sisestatud matemaatilised algoritmid.

Niiskusemõõturi mõõteelektroodideks on korrosioonivabad isoleeritud süsinikkiud- nõel-elektroodid. Need võivad olla valmistatud ka roostevabast terasest või alumiiniumsulamist.

Puidu elektrilise laadumise efektiga niiskusemõõturi kalibreerimise meetodi kohaselt sisaldab mõõtmisprotsess puidu elektritakistuse ja laadumisvoolu mõõtmist ajast sõltuvana, eelnevalt valitud mõõteintervalliga, konstantse laadumispinge juures ette nähtud pikkusega mõõtettsükli korral, kusjuures mõõdetud laadumisvoolu ajalise käigu alusel leitakse reaajas puidu elektrimahtuvus eri ajamomentidel ning määratakse puidu laadumisarv optimaalse kalibreerimismudeli koostamiseks ja valideerimiseks, kusjuures mõõtmisprotsessi juhitakse digitaalselt.

Puidu elektrilise laadumise meetodile vastavalt on puidu laadumisarvu järgi puidu elektritakistus pöördvõrdelises sõltuvuses puidu elektrimahtuvusega kõigil kalibreerimismudelil erinevatel puidu tegelikel niiskussisaldustel, kusjuures kasutatakse elektritakistuste hälvete koondamiseks kalibreerimismudelil elektrimahtuvusest sõltuva muutuja integreerimisega kalibreerimismudelisse. Elektrimahtuvusest sõltuvaks muutujaks on laadumisarvu kaudu puidu elektritakistus ning niiskussisaldus.

- Puidu elektrilist laadumist iseloomustavaid muutujaid, elektritakistust ja elektrimahtuvust mõõdetakse parima võimaliku täpsusega konstantsel laadumisingel potentsiostaatilises laadimisrežiimis. Ühe mõõtettsükli jooksul kogutakse hulk katseandmeid, saadud katseandmeid töödeldakse, selleks kasutatakse matemaatilisi seoseid ning selle tulemusena
- 5 parandatakse kalibreerimismudeli kvaliteeti. Kogutud andmeid töödeldakse mikroarvuti abil ning registreeritakse elektritakistuse ja elektrimahtuvuse ajalised käigud.

JOONISTE LOETELU

- Joonisel fig. 1 on kujutatud puidu elektrilise laadumise põhimõtet realiseeriva elektroonikaseadme analoogosa.
- 10 Joonisel fig. 2 on kujutatud puidu elektrilise laadumise efektiga niiskusemõõtuuri põhimõtteskeem.
- Joonisel fig. 3 on kujutatud tüüpilised puidu elektritakistuse $R_x = R_{puit} + R_{kontakt}$ sõltuvused ajast 20 sekundi pikkuse mõõtettsükli jooksul.
- Joonisel fig. 4 on kujutatud puidu elektrimahtuvuse C sõltuvused ajast 20 sekundi pikkuse
- 15 mõõtettsükli jooksul.
- Joonisel fig. 5 on kujutatud puidu laadumisarvu logaritmi graafik, mis vastab valemile (6).
- Joonisel fig. 6 on kujutatud $\text{Log}R_{1n}$ -st sõltuv kalibreerimismudel puidu niiskussisalduse prognoosimiseks puidu elektritakistuse mõõtmistulemuste alusel.
- Joonisel fig. 7 on kujutatud võrdlusmudel puidu tegeliku niiskussisalduse ja R_{1n} alusel
- 20 prognoositud puidu niiskussisalduste võrdlemiseks
- Joonisel fig. 8 on kujutatud võrdlusmudel puidu tegeliku niiskussisalduse ja 10 kordusmõõtmise alusel keskmistatud R_{1n} alusel tehtud puidu niiskussisalduse prognoosi võrdlemiseks.

Joonisel fig. 9 on kujutatud kombineeritud muutujast ($R_{1n} + C_{1n}$) sõltuv kalibreerimismudel puidu niiskussisalduse prognoosimiseks.

Joonisel fig. 10 on kujutatud võrdlusmudel puidu tegeliku niiskussisalduse ja muutuja ($R_{1n} + C_{1n}$)_c alusel prognoositud puidu niiskussisalduste võrdlemiseks, juhul kui on ära
5 korrigeeritud puidu tegelikul niiskussisaldusel 105% NS juhuslike vigade kokku surumiseast tekkinud arvutuslik süstemaatiline viga.

Joonisel fig. 11 on kujutatud kombineeritud muutujast $\text{Log}(R_1 + R_{20})$ sõltuv kalibreerimismudel puidu üle 30% tegeliku niiskussisalduse prognoosimiseks

Joonisel fig. 12 on kujutatud võrdlusmudel puidu tegeliku niiskussisalduse ja muutuja
10 $\text{Log}(R_{1n} + R_{20n})$ alusel prognoositud puidu niiskussisalduste võrdlemiseks.

Joonisel fig. 13 on kujutatud võrdlusmudel puidu tegeliku niiskussisalduse ja muutuja $\text{Log}(R_{1n} + R_{20n})$ alusel prognoositud puidu niiskussisalduste võrdlemiseks, kui on tehtud 10 kordusmõõtmist.

Joonisel fig. 14 on kujutatud kalibreerimismudel kombineeritud sõltumatu x-muutujaga $R +$
15 $0.00005 \cdot C^3$, mis on edaspidi nimetatud R+Par5 muutujaks.

Joonisel fig. 15 on kujutatud võrdlusmudel tegeliku niiskussisalduse ja joonisel fig. 14 kujutatud kalibreerimisfunktsiooni abil prognoositud niiskussisalduste võrdlemiseks.

Joonisel fig. 16 on kujutatud R+Par5 kalibreerimismudel juhul, kui on tehtud k=10 kordusmõõtmist.

Joonisel fig. 17 on kujutatud võrdlusmudel puidu tegeliku niiskussisalduse ja joonisel fig. 19 kujutatud kalibreerimismudeli abil prognoositud puidu niiskussisalduste võrdlemiseks, juhul kui on tehtud k=10 kordusmõõtmist.

Joonisel fig. 18 on kujutatud eri mudelite tolerantsi intervallid.

TEOSTUSNÄIDE

Järgnevalt kirjeldatakse leiutist täielikumalt, koos viidetega lisatud joonistele, millel on kujutatud jooniste eelistatud teostus.

- Joonisel fig. 1 on kujutatud puidu elektrilise laadumise põhimõtet realiseeriva elektroonikaseadme analoogosa. Puidu elektriline laadimine toimub konstantsel pingel, näiteks, $U_0=1,024$ volti, mis võetakse tugipingeaallikast. Elektromeetri E, ehk täpsemalt elektromeetrilise sisendiga operatsioonvõimendi, tagasisideahelasse on lülitatud täppistakisti R_0 . Mõõdetav puidu elektritakistus R_x on lülitatud elektromeetri sisendisse. Läbi mõõdetava puidu elektritakistuse kulgeb laadimisvool I_{laad} . Elektromeetri väljundpinge $U_{välj}$ muutub ettenähtud piirides.

Puidu elektrilise laadumise ekvivalentskeem (fig. 2), kus puidu/mõõteelektroodi elektrilise kontakti takistus sõltub ajast logaritmiliselt:

$$R(t) = a \cdot \ln(t) + b, \quad (1)$$

ja puidu/elektroodi kontakti elektrimahtuvus sõltub ajast lineaarselt:

$$C(t) = a_1 \cdot t + b_1, \quad (2)$$

kus a , b , a_1 ja b_1 on konstandid mõõteelektroodide antud konkreetse asukoha jaoks puidus.

- 15 Kui mõõteelektroodide asukohta puidus muuta, siis omandavad konstandid uued väärtused, kuid funktsioonide üldkuju (logaritmiline (1) – lineaarne (2)) jääb samaks.

Elektritakistuse ja elektrimahtuvuse ajaliste sõltuvuste arvutamiseks on kasutatud joonisel fig. 1 kujutatud põhimõtteskeemi, kus puitu elektriliselt laadiv (polariseeruv) pinge võetakse täppis-tugipingeaallikast $U_0=1,024$ V ja puidu ajast sõltuv elektritakistus arvutatakse valemist

$$R_x = U_{väljund} \frac{R_0}{U_0}, \quad (3)$$

kus R_x on puidu elektritakistus oomides, R_0 on elektromeetri tagasiside täppistakisti takistus oomides (100 megaoomi) ja $U_{\text{väljund}}$ on mõõdetud analoog-väljundpinge voltides.

Puidu laadimisvool amprites arvutatakse valemist:

$$I_{\text{laad}} = \frac{U_0}{R_x}, \quad (4)$$

ja puidu elektrihahtuvus arvutatakse valemist:

$$C_x = \frac{Q}{U_0}, \quad (5)$$

- 5 kus C_x on puidu elektrihahtuvus faradites, Q on puidu elektrilaeng kulonites, mille konkreetne väärtus määratakse laadimisvoolu I_{laad} numbrilise integreerimise abil, mis omakorda viiakse läbi seadme tööd juhtiva mikroarvuti abil reaalaajas.

Puidu elektrilise laadimise tsükkel konstantsel laadimisingel kestab, näiteks, 20 sekundit, kusjuures mõõteintervall on eelnevalt valitav vahemikus 0,1 kuni 1,0 sekundit. Seega, antud
10 näite puhul, ühe mõõtettsükli jooksul registreeritakse 200 kuni 20 puidu elektritakistuse R_x ja laadimisvoolu I_{laad} ajast sõltuvat mõõtetulemust.

Leitise olemuse esiletõstmiseks on defineeritud katseandmete analüüsi alusel puidu empiiriline laadumisarv. Kui moodustada mõõdetud elektritakistustest ja arvatud elektrihahtuvustest korrutised iga järgneva mõõteintervalli jooksul, siis selgus, et need
15 korrutised on praktiliselt konstantsed (väga väikese varieeruvusega, vt joonis fig. 3), ning ei sõltu ka puidu niiskussisaldusest üle 30% puidu niiskussisalduste piirkonnas. See väga väikese varieeruvusega empiiriline konstant nimetati puidu laadumisarvuks. Logaritmidest puidu laadumisarvu, saame lihtsa matemaatilise seose, mida on mugav esitada graafikuna (joonis fig. 3):

$$\log(LA) = \log R_{1n} + \log C_{1n}, \quad (6)$$

- 20 kus LA on puidu laadumisarv, R_{1n} on vastavalt puidu elektritakistused ja C_{1n} puidu elektrihahtuvused n -da mõõtmisttsükli esimesel sekundil.

Kommentaariid puidu empiirilise tunnuse, laadumisarvu, kohta on järgmised.

1. Kuna puidu laadumisarv ise ei sõltu puidu niiskussisaldusest, siis ei sobi see muutujaks kalibreerimismudelisse, mille eesmärgiks on prognoosida puidu niiskussisaldust puidu kiu küllastuspunktist suurema, see on puidu üle 30% niiskussisaldusel.
2. Puidu laadumisarv matemaatiliselt esitab empiirilisel tunnust, et puidu elektritakistus on pöördvõrdelises sõltuvuses puidu elektrimahtuvusega kõigil kalibreerimismudelid esinevatel puidu tegelikel niiskussisaldustel. Seda asjaolu on teoreetiliselt võimalik ära kasutada elektritakistuse suurte hälvete kokkusurumiseks kalibreerimismudelid elektrimahtuvusest sõltuva uue muutuja integreerimisega mudelisse. Seda protseduuri võib nimetada kalibreerimismudelid signaal-müra- suhte parandamiseks, või ka kalibreerimismudelid kvaliteedi tõstmiseks.

Joonisel fig. 2 on kujutatud puidu elektrilise laadumise efektiga niiskusemõõduri põhimõtteskeem, kusjuures niiskusemõõduri funktsionaalsed elemendid on näidatud plokkiskeemina. Niiskusemõõdur sisaldab mõõteelektroode 1 ja 2, stabiliseeritud tugipingeallikat 3, analoogmõõteahela plokki 4, analoog-digitaalmuundurid 5, mikroarvutid 6 ja LCD-displeid 7. Analoogmõõteahela plokk 4 sisaldab elektromeetrilise sisendiga eelvõimendit A1, elektrooniliste aktiivfiltrite plokki 8 ja lülitust 9 (R2 ja R3) analoogvõimendi väljundpinge ja nullimispinge summeerimiseks. Mõõteelektroodid 1 ja 2 on ette nähtud surumiseks puidu 11 sisse niiskussisalduse (NS) mõõtmiseks.

Joonisel fig. 2 on seadme funktsionaalsed elemendid näidatud skemaatiliselt plokkiskeemina. Analoogmõõteahela plokk 4, mis sisaldab elektromeetrilise sisendiga eelvõimendit A1 signaali eelvõimendina, tagasiside täppistakistid 10 (R0), potentsiomeetrilist lülitust R1 võimendi nulli seadistamiseks, lülitust 9 (näiteks takistid R2 ja R3) võimendi väljundpinge ja nullimispinge summeerimiseks, elektrooniliste aktiivfiltrite plokki 8 (joonisel fig. 2 tähistatud plokkina „Filter“), mis sisaldab filtreid madalsageduslike ja kõrgsageduslike mõõtemürade filtreerimiseks operatsioonvõimendi A2 ja kondensaatori C1 abil. Stabiliseeritud tugipingeallikas 3 väljastab mõõteelektroodile 2 stabiliseeritud alalispinge väärtusega U_0 , milline pinge mõõteelektroodil 2 langeb mõõtmisprotsessis puidu 11 või puitmaterjali ekvivalenttakistusel R_x kuni null volti potentsiaalini mõõteelektroodil 1, mis on

ühendatud elektromeetrilise sisendiga eelvõimendi A1 sisendi nullpotentsiaali tähistava punktiga O analoogmõõteahela plokis 4. Analoogmõõteahela ploki 4 üldine otstarve on konvertida eelvõimendi A1 sisendis mõõdetud elektritakistuse R_x väärtus võimalikult lineaarselt ja müravabalt analoogväljundpingeks $U_{välj.}$, luues sellega eeldused

5 analoogväljundi signaali muundamiseks digitaalseks signaaliks analoog-digitaalmuunduri 5 abil. Mõõtetulemuse edasine digitaalne töötlus toimub mikroarvuti 8 abil, töötlemise tulemus väljastatakse numbriliselt LCD-displeil 7. Niiskusemõõturi elektrooniliste elementide 3, 5, 6, 7, 8, 9 toiteahelaid ei ole joonisel fig. 2 kujutatud, samuti ei ole kujutatud mõõtmistsükli markeerivat heliallikat (summerit) ega valgusallikat (valgusdiodi).

10 Joonisel fig. 3 on kujutatud tüüpilised puidu 11 elektritakistuse $R_x = R_{puit} + R_{kontakt}$ sõltuvused ajast 20 sekundi pikkuse mõõtettsükli jooksul. Mõõtmised on tehtud 21 puidus juhuslikult valitud asukohas, ühe puuliigi korral, ja 1/3 puidu paksuse sügavusel. Puuliigiks oli sanglepp, tegeliku keskmise niiskussisaldusega 105%, mis määrati kuivkaalu meetodil

15 mõõdeti puidus 1/3 materjali paksuse sügavusel pinnast. Igale mõõtmistsükliile vastab üks graafik. Maksimaalseid puidu elektritakistuste mõõtetulemusi kujutavale graafikule ja minimaalseid mõõtetulemusi kujutavale graafikule parves on lisatud trendijoon. Graafikutelt on visuaalselt tuvastatav, et kõige väiksem hajuvus on puidu elektritakistusel mõõtmise algul punktis R_{1n} . Võrdlev kirjeldav statistika mõõtepunktides R_{1n} ja mõõtepunktides 20 sekundi

20 mõõdudes R_{20n} kinnitab seda järeldust. Arvutatud vastavad variatsioonikordajad ($\sigma/average$) 100% on vastavalt: ($R_{1n}=9,7\%$ ja $R_{20n}=15,9\%$), st variatsioonikordaja suureneb 20. sekundil alates mõõtmise algusest oluliselt.

Joonisel fig. 4 on kujutatud tüüpilised puidu elektrimahtuvuse C sõltuvused ajast 20 sekundi pikkuse mõõtettsükli jooksul. Mõõtmised on tehtud 21 puidus juhuslikult valitud asukohas

25 (joonise selguse huvides on kujutatud ainult min, max ja 4 vahepealset mahtuvuse ajast sõltuvuse graafikut 21 tegelikult määratud graafikust), ühe puuliigi korral, ja 1/3 puidu paksuse sügavusel. Puuliigiks on toodud näites sanglepp, tegeliku keskmise niiskussisaldusega 105%, mis määrati kuivkaalu meetodil vastavalt standardile ISO 3130:1975 ja temperatuuril 50 kraadi Celsiuse järgi, elektrimahtuvus, nagu ka

30 elektritakistus, mõõdeti puidus 1/3 materjali paksuse sügavusel pinnast. Igale mõõtmistsükliile vastab üks graafik. Maksimaalseid puidu elektrimahtuvuse mõõtetulemusi

kujutatavale graafikule ja minimaalseid mõõtetulemusi kujutatavale graafikule parves on lisatud trendijoon. Graafikutelt on visuaalselt tuvastatav, et kõige väiksem hajuvus on puidu elektrimahtuvusel mõõtmise algul punktis C_{1n} . Võrdlev kirjeldav statistika mõõtepunktides C_{1n} ja mõõtepunktides C_{20n} kinnitab seda järeldust. Arvutatud vastavad variatsioonikordajad

5 (s.o standardhälve jagatuna aritmeetilise keskmisega protsentides: $(\sigma/average) \cdot 100\%$ on ($C_{1n}=10,4\%$ ja $C_{20n}=14\%$), seega 20 sekundit mõõtmise algusest kasvas hajuvust kvantitatiivselt iseloomustav variatsioonikordaja oluliselt.

Joonisel fig. 5 on kujutatud puidu laadumisarvu logaritmi graafik, mis vastab valemile (6). Laadumisarv ise puidu niiskussisaldusest ei sõltu, kuid selle tähtsus seisneb selles, et

10 laadumisarvust lähtuvalt koostatud statistiliste muutujate abil on teoreetiliselt võimalik kokku suruda puidu niiskussisalduse kalibreerimise regressioonimudeli hajuvust eriti puidu suurtel niiskussisaldustel, kus traditsioonilised puidu elektritakistus kasutatavad mudelid muutuvad niiskussisalduse suurenedes progresseeruvalt ebatäpsemateks (st annavad ebatäpsema prognoosi puidu niiskussisaldusele).

15 Järgnevad joonised fig. 6, fig. 7 ja fig. 8. hõlmavad sellist teostusnäidet, kus kalibreerimismudelis sõltumatuks muutujaks on valitud puidu elektritakistus R_{1n} kui kõige väiksema algse hajuvusega muutuja (vt fig. 3).

Joonisel fig. 6 on kujutatud $\text{Log}R_{1n}$ -st sõltuv kalibreerimismudel puidu niiskussisalduse prognoosimiseks puidu elektritakistuse mõõtmistulemuste alusel. Mõõtmiste koguarv

20 mudeli kohta oli $n=63$.

Joonisel fig. 7 on kujutatud võrdlusmudel puidu tegeliku niiskussisalduse ja R_{1n} alusel prognoositud puidu niiskussisalduste võrdlemiseks. Selline võrdlusmudel võimaldab hinnata joonisel fig. 6 antud kalibreerimismudeli ennustuspotentsiaali, kuna puidu tegelik niiskussisaldus on määratud suure täpsusega kuivkaalumise meetodil vastavalt standardile

25 ISO 3130:1975.

Joonisel fig. 8 on kujutatud võrdlusmudel puidu tegeliku niiskussisalduse ja 10 kordusmõõtmise alusel keskmistatud R_{1n} alusel tehtud puidu niiskussisalduse prognoosi võrdlemiseks. 10 kordusmõõtmist on praktikas enim aktsepteeritud võtte prognoosi

usaldusväärseuse tõstmiseks, kuna see ei ole eriti töömahukas. Seda võtet nimetatakse ka kalibreerimismudeli valideerimiseks 10 kordusmõõtmise juures.

Võrreldes kirjanduses (Tamme, V., Muiste, P., Padari, A., Tamme, H. 2014. Modelling of Resistance-Type Wood Moisture Meters for Three Deciduous Tree Species (Black Alder, Birch, Aspen) in Moisture Contents Above Fibre Saturation Point. *Baltic Forestry*, 20 (1): 157-166) tuntud üksikmõõtmisele prognoositud tolerantsi intervalliga 35% NS sanglepa puidu tegelikul niiskussisaldusel 90% on joonise fig. 6 kalibreerimismudeli abil prognoositud 105% tegeliku niiskussisalduse (NS) jaoks üksikmõõtmise tolerantsi intervall 20% NS. Seega üksikmõõtmise prognoos paranes 15% NS. Kui aga võrrelda mudeli fig. 7 üksikmõõtmise prognoosi, ja mudeliga fig. 8, 10 kordusmõõtmise abil tehtud tolerantsi intervalli prognoosi samal tegelikul niiskussisaldusel 105%, siis oli paranemine 20% NS – 8,5% NS = 11,5% NS. Puidu niiskussisalduse tolerantsi intervalli prognoosi paranemine on ilmselt seotud mitme asjaoluga. Esiteks, praktikas läbi viidud eelnevalt kalibreeritud puidu niiskussisalduse ümberkalibreerimine, aga joonisel fig. 6 toimus originaalis elektrilise takistusmõõtja otsene kalibreerimine puiduniiskussisalduse mõõtjaks. Teiseks, tuntud puiduniiskussisalduse mõõtja oli elektritakistuste skaalas ülimalt laia mõõtepiirkonnaga (10 giga-oomi kuni mõnikümmend kilo-oomi), mis viis ilmselt alla elektritakistuse mõõtmistäpsuse üle 30% puidu niiskussisaldustel, lõppkokkuvõttes suurendades mõõtmistulemuste hajuvust.

Joonistel fig. 9, fig. 10 ja fig. 11 kasutatakse puidu laadumisarvu ideoloogia alusel koostatud kombineeritud muutujat ($R_{1n} + C_{1n}$) kalibreerimismudeli sõltumatu muutujana, et suruda kokku kalibreerimismudeli suurt hajuvust eeskätt puidu suurematel niiskussisaldustel.

Joonisel fig. 9 on kujutatud kombineeritud muutujast ($R_{1n} + C_{1n}$) sõltuv kalibreerimismudel puidu niiskussisalduse prognoosimiseks. Mõõtmiste koguarv mudeli kohta on $n=63$.

Joonisel fig. 10 on kujutatud võrdlusmudel puidu tegeliku niiskussisalduse ja muutuja ($R_{1n}+C_{1n}$)_e alusel prognoositud puidu niiskussisalduste võrdlemiseks, juhul kui on ära korrigeeritud puidu tegelikul niiskussisaldusel 105% NS juhuslike vigade kokkusurumisest tekkinud arvutuslik süstemaatiline viga 11,17% NS.

Võrreldes joonisel fig. 6 (R_{1n}) kujutatud mudelit ja joonisel fig. 9 kujutatud ($R_{1n} + C_{1n}$) mudelit, võib teha järelduse, et näiteks puidu tegelikul niiskussisaldusel 105% vähenes

üksikmõõtmise tolerantsi intervall vastavalt 20% NS kuni 7% NS. See tähendab, et elektrimahtuvuse lisamine kalibreerimismudelisse vähendab oluliselt üksikmõõtmise veahinnangut, ehk parandab kalibreerimismudeli kvaliteeti, eriti üle 100% puidu tegelikul niiskussisaldusel. Kui joonisel fig. 9 kujutatud mudeli korral kasutada 10 kordusmõõtmise võtet hajuvuse vähendamiseks, siis puidu 105% tegeliku niiskussisalduse prognoosimisel üksiku (antud juhul 10 kordusmõõtmise keskmine tulemus on mõistetav üksikmõõtmise tähenduses) mõõtmise alusel võib sattuda tolerantsi intervalli 7% NS asemel vaid intervalli 2,2% NS (vt joonis fig. 9). Joonisel fig. 10 võib täheldada väga kõrget $R^2=0,9885$ väärtust, mis viitab korregeeritud süstemaatilise veaga mudeli väga heale ennustuspotentsiaalile. Kui joonise fig. 10 põhjal on parima mudeliga puidu tegelikul niiskussisaldusel 105% üksikmõõtmisele prognoositud tolerantsi intervall 7% NS, siis puidu tegelikul niiskussisaldusel 77% NS on see 14,5% NS ja tegelikul puidu niiskussisaldusel 34% NS on üksikmõõtmise tolerantsi intervall vastavalt 12,1% NS. Niisiis on täheldatav üksikmõõtmisele prognoositud tolerantsi intervalli vähenemine suurematel, eelistatult üle 100% puidu niiskussisaldustel. Tulemus on täielikult vastuolus ainult puidu elektritakistusest sõltuva mudeli (vt joonis fig. 6) käitumisega.

Võrreldes joonisel fig. 9 kujutatud $(R_{1n} + C_{1n})$ mudelit ja joonisel fig. 12 kujutatud $(R_{1n} + C_{1n} + 1/(R_{1n} + C_{1n}))$ mudelit, võib täheldada, et komplitseerituma mudeli kasutamine ei anna erilist efekti lihtsama mudeliga (fig. 9) võrreldes. Näiteks 105% sanglepa puidu korral paranes prognoositud üksikmõõtmise tolerantsi intervall 7,17% NS kuni 7,15% NS, seega vaid 0,02%.

Kaudselt on puidu laadumisarvu ideoloogiaga seotud ka $(R_{1n} + R_{20n})$ kombineeritud muutujaga kalibreerimismudel, sest puidu elektritakistuse (R_{20n}) kasv laadumise 20. sekundiks on teatavas sünkroonis puidu elektrimahtuvuse kasvuga laadumise 20. sekundiks (vt. joonised fig. 3 ja fig. 4). Järgnevatel joonistel fig. 14, fig. 15 ja fig. 16 on kujutatud $(R_{1n} + R_{20n})$ tüüpi mudelite kasutusnäidised (lihtsuse huvides on graafikute pealkirjades alaindeksid ära jäetud).

Joonisel fig. 11 on kujutatud kombineeritud muutujast $\text{Log}(R_1 + R_{20})$ sõltuv kalibreerimismudel puidu üle 30% tegeliku niiskussisalduse prognoosimiseks. Mõõtmiste koguarv mudeli kohta on $n=63$.

Joonisel fig. 12 on kujutatud võrdlusmodel puidu tegeliku niiskussisalduse ja muutuja $\text{Log}(R_{1n} + R_{20n})$ alusel prognoositud puidu niiskussisalduste võrdlemiseks.

Joonisel fig. 13 on kujutatud võrdlusmodel puidu tegeliku niiskussisalduse ja muutuja $(R_{1n} + R_{20n})$ alusel prognoositud puidu niiskussisalduste võrdlemiseks, kui on tehtud $k=10$ kordusmõõtmist, st eelmisel joonisel fig. 15 kujutatud võrdlusmodelit on hajuvuse vähendamiseks valideeritud 10 kordusmõõtmise korral.

Joonisel fig. 14 on kujutatud kalibreerimismudel kombineeritud sõltumatu x -muutujaga $R+0.00005 \cdot C^3$ ehk edaspidi lühendatult nimetatud (R+Par5) kalibreerimismudel, mis ei vaja enam süstemaatilise vea korrigeerimist nagu R+C mudel (vt joonis fig. 10), sest R+Par5 muutuja kasutamisel süstemaatilist viga ei teki.

Joonisel fig. 15 on kujutatud võrdlusmodel tegeliku niiskussisalduse ja joonisel fig. 17 kujutatud kalibreerimisfunktsiooni abil prognoositud niiskussisalduste võrdlemiseks ja mudeli ennustuspotentsiaali hindamiseks.

Joonisel fig. 16 on kujutatud R+Par5 kalibreerimismudel juhul, kui on tehtud $k=10$ kordusmõõtmist.

Joonisel fig. 17 on kujutatud võrdlusmodel tegeliku puidu niiskussisalduse ja joonisel fig. 19 kujutatud kalibreerimismudeli abil prognoositud puidu niiskussisalduste võrdlemiseks, juhul kui on tehtud $k=10$ kordusmõõtmist.

Joonisel fig. 18 on kujutatud eri mudelite tolerantsi intervallid: a) tavalise elektritakistusest R oleneva kalibreerimismudeli prognoositud üksikmõõtmise tolerantsi intervall (joonisel punktirjoon), b) kombineeritud muutujaga R+C mudeli abil leitud üksikmõõtmise tolerantsi intervall (joonisel paks pidevjoon) ja c) tegeliku puidu niiskussisalduse tolerantsi intervall (joonisel kriips-punktjoon) omavaheliseks võrdlemiseks.

Jooniselt fig. 18 nähtub graafiliselt, kuidas käituvad eri sõltumatu x -muutujaga mudelite tolerantsi intervallid puidu tegeliku niiskussisalduse kasvades. Punkt-kriipsjoon tähistab puidu tegeliku niiskussisalduse tolerantsi intervalli, aga kuna see on nii kitsas (alla 1% NS),

- ei tule siis joonisel vahemik nähtavale, on ainult üks punkt- kriipsjoon. Punktirjoon tähistab tavalise elektritakistusest R oleneva kalibreerimismudeli poolt prognoositud tolerantsi intervalli üksikmõõtmise jaoks. Sellise trendi tõi esmakordselt välja Edwards 1974 aastal. Paks pidevjoon joonisel tähistab kombineeritud muutujaga R+C mudeli abil leitud tolerantsi intervalli käitumist. On näha, et esialgu on käitumine samane Edwardsi trendiga, kuid alates 5 puidu tegelikust niiskussaldusest 78% NS pöördub trend Edwardsi trendiga vastupidiseks, ja algab tolerantsi intervalli kokku surumine puidu suurematel tegelikel niiskussaldustel, mis tähendab, et hakkab toimima laadumisarvu ideoloogia. Selline tolerantsi intervalli kokkusurumine on uus võrreldes tuntud tehnika tasemega.
- 10 Võrreldes omavahel joonisel fig. 9 kujutatud ($R_{1n}+C_{1n}$) mudelit ja joonisel fig. 14 kujutatud ($R_{1n}+R_{20n}$) mudeleid puidu 105% tegeliku niiskussalduse juures, võib täheldada (R_1+R_{20}) mudeli ligikaudu kaks korda suuremat hinnangut üksikmõõtmise tolerantsi intervallile, mis suurenes 7%NS kuni 13,44%NS ja 10 kordsmõõtmise jaoks (vt joonis fig. 16) vastavalt 2,2% NS kuni 8,1% NS. Teiselt poolt aga, võrreldes fig. 16 ja fig. 10 üksikmõõtmise 15 tolerantsi intervalle ülejäänud kahes niiskusrühmas puidu tegeliku niiskussaldusega 78% NS (T. I.=21% vs. 14,5%) ja 34%NS (T. I.=8,6% vs 12,1), võib täheldada, et tolerantsi intervall väheneb mudelis fig. 10 niiskusrühmas 78%NS ja vähesel määral suureneb niiskusrühmas 34%NS.
- 20 Käesolevas tehnilises lahenduses sisaldavad mõõte-elektroodid kahte sümmeetrilist, ettenähtud omavahelise distantsiga isoleeritud nõel-elektroodi, mis on sisestatud puitu teatavale sügavusele puidu pinnast (tavaliselt 1/3 puidu paksust), ja mille vahele on rakendatud konstantne alalispinge ehk puidu laadumispinge.
- Kalibreerimismudeli ennustuspotentsiaali on võimalik vastavalt kasutaja soovidele kohandada (näiteks võib sobiva mudeli valikuga garanteerida parema ennustuspotentsiaali 25 puidu suurematel niiskussaldustel).
- Niiskusmõõturi kalibreerimise mudel on oma olemuselt statistiline regressioonmudel. Kalibreerimismudel koostatakse konkreetse empiiriliste katseandmete hulga ehk valimi põhjal. Kalibreerimismudeli kõige olulisemaks elemendiks on kalibreerimisfunktsioon, mis esitatakse matemaatilise avaldise kujul ja seda teades on võimalik iga mõõdetud sõltumatu

x-muutuja (puidu elektritakistus R, puidu elektrimahtuvus C, või mõni nende kahe parameetri summa) jaoks välja arvutada puidu niiskussisalduse väärtus, mis on kalibreerimisfunktsiooni seisukohalt sõltuv y-muutuja.

- 5 Kalibreerimismudelid on leitud empiirilisel, katse-eksimuse meetodil, mistõttu ei ole nende puhul tegemist teoreetilisel tuletatud matemaatiliste avaldistega.

Niiskusemõõtur töötab järmselt. Niiskusemõõturi töö kirjeldamisel eeldatakse, et seade on töökorras, st enne mõõtmiste alustamist on seadet testitud mõõtepiirkonnale vastavalt valitud täppistakistitega. Niiskusemõõturi töökorras oleku testimine ei ole kokkuleppeliselt mõõtmisprotsessi osa.

- 10 Mõõtmisprotsessi võib tinglikult jagada üksteisele järgnevateks sammudeks või toiminguteks või etappideks.

- Esimene samm on järgmine. Mõõteelektroodid 1 ja 2 vajutatakse puitmaterjali 11 (tavaliselt laud, plank või pruss üle 30% algniiskussisaldusega) sisse, tavaliselt 1/3 materjali paksuse sügavusele, nii et puidu elektritakistus R_x moodustuks puidu pikikiudu suunaga risti olevas suunas, tavaliselt 30 mm elektrootide vahekaugusega (juhul kui kalibreerimismudeli korratavuse tingimused ei näe ette teistsugust suunda või teistsugust vahekaugust). Vältimaks voolu teekonda mööda puidu pinnakihti, peavad mõõte-elektroodid olema osaliselt isoleeritud, nii et voolu juhiks ainult nõelelektroodide 1 ja 2 puitu sisestatud koonusekujuline osa. Seejärel ühendatakse mõõteelektroodid varjestatud koaksiaalkaabliga,
- 20 nii et elektroot 2 ühendatakse niiskusemõõturi mittetundliku terminaali abil tugipinge allikaga 3 ja tundliku terminaali abil plokiga 5 punktiga O. Seejuures tuleb jälgida, et seadme tundlik osa ei saaks juhmete paigaldamise käigus elektrostaatilist laengut, mis võib parimal juhul moonutada mõõtmistulemusi, halvimal juhul aga ka seadme rikkuda. Mõõtmisprotsessi esimene samm on vajalik teha käsitsi (kui seda ei tee robot). Kuna
- 25 niiskusemõõturi mõõtmisprotsess on eelprogrammeeritav ja mikroarvuti 6 poolt juhitud, siis edasine toimub automaatselt.

Teine samm on tegelik mõõtmine. Võimendile A1 tehakse nullikontroll ja sellele järgneb katseandmete kogumine 20 sekundi jooksul varem seadistatud mõõteintervalliga. Mõõtmise toorandmetes filtreeritakse täiendavalt digitaalselt müra, arvutatakse reaalaajas puidu

elektritakistus ja elektrimahtuvus, salvestatakse katseandmete ja varustatakse failinimega. Järgneb etteantud pikkusega paus, seejärel algab mõõtmise katseandmete kogumine 20 sekundi jooksul otsast peale. Mõõtmistsükkel 20 sekundit ja etteantud pikkusega paus on seadme kasutamise mugavuse huvides markeeritud nii heli- kui ka valgussignaaliga. Pausi

5 võib mikroarvuti vastavalt programmile kasutada eelmise mõõtmise katseandmete esmaseks statistiliseks töötlemiseks. Samuti võib pausi kasutada mõõteelektroodide puidul järgmisse asukohta sisestamiseks.

Kolmas samm on andmeanalüüs mikroarvutis 6 ja puidu niiskussisalduse mõõtetulemuse väljastamine numbriliselt displeile 7 koos statistiliste usalduspiiridega. Andmeanalüüsil

10 kasutatakse käesoleva seadme jaoks spetsiaalselt välja töötatud kalibreerimismeedotid, mille rakendamise tulemusena leitakse teaduslikult põhjendatud hinnang puidu niiskussisaldusele üle kiu küllastuspunkti niiskussisaldustel.

Puidu elektrilise laadumise efektiga niiskusemõõtur puidu küllastuspunkti suurema niiskussisalduse mõõtmiseks võimaldab reaajas registreerida ja salvestada mikroarvuti

15 mallu puidu elektritakistuse ja puidu elektrimahtuvuse ajalised käigud puidu elektrilise laadimise tsükli jooksul, eelnevalt valitava mõõtmiskiirusega.

Pärast mõõtmiste lõppu töödeldakse mõõtmisandmete fail seadme mikroarvutis vastavalt valitud kalibreerimismudelile ja väljastatakse puidu niiskussisalduse prognoos koos statistilise vea hinnanguga. Puidu elektrilise laadumise meetod puidu niiskussisalduse

20 määramiseks puidu kiu küllastuspunkti kõrgema niiskussisalduse korral iseloomulikuks tunnuseks on see, et toimub puidu kiu küllastuspunkti kõrgema niiskuse mõõtmisel mõõtemääramatuse oluline kahanemine puidu niiskussisalduse kasvades. Mõõtemääramatuse kahanemine, eriti puidu suurtel niiskussisaldustel 100% ja enam, on saavutatud originaalse puidu laadumisarvu kasutusele võtuga ja selle arvestamisega

25 kalibreerimismudeli koostamisel.

Niiskusemõõturi mõõtmistäpsust on suurendatud kalibreerimismudelite kasutusele võtuga. Niiskusemõõturi kalibreerimismudelite tekitamisega ehk sisuliselt niiskusemõõturi ümberkalibreerimisega ei õnnestunud kõrvaldada suuri juhuslikke vigu üksikmõõtmisele antavas veahinnangus. Näiteks 90% tegeliku niiskussisaldusega (tegelik niiskussisaldus

määrati kuivkaalu meetodil vastavalt standardile ISO3130:1975) puidu jaoks mudeli abil prognoositud üksikmõõtmine võis sattuda 95% usaldatavusega niiskussisalduste vahemikku 72,5% kuni 105,5% niiskussisaldust. Toodud näites oli üksikmõõtmisele hinnanguliselt omistatav niiskussisalduse tolerantsi intervall 35% niiskussisaldust, ja seda 95%
 5 usaldusnivool. Saadud statistiliste regressioonimudelite (st niiskusmõõturite uute kalibreerimismudelite) usaldusväärsust kontrolliti mitteparameetriliste Kolmogorov-Smirnov- ja Shapiro-Wilk-testidega. Leiti, et kõik leitud mudelid olid statistiliselt usaldusväärsed.

10 Modelleerimise teiseks oluliseks järelduseks on fakt, et leitud regressioonimudelite jääkstandardhälve vähenes üllatavalt kiiresti koos tehtud kordusmõõtmiste arvuga – see tähendab seda, et mudelid olid statistilises mõttes hästi koonduvad. Seega optimaalselt valitud kordusmõõtmiste arv (10 ja enam) võimaldas oluliselt parandada kalibreerimismudelite kvaliteeti ja alla suruda puidu niiskussisalduse juhuslikke mõõtmisvigu üle 30% niiskussisalduse piirkonnas.

15 Käesolevas tehnilises lahenduses sisaldavad mõõte-elektroodid kahte sümmeetrilist isoleeritud nõel-elektroodi, omavahelise distantsiga 30 mm, mis on sisestatud puitu teatavale sügavusele puidu pinnast (tavaliselt 1/3 puidu paksust), ja mille vahele on rakendatud konstantne alalispinge ehk puidu laadumispinge.

20 Puidu elektrilise laadumise efektiga niiskusemõõturite abil on osutunud võimalikuks vabaneda tuntud takistustüüpi puidu niiskusemõõturitele iseloomulikust progresseeruvast laienevast veakoridorist, ja seda ilma puidu elektritakistust logaritmitamata ning kordusmõõtmisi sooritamata.

25 Leuitise olemus ei piirdu kitsalt ülaltoodud teostusnäitega, vaid võimaldab mitmeid edasiarendusi modelleerimise valdkonnas. Näiteks ei ole ülaltoodud teostusnäites esitletud ajahetke $t = 0,1$ sekundit jaoks $R(0,1)_{1n}$, $C(0,1)_{1n}$ ja nende kombinatsioonide alusel saadud kalibreerimismudeleid. Ka kombineeritud muutujate võimalik valik ei ole selles teostusnäites sugugi ammendav.

PATENDINÕUDLUS

1. Niiskusmõõtur puidu elektrilise laadumise efektiga puidu küllastuspunktist suurema niiskussisalduse mõõtmiseks, mis sisaldab kahte mõõteelektroodi (1) ja (2), stabiilset tugipingeallikat (3), elektromeetrilise sisendiga eelvõimendit (A1) ning analoog-
 5 digitaalmuundurit (5), **mis erineb selle poolest**, et sisaldab täppistakistit (10) elektromeetrilise sisendiga eelvõimendi (A1) tagasisideahelas, elektrooniliste aktiivfiltrite plokki (8), mis sisaldab filtreid madalsageduslike ning kõrgsageduslike mõõtemürade filtreerimiseks operatsioonivõimendi A2 ja kondensaatori C1 abil, mikroarvutit (6) mõõtmisprotsessi juhtimiseks ning LCD displeid (7), kusjuures mikroarvutisse (6) on
 10 sisestatud matemaatilised avaldised, mistõttu mõõtmisprotsess on täielikult automatiseeritud.
2. Niiskusmõõtur vastavalt nõudluspunktile 1, **mis erineb selle poolest**, et mõõteelektroodideks (1) ja (2) on korrosioonivabad isoleeritud süsinikkiud-nõel-elektroodid.
- 15 3. Niiskusmõõtur vastavalt nõudluspunktile 1, **mis erineb selle poolest**, et mõõteelektroodideks (1) ja (2) on korrosioonivabad isoleeritud elektroodid, mis on valmistatud roostevabast terasest.
4. Niiskusmõõtur vastavalt nõudluspunktile 1, **mis erineb selle poolest**, et
 20 mõõteelektroodideks (1) ja (2) on korrosioonivabad isoleeritud elektroodid, mis on valmistatud alumiiniumsulamist.
5. Meetod puidu elektrilise laadumise efektiga puidu küllastuspunktist suurema niiskussisalduse mõõtmiseks, mille kohaselt mõõdetakse puidus puidu elektritakistust (R_x),
mis erineb selle poolest, et mõõdetud laadumisvoolu ajalise käigu alusel leitakse reaalarvas puidu elektrimahtuvus (C) eri ajamomentidel ning määratakse puidu laadumisarv
 25 kalibreerimismudeli koostamiseks ja valideerimiseks, kusjuures mõõtmisprotsessi juhitakse digitaalselt.
6. Meetod vastavalt nõudluspunktile 5, **mis erineb selle poolest**, et puidu laadumisarvu, mille järgi puidu elektritakistus on pöördvõrdelises sõltuvuses puidu elektrimahtuvusest

kõigil kalibreerimismudelil erinevatel puidu tegelikel niiskussisaldustel, kasutatakse elektritakistuste hälvete koondamiseks kalibreerimismudelil elektrimahtuvusest sõltuva muutuja integreerimisega kalibreerimismudelisse, kusjuures kalibreerimismudelina kasutatakse statistilist regressioonimudelit, mis koostatakse empiiriliste katseandmete hulga

5 põhjal.

7. Meetod vastavalt nõudluspunktidele 5 ja 6, mis **erineb selle poolest**, et elektrimahtuvusest sõltuvaks muutujaks on laadumisarvu kaudu puidu elektritakistus ning niiskussisaldus.

8. Meetod vastavalt nõudluspunktidele 5 kuni 7, mis **erineb selle poolest**, et puidu elektrilist laadumist iseloomustavate muutujate, elektritakistuse R_x ja elektrimahtuvuse C_x mõõdetakse

10 parima võimaliku täpsusega konstantsel laadumisingel potentsiostaatilises laadimisrežiimis.

9. Meetod vastavalt nõudluspunktidele 5 kuni 8, mis **erineb selle poolest**, et ühe mõõtetsükli jooksul kogutakse hulk katseandmeid, saadud katseandmeid töödeldakse, milleks kasutatakse matemaatilisi seoseid ning mille tulemusena parandatakse kalibreerimismudeli

15 kvaliteeti.

10. Meetod vastavalt nõudluspunktidele 5 kuni 9, mis **erineb selle poolest**, et kogutud katseandmed töödeldakse mikroarvuti abil, ning millega registreeritakse elektritakistuse ja elektrimahtuvuse ajalised käigud.

1/9

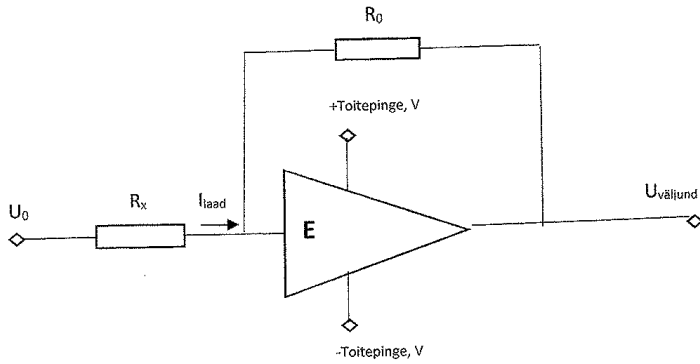


Fig 1

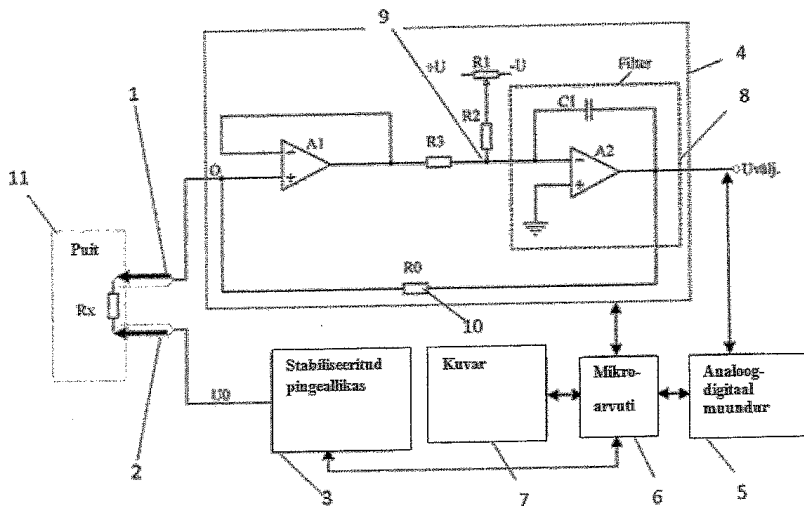


Fig 2

2/9

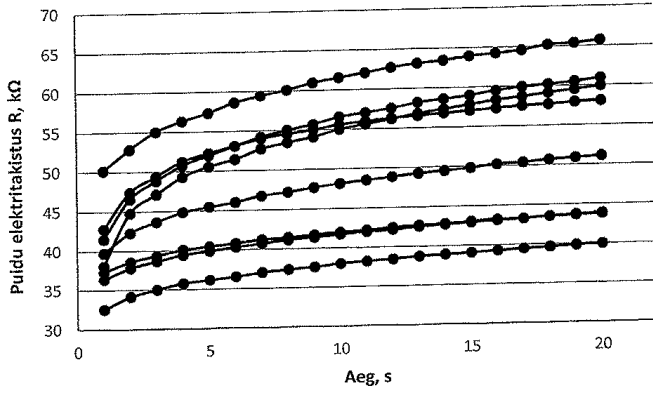


Fig 3

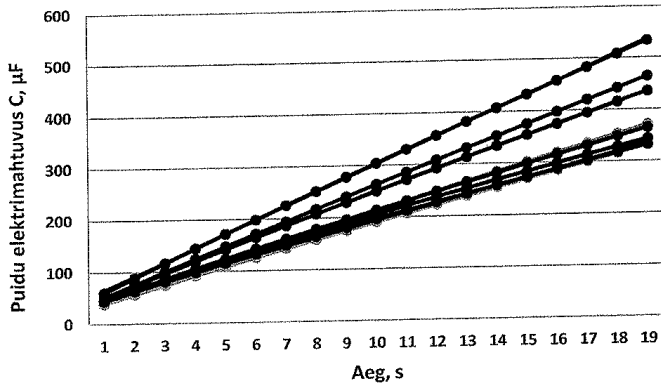


Fig 4

3/9

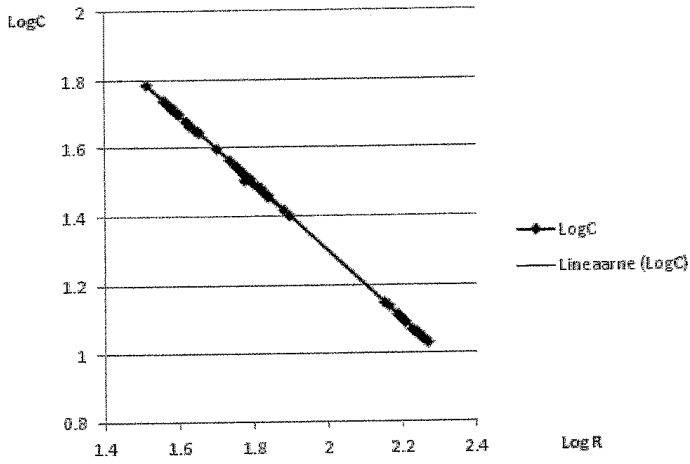


Fig 5

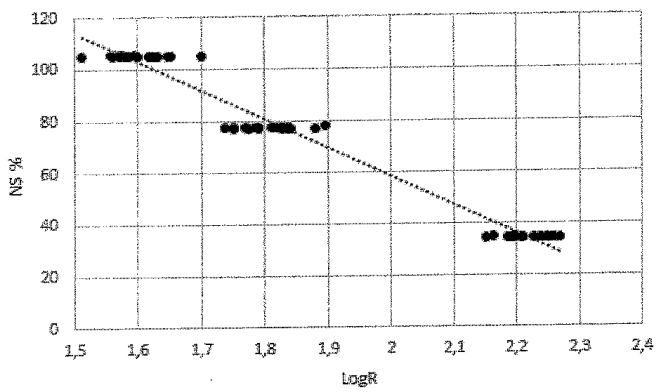


Fig 6

4/9

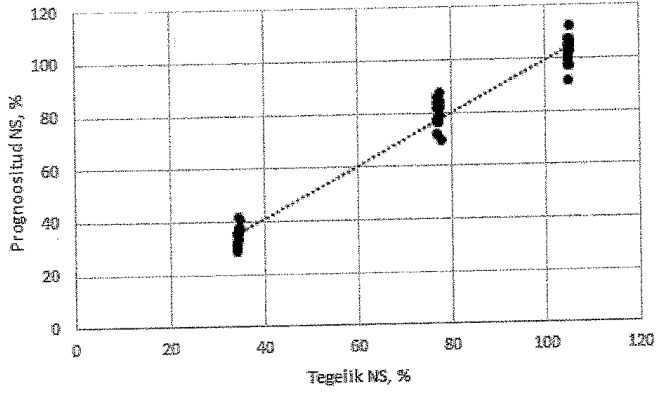


Fig 7

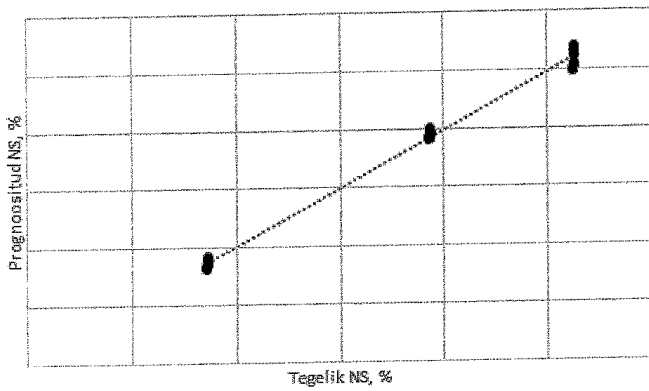


Fig 8

5/9

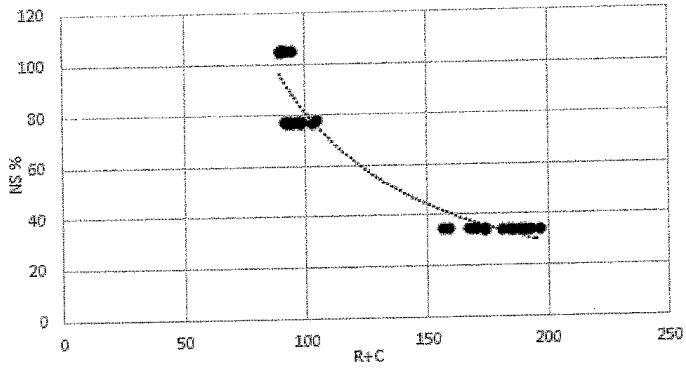


Fig 9

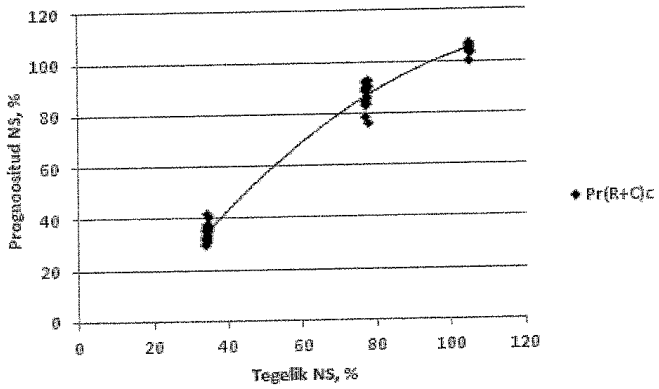


Fig 10

6/9

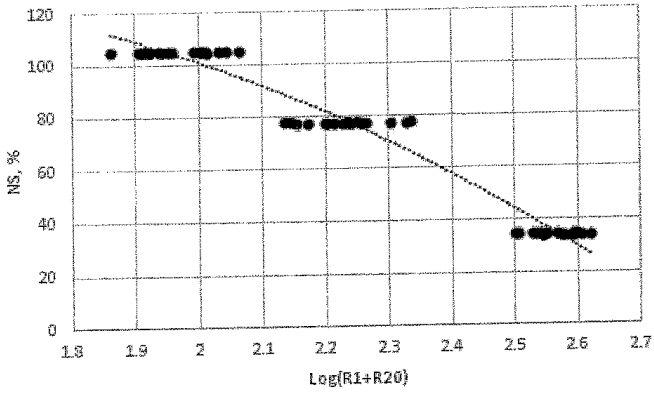


Fig 11

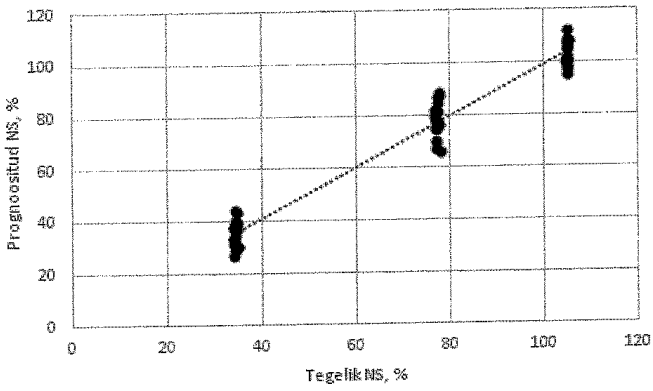


Fig 12

7/9

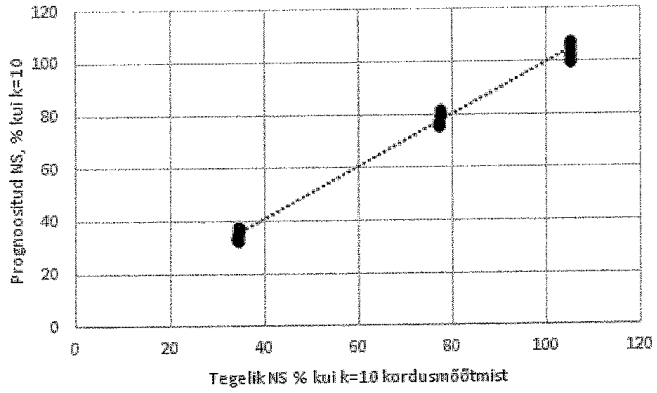


Fig13

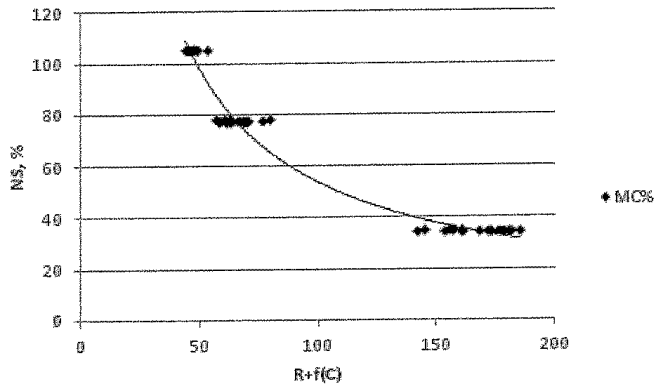


Fig 14

8/9

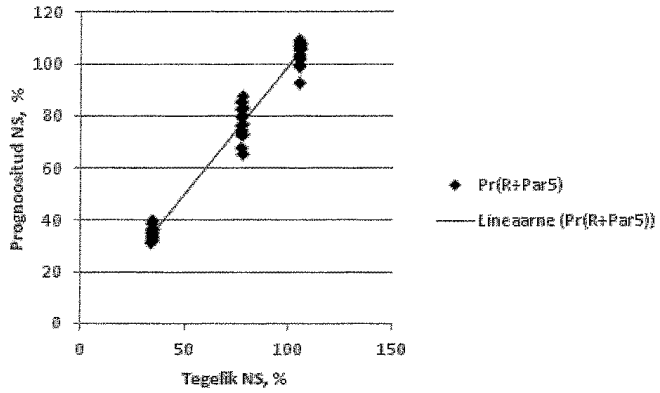


Fig 15

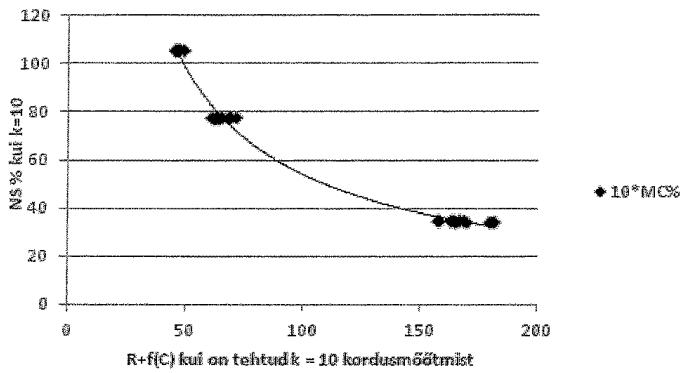


Fig 16

9/9

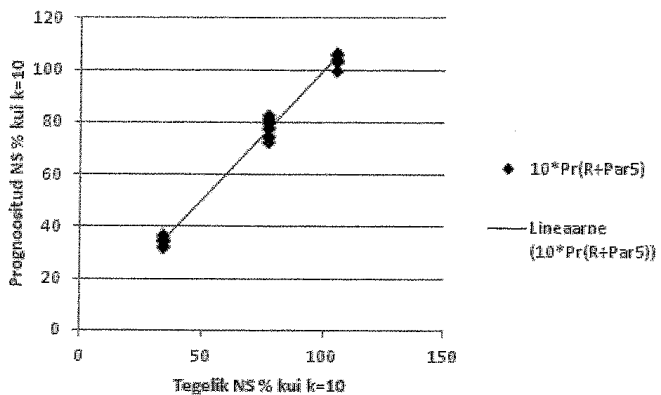


Fig 17

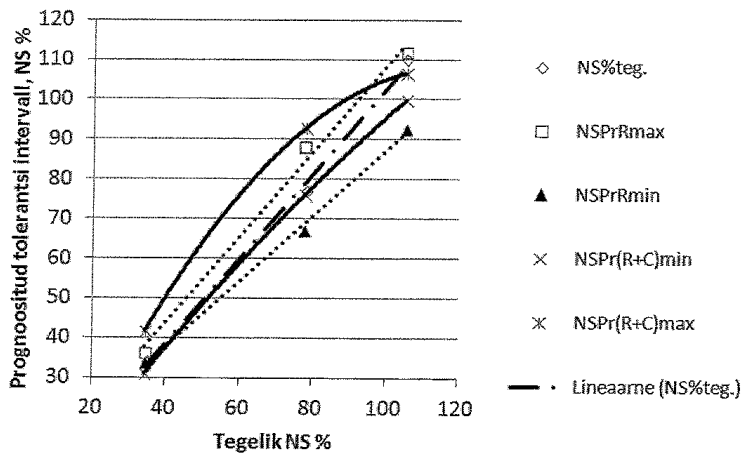


Fig 18



Tamme, V., **Tamme, H.**, Miidla, P., Muiste, P., 2021. Novel polarization-type moisture meter for determining moisture content of wood above fibre saturation point. *European Journal of Wood and Wood Products*, 79: 1577–1587.



Novel polarization-type moisture meter for determining moisture content of wood above fibre saturation point

Valdek Tamme¹ · Hannes Tamme¹ · Peep Miidla² · Peeter Muiste¹

Received: 18 March 2020 / Accepted: 1 March 2021

© The Author(s), under exclusive licence to Springer-Verlag GmbH Germany, part of Springer Nature 2021

Abstract

Resistance-type wood moisture meters are not reliable at moisture contents above the fibre saturation point. The aim of this study was to develop an alternative polarization-type wood moisture meter and to analyse the different calibration methods of this moisture meter in comparison with the traditional resistance-type wood moisture meter calibration method. A significant decrease (up to 3.5% of moisture content) in the tolerance interval of a single measurement was attained by introducing and integrating the original electrical wood charging number into the calibration model of the novel wood moisture meter with electric polarization effect for a high wood moisture content (MC) above 100%. The tolerance interval convergence was analysed using the traditional method of increasing the number of measurements and averaging the results and was compared to the novel method of compensating for random deviations, as used in this study. To calibrate the wood moisture meter, the wood's electrical resistance and electrical capacitance timelines during the electrical charging cycle were registered in real time (online) with a preselected measuring speed and saved to the microcomputer memory. When the measurements were completed, the measurement data was processed by the device's microcomputer. This novel polarization-type moisture meter allows for the moisture content of specific tree species to be predicted by selecting a suitable calibration model from a set of eight. The novel wood moisture meter can be used to monitor wood drying and to determine seasonal variations in the moisture content of growing trees.

1 Introduction

Stamm (1927) presented the idea of determining wood moisture content on the basis of measuring wood electrical conductance. Since then, wood moisture meters operating on that principle have been industrially manufactured in series and are still widely used today. Well-known producers include Gann (2019), NdtJames (2020), Brookhuis (2009), BES Bollmann (2020), and others. Both the direct current (DC) method (Stamm 1927; Vermaas 2002; Tamme 2016) and alternating current (AC) method (James 1993; Zelinka et al. 2007; Tiitta et al. 1999) have been used to study wood electrical resistance. Zelinka et al. (2007) compared Stamm's results for wood DC resistance to the alternating current method. Comprehensive research comparing the

electrical resistance of wood using the DC and AC methods has also been carried out by Gao et al. (2018) and Berga et al. (2019). For the moisture content range below the wood fibre saturation point (FSP), the electrical resistance method may be considered a reliable method of measurement (Forsén and Tarvainen 2000).

For moisture contents above the FSP, the electrical resistance method is generally deemed to be unreliable (Edwards 1974; ASTM D4444-08 2008; Vermaas 2002; Tamme et al. 2014). For that moisture content range above FSP, wood electrical resistance becomes dependent on time, and deposits may appear on the measuring electrodes during long-duration measurements (Skaar 1964). However, the appearance of the deposits—or in other words, an absorption layer and hydrogen bubbles on the measuring electrodes—can be minimized by selecting optimal values of current density and voltage (Romann et al. 2014). Tamme et al. (2013) and Tamme (2016) described the polarization-depolarization (PD) method for determining wood electrical resistance. For moisture contents above the FSP this allows the wood electrical resistance and wood electrical capacitance to be established in moisture contents above FSP during a 20-s

✉ Valdek Tamme
valdek.tamme@emu.ee

¹ Estonian University of Life Sciences, Kreutzwaldi 1,
51006 Tartu, Estonia

² University of Tartu, Ülikooli 18, 50090 Tartu, Estonia

polarization cycle followed immediately by a 20-s depolarization cycle. The PD method has been the basis for developing and patenting a wood moisture meter with wood electric charging effect (so-called polarization-type wood moisture meter) (Tamme et al. 2020).

The main objective of this research was to develop the concept of a polarization-type moisture meter and a prototype thereof using the PD method for determining wood moisture content above the FSP, and to formulate principles for calibrating such a moisture meter.

2 Materials and methods

2.1 Theoretical background

2.1.1 Dependence of wood electrical resistance and wood electrical capacitance on time

Tamme et al. (2013) discovered that wood electrical resistance depends on time (t) logarithmically at wood moisture contents above the FSP, and wood electrical capacitance depends on time linearly:

$$R(t) = a \cdot \ln(t) + b \quad (1)$$

$$C(t) = c \cdot t + d \quad (2)$$

where $R(t)$ is resistance, $C(t)$ is wood electrical capacitance, and the a , b , c and d constants are the location at which the specific moisture content of wood is measured.

In the doctoral thesis by Tamme (2016), it was demonstrated that above the wood FSP, the time-dependent electrical resistance $R(t)$ or polarization resistance also depends significantly on moisture content. He found that the increase in the moisture content (MC) results in a greater relative gain of the polarization resistance. He also found that the electrical resistance of wood below the FSP is no longer time dependent, but rather depends on the MC according to the modified Stamm formula. Electrical resistance was found using the PD method, as a result of measuring the voltage polarized in wood and the polarization current. It was established that it is possible to improve the accuracy of prediction of wood moisture content when using both resistance and capacity measurements (Sect. 3.4: Model types A, B, and C).

2.1.2 Statistical processing of measurement data on actual wood moisture content, wood electrical resistance and wood electrical capacitance

The statistical processing of experimental data is methodologically based on a linear and non-linear regression

analysis, which allows independent properties to be studied in association (Sachs 1982), and on retrieving measurement or calibration models (ISO 1993), as well as implementation models or calibration reference models. By using the calibration function, the calibration model allows the value of MC to be calculated for any electrical resistance, electrical capacitance, or combination thereof. The reference model allows any measured average MC (for example, the dry mass method or gravimetric method) to be compared to the respective MC predicted with the calibration model. The reference model does not require the mathematical presentation of the calibration function. Essentially, the reference model is a calibration model validation test, done under repeatability conditions (ISO/EIC 2008; Laaneots and Mathiesen 2006).

In the case of Student t-distribution and linear regression for the single measurement, the upper and lower tolerance lines (confidence limits) of the regression line are presented in MS Excel at the 95% confidence level as follows (Kiviste 1999):

$$\text{Intercept } b_{0\text{lower}} = b_0 - TINV(\alpha;n-2) * s_{b_0} \quad (3)$$

$$\text{Intercept } b_{0\text{upper}} = b_0 + TINV(\alpha;n-2) * s_{b_0} \quad (4)$$

$$\text{Slope } b_{1\text{lower}} = b_1 - TINV(\alpha;n-2) * s_{b_1} \quad (5)$$

$$\text{Slope } b_{1\text{upper}} = b_1 + TINV(\alpha;n-2) * s_{b_1} \quad (6)$$

where s_{b_0} and s_{b_1} are the standard errors of the regression line intercept and slope (Kiviste 1999).

To obtain the convergence of measuring deviations, non-linear regression analysis was carried out for the focusing reference models (Sect. 3.4: Model types A, B, and C). The tolerance intervals, presented as linear functions, were calculated using formulae (3)–(6). For both methods the formulae used for calculating the tolerance intervals are presented in Table 1, column 3: “Equations for calculating single measurement tolerance intervals (T. I.)”.

Calibration models and reference models can also be constructed using single measurements which are not exactly single measurements, but rather arithmetic average values of a given number (e.g., $k=4, 10, 16$, etc.) of single measurements (that is, they are a series of measurements) (Laaneots and Mathiesen 2006) that are viewed as single measurements when producing regression models. Such models could also be called multiple models.

2.2 Materials and calibration procedure of moisture meter with electrical polarization effect

The compilation of a regression model for the calibration of the wood moisture meter first requires that the actual

Table 1 Relevant reference models (RM) with the statistical characteristics for above FSP wood moisture content

Mod. No. Obs. No. Fig. No.	Model type	Equations for calculating single measurement tolerance intervals (T. I.)	R ²	p-value	Focal point on MC% ^a	Calculated MC range where T. I. < 3.5% MC (acc. Rozema 2010)
RM2 N = 63 Figure 9	R-mod	$y_{upper} = 1.2075x - 4.888$ $y_{lower} = 0.796x + 3.897$	0.96	< 0.01	30	> 3.5%
RM3 N = 63 Figure 9	LogR	$y_{upper} = 1.0071x + 7.6164$ $y_{lower} = 0.8924x - 1.14$	0.99	< 0.01	30	> 3.5%
RM4 N = 63 Figure 10	(R + C) (Type A)	$y_{upper} = -0.0015x^2 + 1.14x + 4.01$ $y_{lower} = 0.0052x^2 + 0.2717x + 14.2$	0.99	< 0.01	117	110–120
RM5 N = 63 Figure 11	R + f(C) (Type A)	$y_{upper} = -0.0009x^2 + 1.12x + 1.07$ $y_{lower} = 0.0033x^2 + 0.407x + 13.8$	0.98	< 0.01	151	142–151
RM6 N = 63	R _{1a} + R _{30n} (Type B)	$y_{upper} = -0.0012x^2 + 1.09x + 11.2$ $y_{lower} = 0.0061x^2 - 0.022x + 31.5$	0.97	< 0.01	129	123–133
RM7 N = 63 Figure 12	f(R ₁ + R ₂₀) (Type B)	$y_{upper} = -0.0042x^2 + 1.549x - 5.47$ $y_{lower} = 0.0072x^2 - 0.1469x + 32.7$	0.97	< 0.01	120	116–124
RM8 N = 18 k = 16 Figure 13	k*R (Multiple model)	$y_{upper} = 0.998x + 1.3446$ $y_{lower} = 0.9852x + 0.3413$	0.99	< 0.01	30	30–151
RM9 N = 63 Figure 14	f(R) + f(C) (Type C)	$y_{upper} = 1.03767x - 2.0483$ $y_{lower} = 1.01872x - 3.5253$	0.99	< 0.01	78	30–105

The independent x variable in all RMs is the actual wood moisture content, the dependent y variable in all RMs is the predicted wood moisture content

^aThe model focal point has been defined as the specific value of actual wood moisture content, when the calculated tolerance interval reaches the minimal value

average MC be determined by successively weighing the specimen while it is drying at randomly selected moments of time and thereafter establishing the dry weight of the specimen according to ISO 3130:1975 (1975). The wood electrical resistance and wood electrical capacitance are measured almost simultaneously with the weight, at the same moisture content. The described procedure was repeated 63 times at a constant temperature of 50 degrees Celsius, but each time at a different average moisture content level of *Alnus glutinosa* wood, whereas the electrical resistance and electrical capacitance were measured by inserting the electrodes in a new location in the wood specimen for each measurement. The selected specimen was a massive board with dimensions of 500 mm in length (along the fibres), 150 mm in width (perpendicular to the grain in the tangential direction), and 35 mm thick (in a radial direction perpendicular to the grain). The tangential distance between the corrosion-free pin electrodes was 30 mm and remained the same throughout all the measurements (Brookhuis 2009 instruction manual; Tamme et al. 2011). The electrodes were inserted into the specimen at a depth of one-third of the board's thickness (EDG 2010)

(about 12 mm deep). The random spots of insertion of the two measuring electrodes, 30 mm apart on the test specimen, were generally called measuring points.

2.3 Technical background

Figure 1 presents the circuit diagram of the moisture meter with wood electrical polarization effect, whereas the functional elements of the moisture meter are shown as a block diagram with arrows. The circuit diagram given in Fig. 1 has no analogue power circuits or chains of noise signal analogue filters. The advantage of the principle circuit shown in Fig. 1 lies in the simple calculation formulae (Keithley 2004) that apply at any moment of time in the case of a one-second measurement interval:

$$R_x = U_{out} \frac{R_0}{U_0} \tag{7}$$

where R_x is wood electrical resistance in ohms, U_{out} is the output voltage of the electrometer in volts, R_0 is the

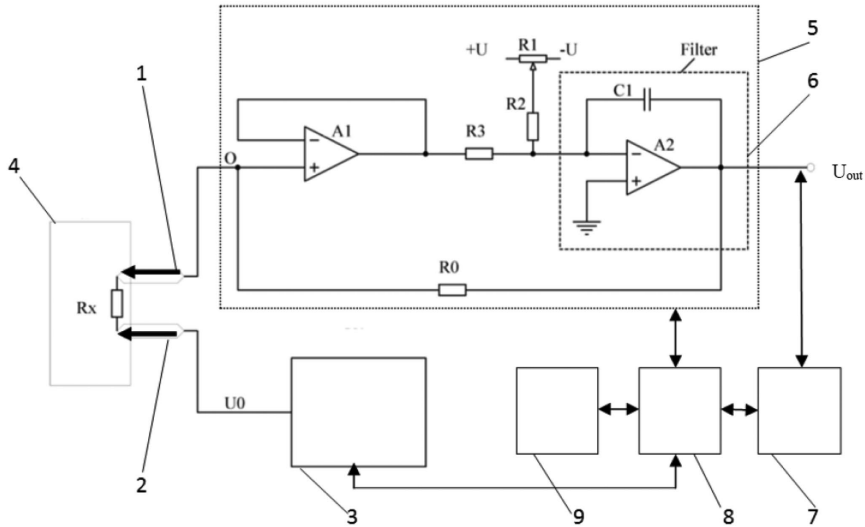


Fig. 1 Block scheme of the wood moisture meter prototype. 1,2—measuring electrodes; 3—stabilised support voltage source 1.024 V; 4—wood being measured for electrical resistance R_x ; 5—analogue

part of the wood moisture meter; 6—analogue noise filter block; 7—analogue/digital converter; 8—microcomputer; 9—LCD display

resistance of the electrometer feedback resistor in ohms, U_0 is the stabilized support (or reference) voltage, 1.024 V.

The wood polarization current I_{pol} in amperes is calculated using the following formula (Keithley 2004; Eco Chemie 2019a):

$$I_{pol} = \frac{U_0}{R_x} \quad (8)$$

and wood electrical capacitance is calculated using the following formula (Eco Chemie 2019b):

$$C_x = \frac{Q}{U_0} \quad (9)$$

where C_x is wood electrical capacitance in farads, and Q is wood electrical charge in coulombs.

The specific value of Q is determined at any given moment with a one-second interval by numerical integration of the polarization current I_{pol} which, in turn, is carried out in real time with a microcomputer controlling

the operation of the device. The method described above for determining electrical capacitance C_x generally corresponds to the current integrator method (Eco Chemie 2019b).

3 Results and discussion

3.1 Linearity and noise study of moisture meter

Figure 2 shows a simple check on the output of the moisture meter using a reference resistor (not wood) to illustrate the linearity of response.

Figure 2 indicates the excellent linearity of the useful signal (solid line). The figure shows a signal-to-noise ratio (SNR) of about 1000, a positive result.

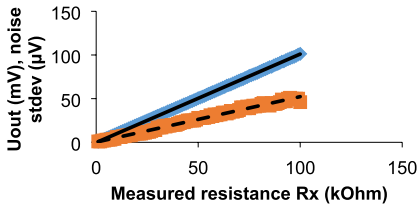


Fig. 2 Input-output connection linearity test of the analogue part of the moisture meter prototype, with the useful signal (solid line) and noise signal standard deviation (dashed line). Number of measurements $N = 123$

3.2 Wood electrical resistance and wood electrical capacitance in moisture contents above the FSP

Typical experimental time dependence of wood electrical resistance and wood electrical capacitance at 105% MC (above the FSP) fitted to formulae (1) and (2) are given in Figs. 3 and 4.

The figures indicate that electrical resistance and electrical capacitance measured at the first second have the smallest variance. The variation coefficient for R_{1s} is 9.7% and for electrical resistance R_{20s} measured at the 20th second, 15.9%. The respective variation coefficients for the electrical capacitance measured at the first second and at the 20th

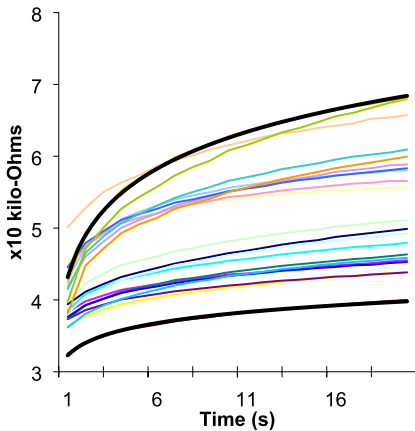


Fig. 3 Typical wood electrical resistance dependence on time for above FSP moisture content, 20-s monitoring period and 21 different locations of measuring electrodes. No of measurements $N = 440$

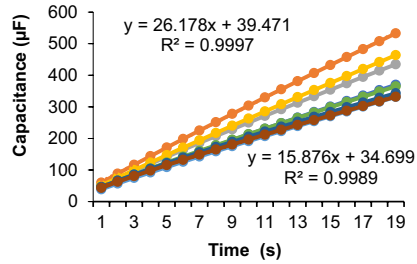


Fig. 4 Typical wood electrical capacitance C dependence on time for above FSP moisture content, 20-s measuring cycle. No of measurements $N = 440$

second are $C_{1s} = 10.4\%$ and $C_{20s} = 14\%$. Consequently, it is more reasonable to choose experimental data with a smaller variation coefficient (Table 3, columns 9 and 13: “Var. coef. %”) as the source data for calibration regression models.

Figure 3 depicts typical wood electrical resistance dependence on time, $R(t)$, with a 20-s measuring cycle, according to Formula (1). The measurements were carried out at 21 random locations in the wood, a single tree species, at one-third the thickness of the wood (EDG 2010). The species in this case was *Alnus glutinosa* (common alder), with an actual average moisture content of 105%, determined by the dry weighing method according to Standard ISO3130:1975 and at 50 °C. Maximum $R(t)$ and minimum $R(t)$ curves in the figure have been fitted to Formula (1).

Figure 4 depicts typical wood electrical capacitance dependence on time, $C(t)$, with a 20-s measuring cycle, according to Formula (2). Measurements were taken at 21 random locations in the wood, a single tree species, at one-third the thickness of the wood (for the sake of clarity, the figure depicts only the graphs for the minimum, maximum, and four intermediate results of the dependence of capacitance on time, not all the actually determined graphs). The species in this case was *Alnus glutinosa* (common alder), with an actual average moisture content of 105%, determined by the dry weighing method according to Standard ISO3130:1975 and at 50 °C. Maximum $C(t)$ and minimum $C(t)$ curves in the figure have been fitted to Formula (2).

In relation to the above, it is evident that the arithmetic averaging of 20 electrical resistances varying in time, which is common in practice (Scantronik Mugrauer GmbH 2019), would not result in the minimum possible variation coefficient being obtained.

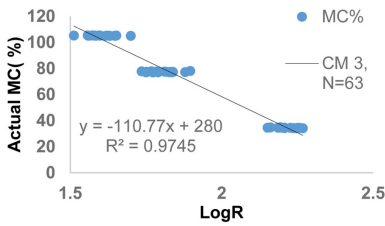


Fig. 5 LogR-type independent x-variable calibrating model (Table 2, CM3). Number of measurements N=63

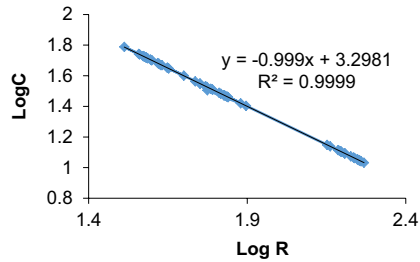


Fig. 7 Wood charging number graph according to Formula (11). Number of measurements N=63

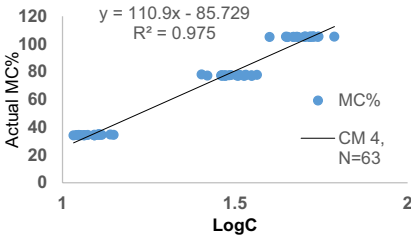


Fig. 6 LogC-type independent x-variable calibrating model (Table 2, CM4). Number of measurements N=63

For a better graphical representation of the wood charging number and its association with Figs. 5, 6 and 7, formula (10) can be given in a logarithmic form:

$$\text{Log}(R) + \text{Log}(C) = \text{Log}(ChN) \tag{11}$$

The value of the variation coefficient characterizing the dispersion of the empirical charging number is 0.597%. Comparing the charging number variation coefficient and the variation coefficients of electrical resistance R and electrical capacitance C (Table 3, columns 9 and 13), it can be concluded that the variation coefficient of the charging number is considerably (about 16 times) smaller than for the electrical variables (0.597% for $R * C$ versus 9.85% for electrical resistance R and 9.47% for electrical capacitance C).

The definition of wood charging number was first presented in a patent application (Tamme et al. 2020). For this research, the definition of wood charging number is the basis for the authors' hypothesis:

Random deviations of electrical resistance R and electrical capacitance C at a given measuring point are inversely proportional and may cause the tolerance interval convergence predicted for a single measurement at high moisture levels of wood, if used with an appropriately selected calibration function of two variables $f(R, C)$.

3.3 Wood charging number

Figures 5 and 6 present linearized calibration models for electrical resistance and electrical capacitance. When comparing the figures, a particular mirror symmetry caught the authors' attention. This led to the idea of comparing the respective values of electrical resistance R and electrical capacitance C measured at each measuring point. It was found that $R * C$ proved nearly constant for every actual moisture content value used in the calibration model, thus showing that the obtained empirical constant is independent of the wood moisture content. The consistency of $R * C$ means that in any wood moisture content above the FSP, wood electrical resistance and electrical capacitance are in an inversely proportional and non-linear dependence. This empirical constant, thus found to be independent of the moisture content, was called the wood empirical charging number, or for short, the wood charging number:

$$RC = 1994.993 \text{ (k}\Omega \cdot \mu\text{F)} = 1.995 \text{ s} = \text{const} = ChN \tag{10}$$

where ChN is the charging number.

3.4 Moisture meter modelling: calibration, reference and focusing models

As according to its definition, the wood charging number (Sect. 3.3) does not depend on wood moisture content, the multiplication of variables $R * C$ is a prohibited combination of R and C in the sought calibration function of two

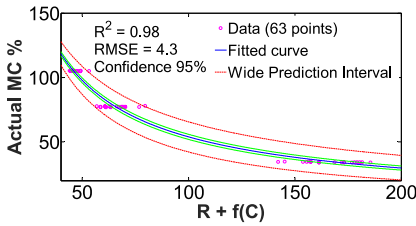


Fig. 8 Calibration model for the independent x variable type $R+f(C)$, where $f(C)$ is the power function of wood capacitance C . The non-linear function regression depicted was carried out with the program MATLAB™ platform with the curve fitting toolbox

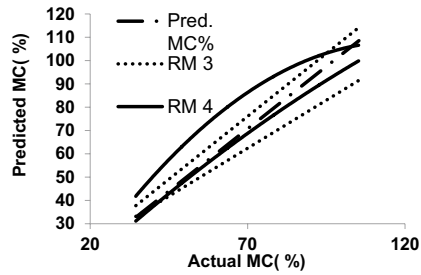


Fig. 10 Calculated single measurement tolerance intervals for $(R+C)$ reference model (RM4, solid line) versus traditional $LogR$ reference model (RM3, dotted line)

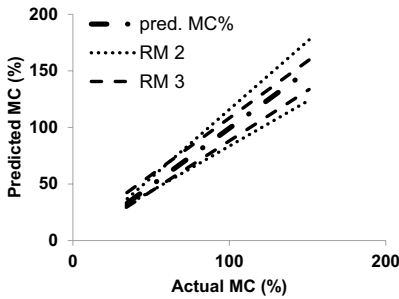


Fig. 9 Calculated single measurement tolerance intervals for traditional $LogR$ independent variable reference model (RM3, dashed line) versus traditional R independent variable reference model (RM2, dotted line)

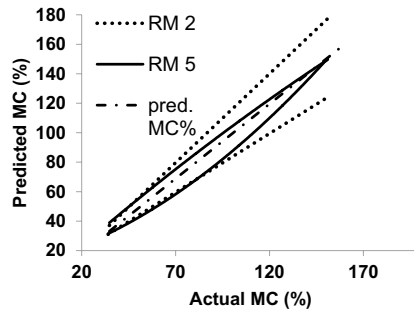


Fig. 11 Calculated single measurement tolerance intervals for $R+f(C)$ reference model (RM5, solid line) versus traditional R reference model (RM2, dotted line). The dash-dotted line depicts the actual average moisture content of wood

variables. Probably the general form of the target calibration function is $f(R+C)$ or $f(R)+f(C)$.

As a result of actual modelling, some evidence was found to support the present hypothesis with the trial and error method (Sect. 3.3):

- (A) The sum of electrical variables R and C and the sum of $R+f(C)$, where $f(C)$ is a power function of C , cause the tolerance interval convergence phenomenon predicted for single measurements (Figs. 8, 9, 10, 11).
- (B) The sum of electrical variables R_{1n} and R_{20n} and the power function $f(R_{1n}+R_{20n})$ also cause the tolerance interval convergence phenomenon predicted for single measurements (Fig. 12).
- (C) The functions $f(R)$, $f(C)$, and $f(R)+f(C)$ compensate for random deviations within the entire validity range of the calibration model; therefore, the tolerance interval

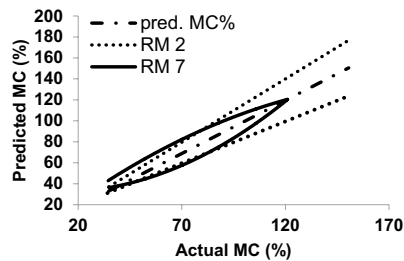


Fig. 12 Calculated single measurement tolerance intervals for $f(R_1+R_{20})$ reference model (RM6, solid line) versus traditional R reference model (RM2, dotted line)

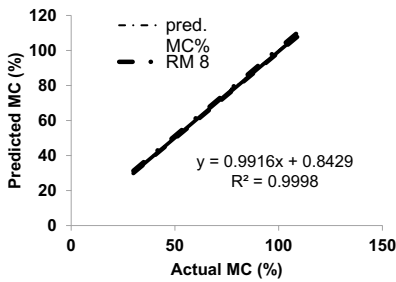


Fig. 13 Calculated single measurement tolerance intervals (RM8, dashed line) for multiple ($k=16$) R reference model

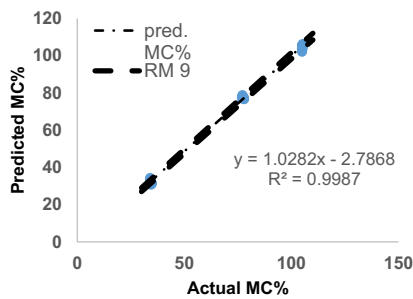


Fig. 14 Calculated single measurement tolerance intervals (RM9, dashed line) for $f(R)+f(C)$ with the real focal point (78% MC) reference model

converges within the entire measurement range without the need to apply the method of averaging repeated measurements (compare Figs. 13, 14).

Model types A, B, and C above are known as focusing models. This name derives from the fact that the predicted tolerance interval for individual measurements is at its minimum at certain actual MCs, called the “focus point of the model” (see Figs. 11, 12, 14). The wood moisture meter calibration function of model types A, B, and C is therefore a function of two variables: R_{In} and C_{In} (i.e., $MC\% = f(R_{In}, C_{In})$). For comparison, the traditional resistance-type moisture meter calibration function is a function of one of the independent variables, R or $\text{Log}R$, (i.e., $MC\% = f(R)$ or $MC\% = f(\text{Log}R)$).

The novel polarization-type wood moisture meter gives us the option to choose from several types of calibration models (Table 2): the traditional single-variable resistance model ($MC\% = f(R)$ or $MC\% = f(\text{Log}R)$), the single-variable capacitance model ($MC\% = f(\text{Log}C)$), and the two-variables polarization model (a total of five focusing models of types A, B, and C). Eight different calibration models can therefore be used to predict the moisture content of one specific wood species. If the electrical capacitance measurement data is not used, considering only the electrical resistance data and the calibration function $MC\% = f(\text{Log}R)$ or $MC\% = f(R)$, the polarization-type wood moisture meter will act as a conventional resistance-type wood moisture meter. This allows the characteristics of the polarization-type wood moisture meter to be compared with those of the conventional resistance-type wood moisture meter, based on identical test conditions for data measurement.

Source data for modelling and a few parameters of descriptive statistics are provided in Table 3.

Statistical parameters of different calibration models are provided in Table 2.

Statistical parameters of various reference models are provided in Table 1.

The dash-dotted line in Figs. 9, 10, 11, 12, 13 and 14 depicts the predicted average moisture content of the specimen.

Figures 11 and 12 have fairly similar tolerance-interval behaviour, leading to the assumption that electrical capacitance does occur in the independent variable ($R_{In} + R_{20n}$), although in a hidden or, in mathematical terms, an implicit form. In practice, the use of the model ($R_{In} + R_{20n}$) would save time, as the measuring of electrical capacitance is unnecessary and only electrical resistance would need to be recorded during the experiment.

3.5 Traditional measurement deviations averaging method versus measurement deviations compensation method

3.5.1 Convergence domain prediction models

Table 1 uses modelling to predict the range of wood moisture convergence domains, where the Rozema quality criterion (Rozema 2010) for the necessary measuring precision $MC < 3.5\%$ can be achieved with a minimum of one measurement. The formation of such domains is related to how the random deviation compensation method works in the focusing models (see model types A, B, and C and Table 1, column 7, models RM 4, 5, 6, 7, and 9.)

Table 2 Relevant calibration models (CM) of the moisture meter above FSP *Alnus glutinosa* wood moisture content with the statistical characteristics

Mod.No. Obs. No. Fig No.	Model type	Independent x-variable	Calibration function	R ²	S. E. (RMSE)	p-value	Predicted T. I., MC% ^a
CM1 ^b N=134	Gann(MC%)~ Log(MC%)	Gann(MC%)	$y = 0.037 * x + 0.702$	0.96	0.048	<0.01	35
CM2 N=63	R _{1n} ~ MC(pred.)	R _{1n}	$y = 1895.4x^{-0.78}$	0.98	6.04	<0.01	35
CM3 N=63 Figure 5	LogR _{1n} ~ MC(pred.)	LogR _{1n}	$y = - 110.7x + 280$	0.97	(4.7)	<0.01	20
CM4 N=63 Figure 6	LogC _{1n} ~ MC(pred.)	LogC _{1n}	$y = 110.9x - 85.73$	0.98	(4.68)	<0.01	20
CM5 N=63	(R _{1n} +C _{1n})~ MC(pred.) (Type A)	R _{1n} +C _{1n}	$y = 74,724 * x^{-1.483}$	0.99	3.31	<0.01	7
CM6 N=63 Figure 8	R _{1n} +aC ³ ~MC(pred.) (Type A)	R _{1n} +aC ³	$y = R + aC^3, a = 0.00005$	0.98	(4.7)	<0.01	8
CM7 N=63	(R _{1n} +R _{20n}) ~MC(pred.) (Type B)	R _{1n} +R _{20n}	$y = 0.00058x^2 - 0.4607x + 143$	0.97	4.51	<0.01	13.4
CM8 N=18 k=16	k * R~ k * MC(pred.) (Multiple model)	k * R	$y = 0.058x^2 - 1.76x + 166.6$	0.99	0.38	<0.01	1.3
CM9 ^c N=63	f(R)+f(C) ~MC(pred.) (Type C)	f(R)+f(C)	$y = f(R) + f(C)$	0.99	1.1	<0.01	3.4

^aPredicted tolerance interval at 105% actual MC

^bGann HT 85 T wood moisture-meters recalibration model (Tamme et al. 2014)

^cCM9 calibrating function $y = f(R) + f(C)$ specific format is y (predicted MC%) = $0.0044R^2 - 1.458R + 0.0014C^2 - 0.6834C + 269.32$

Table 3 Results of the measurement of *Alnus glutinosa* wood for the moisture groups

Moisture group Obs. No.	Measured actual MC, %				Measured electrical resistance, kΩ				Measured electrical capacitance, μF			
	Average MC%	Range MC%	St. dev	Var. coef.%	Ave-rage	Range	St. dev	Var. coef.%	Ave-rage	Range	St. dev	Var. coef.%
1. n=21	105.2	0.38	0.11	0.1	40	17.6	3.9	9.7	50	21.5	4.74	9.43
2. n=21	77.34	1.04	0.28	0.36	64	24.3	6.3	9.85	31	11.3	2.96	9.47
3. n=21	34.4	0.8	0.23	0.66	166	43.6	12	7.39	12	3.3	0.92	7.56

3.5.2 Multiple model versus focusing model $f(R) + f(C)$

Table 2 also shows the calibration model for the traditional resistance method (so-called multiple model, CM 8), where the arithmetic mean of a series of 16 electrical resistance repeat measurements was used as a single measurement. Comparing Figs. 13 and 14, it can be observed that the tolerance interval basically is equal to that of the traditional R model with multiple averaged series of 16 measurements

(Fig. 13), so the real focal point $f(R) + f(C)$ model can be achieved with only one measurement (Fig. 14).

A numerical example can be given to illustrate the comparison of Figs. 13 and 14. In Fig. 14, the real focal point of the tolerance interval is near the average moisture content of 78% MC, where the tolerance interval is minimal (i.e., less than 2.5%). For the other two points, the average moisture content was 105% and 34% and the tolerance interval less than 3.5%. In Fig. 13, the $k = 16$ -fold R model for an average MC of 105% gives a tolerance interval of

2.5% MC, which also meets the Rozema quality criteria (Table 1, RM8).

3.5.3 Predicted differences between two types of moisture meters for the high MC range of growing trees

The differences between the predicted measurement precision of the two types of moisture meters (i.e., the resistance-type and the polarization-type) are most remarkable at high MCs.

The following numerical example illustrates the difference. Let's say that the aim is to measure the actual MC, 151%. According to the formula in Table 1 (see RM2), a conventional resistance-type wood moisture meter gives a reading in the range of 125% MC to 175% MC, so the error could be up to 50% MC for a single measurement. The polarization-type wood moisture meter gives an estimated reading of between 149.25 and 152.75% using the non-linear calibration method (Table 2, CM6; Table 1, RM5). That is, the measurement error for a single measurement could be up to 3.5% MC. Thus, the precision of measurements for high MCs can differ up to a factor of 14 (depending on the calibration model used).

4 Conclusion

The novel polarization-type wood moisture meter described in this article allows for a total of eight different calibration models to be used to predict the MC of one variety of wood. For high MCs, such as in the wood of a growing tree (approximately 151% MC) or in raw wood (approximately 130–150% MC), the moisture meter with an electric polarization effect (polarization-type) can give the pre-set tolerance interval (1.5–3.5% MC), depending on the calibration model used, even from a single measurement. This advantage is particularly relevant in determining the moisture content of growing trees in situations where the possibility to repeat measurements (on the same tree at different measuring points) is limited. The Rozema quality criteria across the whole measurement range above the FSP of the novel polarization-type moisture meter was achieved by using focusing model $f(R) + f(C)$.

Acknowledgements This work was partially supported by institutional research funding IUT20-57 of the Estonian Ministry of Education and Research.

Declarations

Conflict of interest On behalf of all authors, the corresponding author states that there is no conflict of interest.

References

- ASTM D4444–08 (2008) Standard test method for laboratory standardization and calibration of hand-held moisture meters. Annual Book of ASTM Standards. ASTM International, West Conshohocken, p 10
- Bes Bollmann® Drying and Control Systems. <https://www.bes-bollmann.com/>. Accessed 3 Mar 2020
- Berga SC, Gil RG, Anton AEN, Muñoz AR (2019) Novel wood resistance measurement method reducing the initial transient instabilities arising in DC methods due to polarization effects. *Electronics* 8:1253
- Brookhuis (2009) Moisture measuring manual version 1.4, 27. Brookhuis Micro-Electronics BV
- Eco Chemie (2019a) Metrohm Autolab B. V. <http://www.ecochemie.nl>. Accessed 13 Apr 2019
- Eco Chemie (2019b) Metrohm Autolab B. V. <https://www.metrohm.com/en/applications/> Accessed 13 Apr 2019
- EDG (2010). Dried Timber- how to specify correctly. In: Welling J (ed), European Drying Group (EDG) and COST E53 2010, pp 38
- Edwards NC (1974) Procedure for the determination of species correction data for electrical resistance type moisture meters. CSIRO Div. Forest Products. (Unpublished divisional report), p 10
- Forsén H, Tarvainen V (2000) Accuracy and functionality of hand held wood moisture content meters. VTT publications, vol 420, p 102. <http://www.vti.fi/inf/pdf/publications/2000/P420.pdf>. Accessed 13 Apr 2019
- Gann Mess-u Regeltechnik GmbH. <http://www.gann.de>. Accessed 13 Apr 2019
- Gao S, Bao Z, Wang L, Yue X (2018) Comparison of voltammetry and digital bridge methods for electrical resistance measurements in wood. *Comput Electron Agric* 145:161–168. <https://www.mdpi.com/2079-9292/8/11/1253/htm>. Accessed 3 Mar 2020
- ISO 3130:1975 (1975) Wood—determination of moisture content for physical and mechanical tests. International Organization for Standardization, Switzerland, p 2
- ISO 3534-1:1993 (1993) Statistics—vocabulary and symbols—part 1: probability and general statistical terms. International Organization of Standardization, Geneva, p 46
- ISO/EIC (2008) GUIDE 98-3:2008(E) uncertainty of measurement—part 3: guide to the expression of uncertainty in measurement (GUM:1995). International Organisation for Standardization, Geneva, p 120
- James WL (1993) Fundamentals of hand held moisture meters: proceedings. ASTM hand held moisture meter workshop, Madison, WI, Forest Product Society, 5 May 1993, pp 13–16
- Keithley (2004) Low level measurements handbook 6th edition, p. 239. <http://web.mit.edu/8.13/8.13d/manuals/LowLevMsHandbk.pdf>. Accessed 3 Mar 2020
- Kiviste A (1999) Matemaatilise statistika MS excel keskkonnas (Mathematical statistics in MS excel environments). GT tarkvara OÜ, Tallinn, p 86
- Laaneots R, Mathiesen O (2006) An introduction to metrology. TUT Press, Tallinn, p 271
- MatLab™ (MathWorks, Natic, MA). URL <https://se.mathworks.com/products/matlab.html>. Accessed 03/03/2020.
- NdtJames (2020) <http://www.coste53.net/downloads/Edinburgh/Edinburgh-Presentation/72.pdf>. Accessed 13 Apr 2019.
- Romann T, Oll O, Pikma P, Tamme H, Lust E (2014) Surface chemistry of carbon electrodes in 1-ethyl-3-methylimidazolium tetrafluoroborate ionic liquid: an in situ infrared study. *Electrochim Acta* 125:183–190

- Rozema P (2010). Dos and don'ts in respect to moisture measurement. The future of quality control for wood & wood products, 4–7th May 2010, Edinburgh. The Final Conference of COST Action E 53: 9.
- Sachs L (1982) Applied statistics: a handbook of techniques. Springer-Verlag, New York, p 734
- Scantronik Mugrauer GmbH (2019). <https://www.scantronik.de/>. Accessed 13 Apr 2019
- Skaar C (1964) Some factors involved in the electrical determination of moisture gradients in wood. For Prod J 14(6):239–244
- Stamm AJ (1927) The electrical resistance of wood as a measure of its moisture content. Ind Eng Chem 19(9): 1021–1025. <https://doi.org/10.1021/e50213a022>. Accessed 13 Apr 2019
- Tamme V, Muioste P, Mitt R, Tamme H (2011) Determination of effective diffusion coefficient and mechanical stress of pine wood during convective drying. Balt For 17:110–117
- Tamme V, Muioste P, Tamme H (2013) Experimental study of resistance type wood moisture sensors for monitoring wood drying process above fibre saturation point. For Stud 59:28–44
- Tamme V, Muioste P, Padari A, Tamme H (2014) Modelling of resistance-type wood moisture meters for three deciduous tree species (black alder, birch, aspen) in moisture contents above fibre saturation point. Balt For 20(1):157–166
- Tamme V (2016). Development of resistance-type control methods for wood drying. Ph.D. Thesis, Estonian University of Life Sciences
- Tamme V, Tamme H, Bernotas T, Muioste P, Olt J (2020) Moisture meter and method for measuring the moisture content of wood above the fibre saturation point of a wood with the electric charging effect. Patent No EE 05822B1 Priority: 16. 07. 2018. https://ee.espacenet.com/publicationDetails/biblio?DB=EPODOC&II=0&ND=3&adjacent=true&locale=ee_EE&FT=D&date=20200217&CC=EE&NR=201800017A&KC=A Accessed 3 Mar 2020
- Tiitta M, Savolainen T, Olkonen H, Kanko T (1999) Wood moisture gradient analysis by electrical impedance spectroscopy. Holzforschung 53:68–76
- Vermaas HF (2002). State of the Art and Latest Technological Advances in the Drying of Fast-Grown Eucalyptus. In: Proceedings of 4th COST E 15 workshop, “methods for improving drying quality of wood”. Santiago de Compostela, Spain, 2002, 17
- Zelinka SL, Stone DS, Rammer DL (2007) Equivalent circuit modelling of wood at 12% moisture content. Wood Fiber Sci 39(4):556–565

Publisher's Note Springer Nature remains neutral with regard to jurisdictional claims in published maps and institutional affiliations.



Tamme, H., Kask, R., Muiste, P., Tamme, V. 2021. Comparative testing of two alternating current methods for determining wood moisture content in kiln conditions. *Forestry Studies*, 74: 72–87.

Research paper

Comparative testing of two alternating current methods for determining wood moisture content in kiln conditions

Hannes Tamme*, Regino Kask, Peeter Muiste and Valdek Tamme

Tamme, H., Kask, R., Muiste, P., Tamme, V. 2021. Comparative testing of two alternating current methods for determining wood moisture content in kiln conditions. – Forestry Studies | Metsanduslikud Uurimused 74, 72–87 ISSN 1406-9954. Journal homepage: <http://mi.emu.ee/forestry.studies>

Abstract. Research into the possibility of applying the electric impedance spectrometry (EIS) method and the dielectric capacitance method (DECM) simultaneously above fibre saturation point (FSP) and in harsh kiln conditions has been relatively scarce. In the framework of this research, tests were carried out on the operational reliability of the measuring capacitor (MEC) prototype used for calibrating the DECM in the harsh internal climate (50°C and 98% RH) of the kiln. Condensation of water vapor on MEC plates, leakage of MEC insulators and the emergence of static electric charges on MEC plates were studied. Quantitative ranges were found for MEC performance-disrupting effects on the parasitic capacities induced by each effect. The DECM was found to be less reliable than the EIS method for application in harsh kiln conditions. Secondly, under the same test conditions and for the same wood species (birch), the possibilities of the DECM method and the EIS method were comparatively modeled with the predetermined Rozema quality criterion of $\pm 1.75\%$ MC for predicting the moisture content (MC) of birch wood above FSP. It was found that, under the same test conditions, the DECM method proved more accurate than the EIS method for predicting birch wood MC above FSP. Based on the tests, it was concluded that DECM can be used in practice by applying a non-destructive method to reliably determine the average moisture content of a wood batch immediately prior to commencing the wood-drying process.

Key words: dielectric capacitance method, electric impedance spectroscopy, wood drying.

Authors' address: Chair of Forest Management Planning and Wood Processing Technologies, Institute of Forestry and Rural Engineering, Estonian University of Life Sciences, Kreutzwaldi 5, 51006 Tartu, Estonia; *e-mail: hannes.tamme@student.emu.ee

Introduction

In drying wood, it is necessary to monitor the moisture content of the wood in order to control the drying process. It is particularly important to reliably determine the average moisture content (MC) of fresh-

ly sawn wood prior to commencing the wood-drying process in order to use a simulation program to assess the drying time, energy consumption, risk of cracks developing during the drying process and other changes in wood quality (Salin, 1990; Tamme, 2016).

DOI: 10.2478/fsmu-2021-0005



© 2021 by the authors. Licensee Estonian University of Life Sciences, Tartu, Estonia. This article is an open access article distributed under the terms and conditions of the Creative Commons Attribution (CC BY) license (<http://creativecommons.org/licenses/by/4.0/>).

In practice, the direct current (DC) electric resistance method (Stamm, 1927; Tammé *et al.*, 2012; Uwizeyimana *et al.*, 2020) for determining and monitoring wood moisture content is widely used, as it is an inexpensive and reliable method for use both at room temperature and in harsh kiln conditions (Gann, 2021; Scantronik, 2021; Brookhuis, 2021; BES Bollmann, 2021; etc.). However, the main disadvantage of the DC resistance method is that the MC readings obtained by this method are not reliable above FSP (ca. more than 30% MC) (ASTM D4444-08, 2008; Tammé, 2016). The alternating current (AC) resistance method has proven approximately 14% more accurate than the DC method (Casans Berga *et al.*, 2019). The EIS method has been used for determining wood MC gradient (Tiitta *et al.*, 1999). The EIS method was used to monitor wood drying in combination with the acoustic emission (AE) method (Tiitta *et al.*, 2010). Another widely utilized method for determining wood MC is the dielectric capacitance method (DECM) (James *et al.*, 1985). This high-frequency capacitance method has also been called the microwave method. Previous research (Moschler, 2004) used the high-frequency (4–6 GHz) capacitance method to determine the average MC of wood in a kiln, leading to the development of a corresponding prototype calibrated into a moisture meter. In the case of the capacitance method, the prevailing geometry of the measuring capacitor (MEC) is a design with carefully electrically insulated flat parallel plates (Moschler, 2004; Tammé *et al.*, 2019). The advantage of the various technical applications of plate capacitor geometry is the simple calculation formula for electric capacitance (Zuleta, 2005):

$$C = \epsilon \epsilon_0 A / d \quad (1)$$

Where C is the capacitance of a parallel plate capacitor, A is the area of one plate in square meters, and d is the distance between the plates in meters. The constant

ϵ_0 is the permittivity of vacuum, and ϵ is the dielectric constant or relative dielectric permittivity. The dielectric constant ϵ depends on the moisture content of the wood placed between the MEC plates. According to formula (1), the electric capacitance C is proportional to the dielectric constant ϵ , hence the specific name of the method for determining the moisture content of wood – the dielectric capacitance method. For comparison: absolute dry (oven-dry) wood $\epsilon = 4$, and water $\epsilon = 80$ (Welling, 2010).

A flat ring capacitor for measuring wood MC below FSP (e.g., Brookhuis, (2020), FMW moisture indicator, 3.5 MHz operating frequency measured with an oscilloscope) and a flat slit capacitor (9.375 GHz operating frequency) for measuring wood MC both below FSP and above FSP have also been used (Johansson *et al.*, 2003).

The objective of our research was to test the MEC prototype developed for the paper in harsh conditions similar to those of a kiln in order to assess risks to the reliability of the MEC. The second objective was to use regression analysis to identify the possibilities of the DECM and EIS methods to establish the predetermined accuracy and to make a reliable determination of wood MC above FSP within the EIS operating frequency range of 1 Mz–10 Hz.

Material and Methods

The relationship between electric capacitance, the wood impedance modulus and average moisture content above and below FSP (FSP is agreed at 30% wood moisture content) was explored using a clear birch board with a thickness of 35 mm, width of 150 mm and length of 470 mm.

The moisture content of the birch wood specimen was varied by means of a specially developed laboratory drying schedule (Tammé *et al.*, 2013). The drying schedule ensured that during the first drying phase (at constant speed), the drying curve decreased linearly and moisture gradients

in the specimen were minimal.

The average MC of wood was determined by weighing the specimen at various randomly selected times using a precision weight with a resolution of 0.1 g. After weighing the specimen at the same average MC, other necessary measurements were also carried out as quickly as possible, such as measurements of the wood electric capacitance and wood impedance. In the final stage of the tests, the dry weight of the specimen was determined by drying it at 103°C. The actual moisture content of the specimen (relative to its dry weight) at the moment of weighing was identified according to ISO 3130:1975 (1975) standard.

An improved version of the parallel plate MEC was developed to determine the electric capacitance of wood at different moisture levels above FSP, compared to that used in our previous paper (Tamme *et al.*, 2019); its circuit diagram is shown in Figure 1(a) and the MEC with the measured specimen is shown in the photograph in Figure 1(b).

The cubic measure between the MEC plates was chosen at about 10% larger than the cubic measure of the specimen. This difference between the cubic measures ensured the necessary slack (tolerance zone) for the specimen when it was replaced between the plates after each weighing. The MEC allowed for the possibility of separate and combined heating of the insulators and plates in the form of a film of water vapor in the climate chamber to study condensation on MEC structural elements and to remove static electric charges of triboelectric origin (Tamme *et al.*, 2019) in the system. Additionally, the developed parallel plate measuring capacitor prototype was tested in conditions similar to kiln climate in the FEUTRON climate chamber (Feutron Klimasimulation GmbH, 2021). The tests were conducted at a temperature of 50°C and at a maximum relative air humidity (RH) of 98%. The purpose of the tests was to check the reliability of the measuring capacitor in the harsh kiln climate and to eliminate the

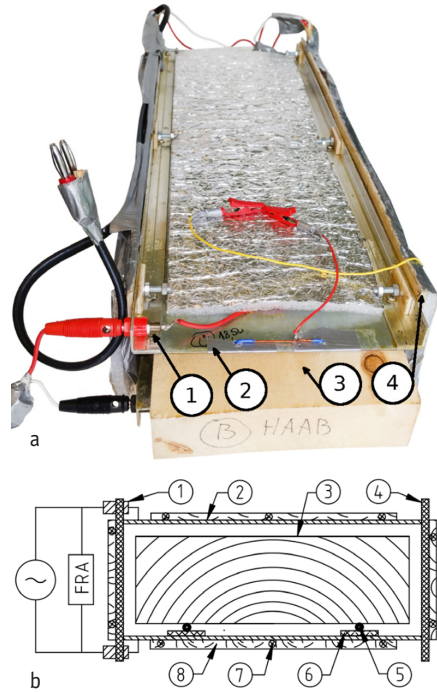


Figure 1. (a) Circuit diagram of the measuring capacitor (MEC) and (b) photograph of the MEC prototype with the tested birch wood specimen. 1 – signal connector, 2 – capacitor plate, 3 – wood specimen, 4 – capacitor insulator, FRA – frequency response analyser, 5 – triboelectric charge collector, 6 – film insulator, 7 – heating cable, 8 – heat insulator.

occurrence of water vapor saturation and condensation of humidity on the measuring capacitor plates and insulators.

According to literature (Moschler, 2004), the microwave measuring capacitor prototype with parallel plates was tested at room temperature and at temperatures of 40°C and 60°C. Moschler (2004) contains no data on the relative humidity in the chamber during the tests, which is an important climate parameter. The measurements of electric capacitance present-

ed in this paper were carried out using the LCR55 (Wavetek Meterman, 2021) capacitance meter (CAM). The LCR55 capacitance meter has an operating frequency of 1,000 Hz as measured with an oscilloscope.

Wood impedance was measured using stainless steel insulated pin electrodes made by the company Gann (Gann 2021), which were nailed into the wood across the grain at a spacing of 30 mm (Brookhuis Micro-Electronics, 2009). The nails were driven to a depth of 1/3 of the thickness of the wooden material (Welling, 2010), which is about 12 mm from the board surface for a 35 mm board thickness. After each impedance measurement, the electrodes were nailed into the next randomly selected location on the board and at the same depth from the surface of the board. The impedance modulus of the measured AC complex electric resistance was calculated on the basis of impedance spectrometry (EIS) measurement data using EIS standard formulas (Krause, 2003; Tamme *et al.*, 2019). Each time, the impedance modulus was determined when the EIS spectrum phase angle had a minimum (ca. 4 to 5 degrees) value. An AUTOLAB PGSTAT 408N impedance analyser with NOVA 1.8 software was used (Metrohm Autolab, 2021).

Interference with the reliability of the measuring capacitor in conditions similar to harsh kiln climate (that is, imitated in a laboratory climate chamber) was also recorded using impedance spectra and processed with the NOVA 1.8 software using the circle-fit analysis tool. To do so, frequency scanning between 1 MHz and 10 Hz and the electric sine wave amplitude of 50 mV were applied.

The possible effect of static electricity on the measurements taken by the measuring capacitor was first investigated indirectly using Keithley's model 6517B with an electrometer (Keithley, 2004) and then directly for potentials safe for the instrument (up to 0.9 V) using LCR55 (Tamme *et al.*, 2019).

Statistical processing of the test results was based on the principles of a metrology standard ISO 3534-1:1993 (1993) and carried out with software R (R Core Team, 2010), MS Excel and NOVA 1.8. In the case of Student t-distribution and linear regression for the single measurement, the upper and lower tolerance lines (confidence limits) of the regression line are presented in MS Excel at 95% confidence level as follows (Kiviste, 1999):

$$\text{Intercept } b_0 \text{ lower} = b_0 - TINV(\alpha; n - 2) * s_{b_0} \quad (2)$$

$$\text{Intercept } b_0 \text{ upper} = b_0 + TINV(\alpha; n - 2) * s_{b_0} \quad (3)$$

$$\text{Slope } b_1 \text{ lower} = b_1 - TINV(\alpha; n - 2) * s_{b_1} \quad (4)$$

$$\text{Slope } b_1 \text{ upper} = b_1 + TINV(\alpha; n - 2) * s_{b_1} \quad (5)$$

Where s_{b_0} and s_{b_1} are the standard errors of the regression line intercept and slope (Kiviste, 1999).

The following formulas were used to estimate the standard error (SE) and the average root-mean-square error (RMSE) of the regression model:

$$SE = \sqrt{\frac{1}{(n-2)} \sum_{i=1}^n (y_i - \hat{y})^2} \quad (6)$$

$$RMSE = \sqrt{\frac{1}{n} \sum_{i=1}^n (y_i - \hat{y})^2} \quad (7)$$

Where y_i = the estimated values and \hat{y} = the actual values.

The non-parametric Kolmogorov-Smirnov test and the Shapiro-Wilk test (Tamme *et al.*, 2014) were used in the R software environment to estimate the reliability of the regression models.

Results and Discussion

Changes in electric parameters caused by water vapor condensation were measured using the LCR55 and the EIS method.

Effect of water vapor condensation on MEC plates

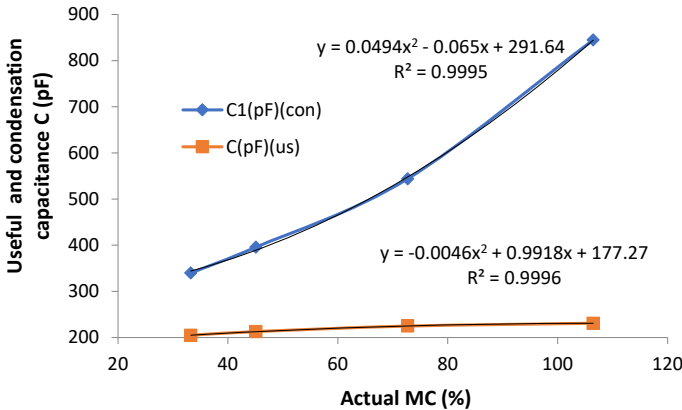


Figure 2. The dependence of MEC useful capacitance and parasitic capacitance caused by water vapor condensation on MEC plates on the actual average moisture content of wood in the same coordinate grid. The upper curve in the figure represents parasitic capacitance, and the lower, useful capacitance.

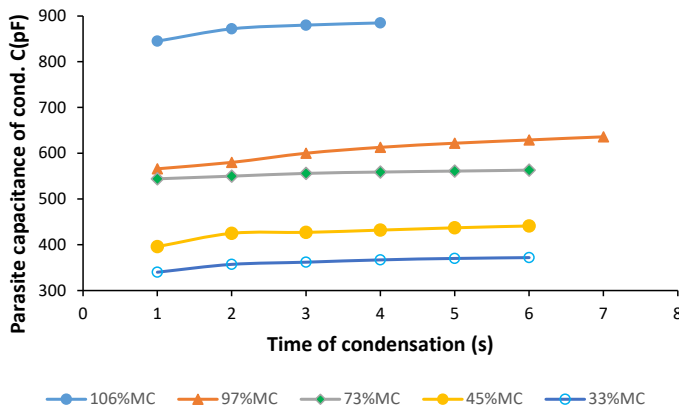


Figure 3. Increment of parasitic capacitance due to condensation of water vapor on MEC plates at varying wood moisture levels.

The parasitic capacitance of condensation observed on MEC plates (indicated as C_{parasite} in Table 1) and the useful capacitance are shown on the same axis in Figure 2, depending on the average moisture content of wood. The EIS method allowed the development dynamics of the condensation process to be monitored (Figure 4, a) and b)) and the quantitative parameters for the electric capacitance C_{parasite} to be calculated.

Figure 3 shows the relative time increments of the parasitic capacitance of condensation on the MEC plates at different wood average moisture levels recorded using the capacitance meter (CAM) LCR55. Both the EIS method and the LCR55 show a similar magnitude for the parasitic capacitance on the MEC plates ($C_{\text{parasite}} = 660$ pF and $C_{\text{parasite}} = 800$ pF, respectively). Based on Figure 3, it may be concluded that the higher the average MC of wood, the greater the value of parasitic capacitance due to water vapor condensation. Parasitic capacitance of approximately 5 times the useful capacitance may completely obscure the correct useful capacitance measurements under conditions favourable for water vapor condensation.

Leakage effect of MEC insulators

The leakage effect of the insulators is characterized by the occurrence of parallel resistance of the condensed water film on the insulators in addition to parasitic capacitance, which shunts the resistance of the insulators. The MEC insulator resistance in normal operation is approximately 10 giga-ohms or greater. The circle-fit analysis found that in the initial phase of leakage, the parallel resistance of a leaking insulator is $R_p = 61$ kOhm and its parasitic capacitance is $C_s = 163$ pF, whereas $R_p = 0.78$ kOhm and $C_s = 681$ pF in the final phase of the leakage.

MEC static charge effect

Figure 5 shows the dynamics of electrostatic charge formation when placing the birch

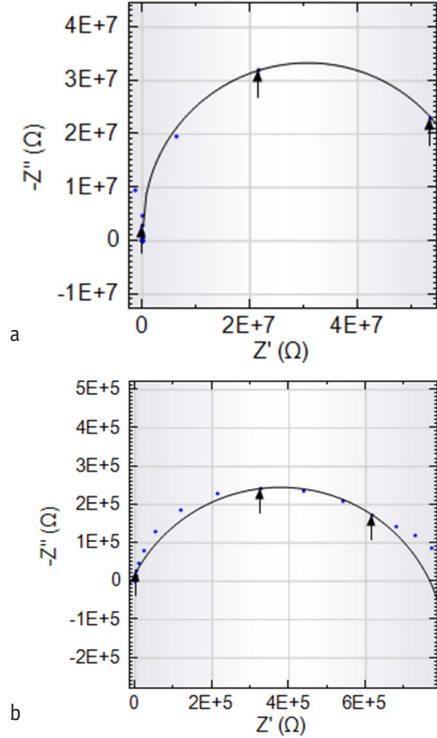


Figure 4. Impedance spectra of leakage of MEC insulators: (a) Start phase of the leakage and (b) End phase of developed leakage.

wood specimen between and removing it from the MEC plates. This procedure was repeated 15 times. A measurement interval of 0.1 seconds was used. In Figure 5, one maximum of impulse voltage generated by static charge corresponds to each cycle of placement and removal of the specimen between the MEC plates. Maximum values (or peaks) with negative potential were predominantly recorded. Because the potential was measured from the electrostatic charge removal system (see Figure 1), the wood itself was oppositely charged; that is, predominantly positive. The potential of electrostatic charges generally decreases when the movement of the specimen in relation to the MEC ceases. However, this

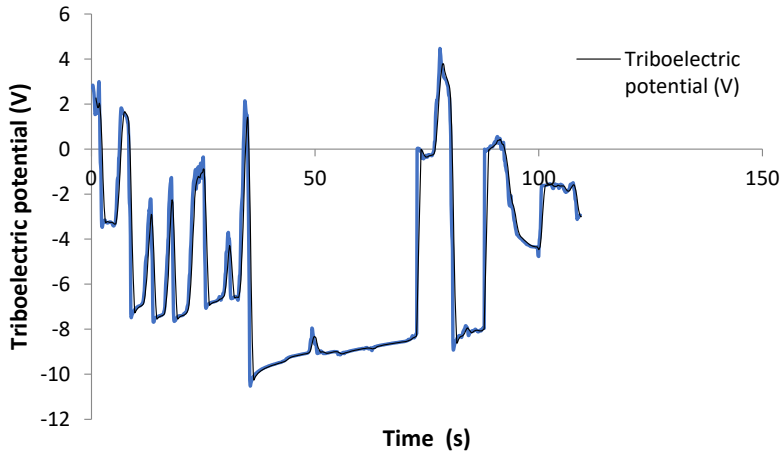


Figure 5. Dynamics of the potential for static electric charges of triboelectric origin when the birch wood specimen is placed between and then removed from the MEC plates.

is not always the case, as Figure 5 shows an exceptional peak where the potential remains high (ca. 10 V) for a considerable time (ca. 30 seconds). The triboelectric potential peak may exceed the CAM LCR55 safe input voltage (up to 0.9V) by about 10 times.

MEC temperature effect

In previous research (Moschler, 2004), the electric capacitance of the measured wood was found to increase slightly with the increase in wood temperature. The same tendency was confirmed in our previous paper (Tamme *et al.*, 2019). In this current study, the measured increase in electric capacitance of MEC with oven-dry wood was from room temperature of 23°C to 105°C: 121 pF to 124 pF. Thus, the effect of temperature on the electric capacitance of oven-dry wood is negligible (only 3 pF) and may be disregarded in a rough approximation. The minor effect of temperature on the capacitance method is also highlighted in industry guidelines (Welling, 2010). On the basis of the above, it was concluded

that due to its low temperature sensitivity, the DECM could be used in practice immediately prior to the start of the wood-drying process by a non-destructive method to reliably determine the average moisture content of the wood batch for the wood drying simulation program.

In addition, an important trend that emerged during testing must be pointed out: namely, condensation effects that obscure the useful capacitance of MEC predominate when the air RH in the climate chamber is higher than 60%, but electrostatic charges occur often on the MEC when the air RH in the climate chamber is lower than 60%.

To summarize, the various physical characteristics and effects influencing the electric capacitance of the MEC are presented in Table 1. Based on the data in the bottom row of Table 1 (useful capacitance), it can be concluded that the DECM in the range below FSP (0–30% MC) is about 8 times more sensitive per percent of MC compared to the range above FSP (30%–105% MC).

Table 1. The main physical reliability characteristics of the dielectric capacitance method (DECM) in kiln climate and the corresponding capacitance meter (CAM) response.

Effect, parameter, figure no.	Effect range	CAM response
Condensation of water vapor on MEC plates, Fig. 2, 3	$C_{\text{parasite}} = 340 \text{ to } 845 \text{ pF}$ $C_{\text{parasite}} = 681 \text{ pF}$, determined using EIS method	CAM reading recorded ca. 5x and moderately increasing**
Leakage of MEC insulators, Fig. 4	$C_{\text{parasite}} = 163 \text{ to } 681 \text{ pF}$ $R_{\text{parallel}} = 61 \text{ to } 0.778 \text{ k}\Omega$	Floating of CAM reading
Triboelectric charges on MEC plates, Fig. 5	$U_{\text{static}} = -10.5 \text{ to } 4.29 \text{ V}$	Floating of CAM reading, CAM spoilage risk
Useful MEC capacitance,* below FSP (0.% to 30%) Useful MEC capacitance, above FSP (30% to 105%)	$C_{\text{useful}} = 121 \text{ to } 205 \text{ pF}$ $MC = 0 \% \text{ to } 30\%$ $C_{\text{useful}} = 205 \text{ to } 231 \text{ pF}$ $MC = 30\% \text{ to } 105\%$	CAM reading stable and reliable

* Useful MEC capacitance depends on the moisture content of wood and the thickness of the wood material according to the MEC, formula 1. Wood moisture content is related to the dielectric constant ϵ in formula 1.

** "Moderately increasing" means that it is possible to manually retrieve a CAM numerical reading, but it slowly increases as the water vapor condensation progresses (see Figure 3).

Useful capacitance of MEC and dielectric capacitance modelling

Useful capacitance is defined as the measured capacitance of MEC with wood, which excludes interfering effects, such as condensation on MEC plates, leakage of MEC insulators and the presence of static charges on MEC plates. Our previous paper (Tamme *et al.*, 2019) indicated that useful capacitance also depends significantly on the selected CAM operating frequency, while being higher in the low frequency range. However, low frequencies proved more sensitive to the effect of water vapor condensation.

For useful capacitance only, it would be reasonable to establish a statistically reliable correlation (generally a linear regression model) between the actual (i.e., determined by weighing) average moisture content of wood and the moisture content predicted by the capacitance method or, in other words, to statistically model the capacitance method. The methodology for modelling the EIS method does not differ from modelling the capacitance method.

Comparatively, the results of modelling the capacitance method and the EIS method are presented in Table 2 and Figures 6, 7, 8, 9, 10, 11.

Formulas in Table 2 and Figure 11, which connect various methods, are presented according to the needs of the wood drying practice. The model RMSE or SE, the p-value and the coefficient of determination R^2 mainly attract theoretical interest. Wood drying practitioners are primarily interested in two issues based on the modelling results: whether a single measurement fall on the 95% confidence level within the desired measurement precision range, and if not, how many repeated measurements are required in the series of measurements in order to achieve the desired prescribed precision. A series of measurements is defined as a certain number (k) of measurements repeated and arithmetically averaged at close moments in time under the same testing conditions (Brookhuis, 2020; Laaneots & Mathiesen, 2006). The Rozema quality criterion was used to define the prescribed measurement accuracy, according to which the standard uncertainty of the wood moisture meter reading must be less than or equal to 3.5% MC (Rozema, 2010). The individual measurement tolerance interval calculated on the Student t-distribution assumption based on formulas 2, 3, 4 and 5 should represent extended uncertainty in metrology

Table 2. Modelling results of the dielectric capacitance method (DECM) and electric impedance spectrometry (EIS) method. In regression models, the independent x -variable is the actual MC (%), and the dependent y -variable is the predicted MC (%). The predicted single measurement tolerance bands on the 95% confidence level, y_{upper} and y_{lower} are calculated using formulas 2, 3, 4 and 5. The SE is calculated according to formula 6. The tolerance interval (TI) is calculated using the formula $TI = y_{upper} - y_{lower}$. N is the number of measurements repeated under the same test conditions and k is the number of measurements averaged per series of measurements (i.e., the averaging period). For models with a series of measurements (k), the identification type shall be “multiple”.

N obs., k -period	Method type, Fig. no.	Equations for predicting single measurement tolerance bands and TI	R^2	p-value and tests*	SE
$N = 63$	DECM (above FSP), Fig. 6	$y_{upper} = 1.0131x + 5.9063$ $y_{lower} = 0.9406x + 0.8399$ $TI = 0.0728x + 5.075$	0.97	<0.01 K-S	4.88
$N = 42$	DECM (below FSP), Fig. 7	$y_{upper} = 1.0135x + 0.2792$ $y_{lower} = 0.9788x - 0.1954$ $TI = 0.0348x + 0.4746$	0.99	<0.01 K-S S-W	0.61
$N = 63$ $k = 16$	DECM (above FSP) (multiple), Fig. 8	$y_{upper} = 1.006x + 0.44$ $y_{lower} = 0.9929x - 0.4163$ $TI = 0.0124x + 0.8775$	0.99	<0.01 K-S S-W	0.46
$N = 63$	EIS (above FSP), Fig. 9	$y_{upper} = 0.9448x + 11.196$ $y_{lower} = 0.787x + 2.41$ $TI = 0.1622x + 8.135$	0.87	<0.01 K-S	5.01
$N = 63$ $k = 16$	EIS (above FSP) (multiple), Fig. 10	$y_{upper} = 1.0134x + 1.728$ $y_{lower} = 0.968x - 0.84$ $TI = 0.0365x + 2.836$	0.99	<0.01 K-S	0.867

* Kolmogorov-Smirnov (K-S) test and Shapiro-Wilk normality (S-W) test

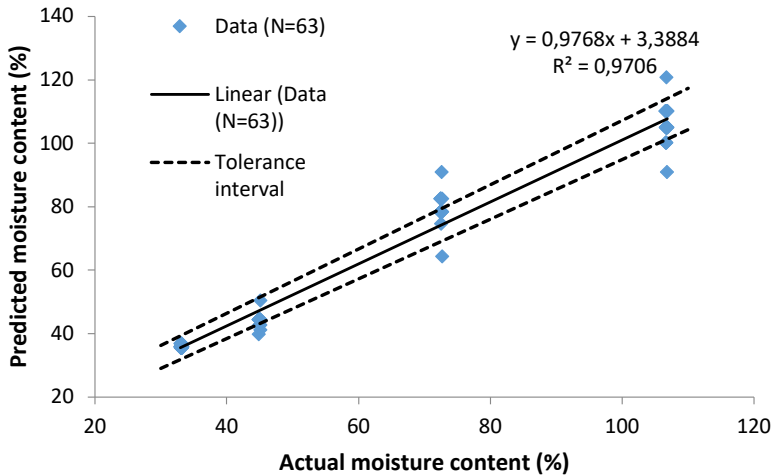


Figure 6. DECM modelling at wood moisture levels above FSP.

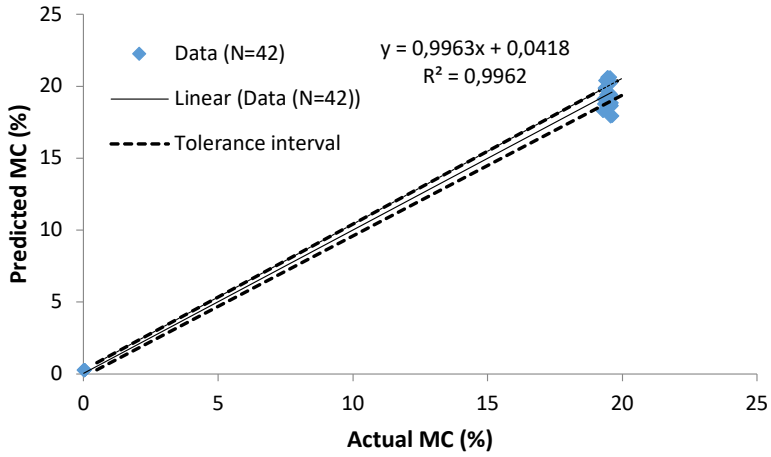


Figure 7. DECM modelling at wood moisture levels below FSP.

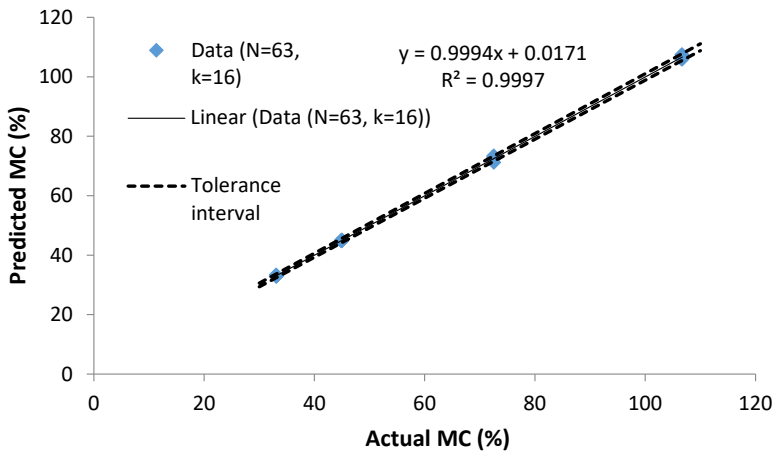


Figure 8. DECM modelling at wood moisture levels above FSP, multiple ($k=16$) model.

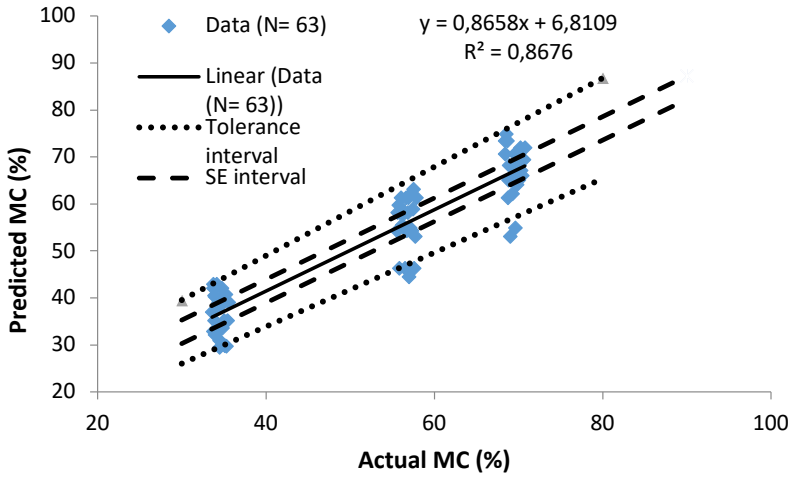


Figure 9. EIS modelling at wood moisture levels above FSP.

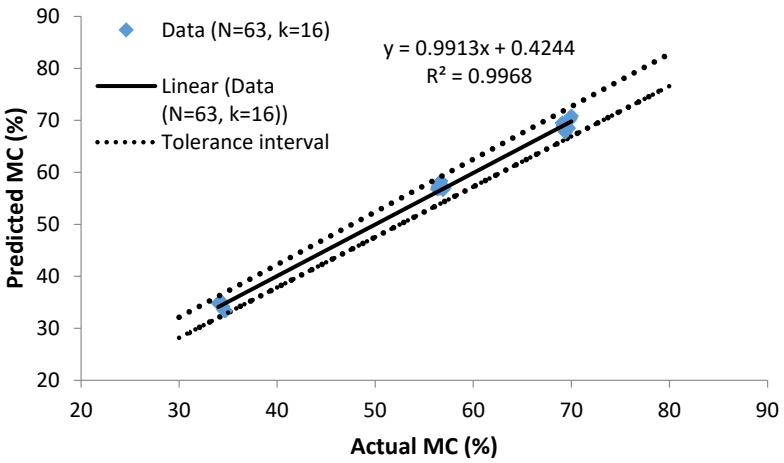


Figure 10. EIS modelling at wood moisture levels above FSP, multiple ($k=16$) model.

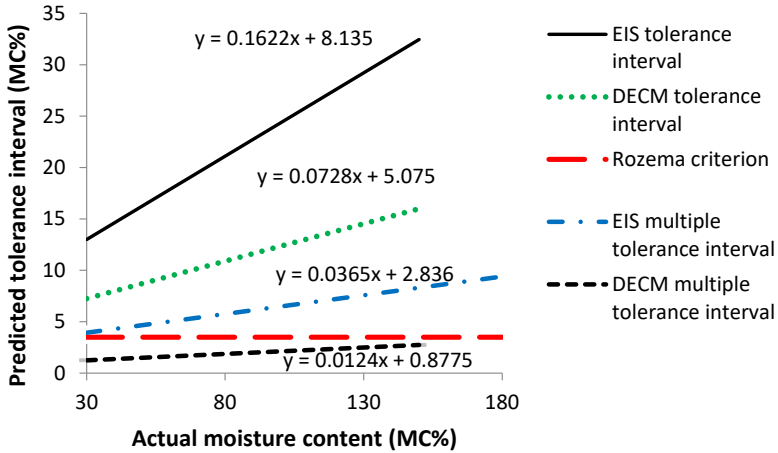


Figure 11. Comparison of the tolerance intervals (TI) predicted for single measurements of different models (using formulas in Table 2) and with the Rozema quality criterion at wood moisture levels above FSP. Corresponding graphs of the predicted TI are given from top to bottom as follows: EIS, DECM, EIS multiple, Rozema quality criterion (dashed line, parallel to x-axis), and DECM multiple.

terms (Laaneots & Mathiesen, 2006). Thus, equating the Rozema 3.5% MC quality criterion with the tolerance interval in this study actually makes the Rozema criterion somewhat more stringent. In Figure 11, the Rozema criterion is marked with a dashed line parallel to the x-axis.

In Moschler’s paper (2004) it was found that the actual MC point of 28.60% of the high frequency capacitance method (4.5 to 6.0 GHz) is estimated to have a predicted expanded uncertainty of $\pm 3.62\%$; thus, the corresponding tolerance interval for this point is 7.24% MC. In comparison, a tolerance interval of 7.26% MC calculated for the same actual MC point of 28.60% was found in this study for the low-frequency capacitance method (see Table 2, second row), using the relevant formulas. Therefore, the consistency of repeated (reproduced) measurements in different laboratories and under different test conditions is surprisingly good. In another paper (Johansson *et al.*, 2003), an RMSEE of 12.52% MC was found for the high-frequency (9.375 GHz) capacitance method for above FSP, and of 0.74% MC for below FSP. This

study found SE values that were very close to the RMSEE, as is shown in Table 2 (see formulas 6 and 7): above FSP SE it was 4.88% MC and below FSP SE it was 0.61% MC. Thus, below FSP the numerical data are comparable, but above the FSP range, the low-frequency capacitance method used in this study provides results that are twice as good as those achieved with the model residual error.

In our research, comparable experiments for the dielectric capacitance and EIS method were conducted under the same test conditions and for the same tree species (birch). In addition, 16 arithmetic averages in a single series of measurements were modelled in the MC range above FSP. The compared results are presented in Figures 6, 7, 8, 9 and 10 and in Table 2. Figure 11 shows that there is a tendency for the tolerance interval (TI) of a single measurement to increase in proportion to the increase of the actual MC, though the increment is different for each model. The results of the modelling summarized in Figure 11 also show that in the actual MC range (30–150%), the Rozema quality

criterion cannot be met either by a single measurement performed with the capacitance method or by a single measurement performed with the EIS method. Using a series of 16 measurements, only the capacitance method can meet the Rozema quality criterion in the actual MC range above FSP (30–150%), whereas the EIS method fails to do so. However, according to Table 2 (row 5), the SE of the EIS method is lower than the Rozema quality criterion (SE = 0.867). Consequently, by increasing the number of measurements (k) to more than 16, it is likely that the Rozema quality criterion can also be met in the case of the EIS method. The wood moisture meter with the recently patented electric charging effect (polarization-type) may prove promising for use in the harsh climatic conditions of a kiln (Tamme *et al.*, 2020). The patented polarization-type wood moisture meter has basically the same reliability as a conventional resistance-type moisture meter given how it is calibrated, but could meet the Rozema quality criterion with just one measurement based on the modelling results (that is, without the series of 16 repeated measurements) (Tamme *et al.*, 2021).

The reliability of the regression models in Table 2 was verified by the Kolmogorov-Smirnov and Shapiro-Wilk non-parametric test of regression residuals in the program R environment, in accordance with the methodology used in a previous paper (Tamme *et al.*, 2014). All the models given in Table 2 passed the Kolmogorov-Smirnov test (marked as “K-S” in the table). The DECM (below FSP) and the DECM (above FSP, multiple) passed the more stringent Shapiro-Wilk normality test (marked as “S-W” in Table 2).

Conclusions

The DECM was found to be less reliable than the EIS method for use in harsh kiln climate. The dielectric capacitance method will require more development in the fu-

ture so that it can be reliably (i.e., without the risk of parasitic capacitance and static charges) used in harsh kiln conditions. However, testing of the DECM and the EIS method under the same test conditions and comparing the modelled test results according to the Rozema quality criterion showed that the dielectric capacitance method exhibits higher accuracy in the MC range above FSP. The DECM of low sensitivity to temperature may prove promising in practice, if the purpose is to quickly and reliably determine prior to the start of the drying process the average moisture content of a wood batch for the wood drying simulation program using a non-destructive method.

Acknowledgements. This work was supported by the Environmental Investment Centre of Estonia (Grant No. 16200).

References

- ASTM D4444-08. 2008. Standard Test Method for Laboratory Standardization and Calibration of Hand-Held Moisture Meters. Annual Book of ASTM Standards, West Conshohocken, PA, ASTM International. 10 pp.
- BES Bollmann Drying and Control Systems. [WWW document]. – URL <https://www.bes-bollmann.com/>. [Accessed 3 March 2021].
- Brookhuis Micro-Electronics BV. 2009. Moisture measuring manual Version 1.4. 27 pp.
- Brookhuis. [WWW document]. – URL <https://brookhuis.com>. [Accessed 3 March 2021].
- Casans Berga, S., Garcia-Gil, R., Navarro Anton, A.E., Rosado-Muñoz, A. 2019. Novel wood resistance measurement method reducing the initial transient instabilities arising in DC methods due to polarization effects. – *Electronics*, 8(11), 1253. <https://www.mdpi.com/2079-9292/8/11/1253/htm>.
- Feutron Klimasimulation GmbH. [WWW document]. – URL <https://www.feutron.de/en/weathering-chamber/>. [Accessed 13 April 2021].
- Gann Mess- und Regeltechnik GmbH. [WWW document]. – URL <http://www.gann.de>. [Accessed 13 April 2021].
- ISO 3130:1975. 1975. Wood – Determination of moisture content for physical and mechanical tests. Geneva, Switzerland International Organization for Standardization. 2 pp.

- ISO 3534-1:1993. 1993. Statistics – vocabulary and symbols – part 1: probability and general statistical terms. Geneva, International Organization of Standardization. 53 pp.
- James, W.L., Yen, Y.-H., King, R.J. 1985. A microwave method for measuring moisture content, density and grain angle of wood. United States Department of Agriculture. [WWW document]. – URL <http://www.treesearch.fs.fed.us/pubs/5792>. [Accessed 13 May 2021].
- Johansson, J., Hagman, O., Oja, J. 2003. Predicting moisture content and density of Scots pine by microwave scanning of sawn timber. – *Computers and Electronics in Agriculture*, 41(1-3), 85 – 90. [https://doi.org/10.1016/S0168-1699\(03\)00044-9](https://doi.org/10.1016/S0168-1699(03)00044-9).
- Keithley. 2004. *Low Level Measurements Handbook* 6th Edition, 239 pp. [WWW document]. – URL <http://web.mit.edu/8.13/8.13d/manuals/LowLevMsHandbk.pdf>. [Accessed 3 March 2020].
- Kiviste, A. 1999. *Matemaatiline Statistika MS Excel Keskkonnas (Mathematical Statistics in MS Excel Environments)*. Tallinn, GT Tarkvara OÜ. 86 pp. (In Estonian)
- Krause, S. 2003. Impedance methods. – Bard, A.J., Stratmann, M., Unwin, P.R. (eds.). *Encyclopedia of Electrochemistry*, Vol. 3, Instrumentation and Electroanalytical Chemistry, Weinheim, Wiley-VCH. 196–229.
- Laaneots, R., Mathiesen, O. 2006. *An Introduction to Metrology*. Tallinn, TUT Press. 271 pp.
- Metrohm Autolab. [WWW document]. – URL <http://www.ecochemie.nl>. [Accessed 13 April 2021].
- Moschler, W. W. 2004. *Wireless microwave wood moisture measurement system for wood drying kilns*. Final Technical Report, Knoxville, Tennessee. University of Tennessee, 18 pp.
- R Core Team. 2010. *R: A language and environment for statistical computing*. R Foundation for Statistical Computing, Vienna, Austria. [WWW document]. – URL <http://www.r-project.org>. [Accessed 13 April 2021].
- Rozema, P. 2010. Do's and don'ts in respect to moisture measurement. – *Proceedings of the Final Conference of COST Action E53: The Future of Quality Control for Wood & Wood Products*, UK, 4-7th May 2010. Edinburgh, 9 pp. <https://www.napier.ac.uk/~media/worktribe/output-208736/e53edinburghproceedingspdf.pdf>.
- Salin, J.G. 1990. *Simulation of the timber drying process. Prediction of moisture and quality changes*. – Doctoral thesis. Helsinki, EKONO Oy. 103 pp.
- Scantronik Mugrauer GmbH. [WWW document]. – URL www.scantronik.de/. [Accessed 13 April 2021].
- Stamm, A.J. 1927. The electrical resistance of wood as a measure of its moisture content. – *Industrial and Engineering Chemistry*, 19(9), 1021–1025.
- Tamme, H., Tamme, V., Kask, R., Muiste, P. 2019. Non-destructive dielectric method for determining the moisture content of newly sawn timber for moisture content above FSP. – Wang, X., Sauter, U.H., Ross, R.J. (eds.). *Proceedings of the 21st International Nondestructive Testing and Evaluation of Wood Symposium*. – General Technical Report FPL-GTR-272. Madison, WI: US. Department of Agriculture, Forest Service, Forest Products Laboratory, 213–224.
- Tamme, V. 2016. *Development of resistance-type control methods for wood drying*. – PhD thesis. Tartu, Estonian University of Life Sciences. 135 pp.
- Tamme, V., Muiste, P., Kask, R., Tamme, H. 2012. Experimental study of electrode effects of resistance type electrodes for monitoring wood drying process above fiber saturation point. – *Forestry Studies / Metsanduslikud Uurimused*, 56, 42–55. <https://doi.org/10.2478/v10132-012-0004-6>.
- Tamme, V., Muiste, P., Padari, A., Tamme, H. 2014. Modelling of resistance-type wood moisture meters for three deciduous tree species (black alder, birch, aspen) in moisture contents above fibre saturation point. – *Baltic Forestry*, 20(1), 157–166.
- Tamme, V., Muiste, P., Tamme, H. 2013. Experimental study of resistance type wood moisture sensors for monitoring wood drying process above fibre saturation point. – *Forestry Studies / Metsanduslikud Uurimused*, 59, 28–44. <https://doi.org/10.2478/fsmu-2013-0009>.
- Tamme, V., Tamme, H., Bernotas, T., Muiste, P., Olt, J. 2020. *Moisture meter and method for measuring the moisture content of wood above the fibre saturation point of a wood with the electric charging effect*. Patent No EE 05822B1 Priority: 16.07.2018. [WWW document]. – URL https://ee.espacenet.com/publicationDetails/biblio?DB=EPODOC&II=0&ND=3&adja cent=true&locale=ee_EE&FT=D&date=20200217&CC=EE&NR=201800017A&KC=A. [Accessed 3 March 2020].
- Tamme, V., Tamme, H., Miidla, P., Muiste, P. 2021. Novel polarization-type moisture meter for determining moisture content of wood above fibre saturation point. – *European Journal of Wood and Wood Products*, 79, 1577–1587. <http://link.springer.com/article/10.1007/s00107-021-01682-6>.
- Tiitta, M., Savolainen, T., Olkkonen, H., Kanko, T. 1999. Wood moisture gradient analysis by electrical impedance spectroscopy. – *Holzforschung*, 53, 68–76.
- Tiitta, M., Tomppo, L., Lappalainen, R. 2010. Combined method for monitoring wood drying process. – *Proceedings of 11th International IUFRO Wood Drying Conference*, Sweden, 18-22 January. Skellefteå, 76–80.

- Uwizeyimana, P., Perrin, M., Eyma, F. 2020. Moisture monitoring in glulam timber structures with embedded resistive sensors: study of influence parameters. - *Wood Science and Technology*, 54, 1463-1478. <https://doi.org/10.1007/s00226-020-01228-8>.
- Wavetek Meterman. [WWW document]. - URL <https://www.tequipment.net/WavetekMetermanLCR55.html>. [Accessed 13 August 2021].
- Welling, J. 2010. Dried timber- how to specify correctly. European Drying Group (EDG), COST E53. 38 pp. [WWW document]. - URL [https://businessdocbox.com/storage/76/74044204/1638107577/Y3f92\]3v0Zn6mj1C96VKOA/74044204.pdf](https://businessdocbox.com/storage/76/74044204/1638107577/Y3f92]3v0Zn6mj1C96VKOA/74044204.pdf). [Accessed 13 April 2021].
- Zuleta, M. 2005. Electrochemical and ion transport characterisation of nanoporous carbon derived from SiC. - Doctoral thesis. Stockholm, KTH-Royal Institute of Technology, Department of Chemical Engineering and Technology. 85 pp. [WWW document]. - URL <http://www.diva-portal.org/smash/record.jsf?pid=diva2%3A7694&dsid=-1261>. [Accessed 13 August 2021].

Puidu niiskussisalduse määramise kahe vahelduvvoolu meetodi katsetamine puidukuivati tingimustes

Hannes Tamme, Regino Kask, Peeter Muiste ja Valdek Tamme

Kokkuvõte

Selles artiklis uuriti kahte erinevat vahelduvvoolu meetodit puidu niiskussisalduse määramiseks. Dielektrilise mahtvusmeetodi (lühidalt *mahtvusmeetod*) korral asetatakse puit, mille niiskussisaldust määratakse, omavahel, ja ühtlasi uuritavast puidust elektriliselt isoleeritud metallplaatide vahele. Moodustub nn. mõõtekondensaator, milles puit täidab dielektriku rolli. Plaatide vahelise elektrimahtvuse mõõtmiseks rakendatakse plaatidele vahelduvpinge. Puidu niiskussisaldus muudab dielektriku (antud juhul puidu) elektrilisi omadusi, ning seetõttu muutub ka mõõtekondensaatori elektrimahtvus, mis mõõdetakse ja seostatakse mõõtemudelise ehk kalibreerimismudelise puidu niiskussisaldusega. Teise vahelduvvoolu meetodi, elektrilise impedantsi spektromeetria meetodi korral antakse vahelduvpinge otseselt puitu sisestatud roostevabast terasest või süsinikkiust nõuelektroodidele, ja mõõdetakse puidu elektrilist kogutakistust (impedantsi), seejärel koostatakse vastav mõõtemudel puidu niiskussisalduse määramiseks.

Elektrilise impedantsi spektromeetria ja mahtvusmeetodi kasutamise võimalusi on üheaegselt üle kiu küllastuspunkti

puidu niiskussisaldustel ja puidukuivati karmides kliimatingimustes suhteliselt vähe uuritud. Selle uurimuse raames tehti mahtvusmeetodi kalibreerimiseks kasutatud mõõtekondensaatori prototüübi töökindluse katsetused puidukuivati karmi sisekliima (50°C ja 98% RH) tingimustes. Uuriti veeauru kondenseerumist mõõtekondensaatori plaatidel, plaatide isolatorite lekkimist ja staatiliste elektrilaengu tekkimist plaatidel. Mõõtekondensaatori töökindlust häirivate efektide jaoks leiti iga efekti poolt esile kutsutud parasitmahtvustele kvantitatiivsed vahemikud. Leiti, et mahtvusmeetod on puidukuivati karmides kliimatingimustes kasutamiseks vähem töökindel kui elektrilise impedantsi meetod. Samuti modelleeriti võrdlevalt samades katsetingimustes ja sama puuliigi (kask) korral mahtvusmeetodi ja elektrilise impedantsimeetodi võimalusi etteantud Rozema kvaliteedikriteeriumiga $\pm 1.75\%$ kasepuidu niiskussisalduse ennustamiseks üle puidu kiu küllastuspunkti niiskussisaldustel. Samades katsetingimustes osutus kasepuidu niiskussisalduse ennustamisel üle kiu küllastuspunkti puidu niiskussisalduste piirkonnas mahtvusmeetod täpsemaks kui elektrilise impedantsi meetod.

Received August 23, 2021, accepted October 04, 2021



Tamme, H., Muiste, P., Tamme, V. 2021. Optimizing the pine wood drying process using a critical diffusion coefficient and a timed moistening impulse. *Forestry Studies*, 75, 150–165.

Research paper

Optimizing the pine wood drying process using a critical diffusion coefficient and a timed moistening impulse

Hannes Tamme*, Peeter Muiste and Valdek Tamme

Tamme, H., Muiste, P., Tamme, V. 2021. Optimizing the pine wood drying process using a critical diffusion coefficient and a timed moistening impulse. – Forestry Studies | Metsanduslikud Uurimused 75, 151–166, ISSN 1406-9954. Journal homepage: <http://mi.emu.ee/forestry.studies>

Abstract. This article demonstrates that it is possible to optimize the drying process for pine wood in two independent ways. Those ways involve either the use of the critical diffusion coefficient (DC) which is determined by the experiment shown below, and/or the drying air moistening impulse in the second drying phase. When processing data which has been gained from the pine wood drying experiment, both coincidences and differences were found when compared to the results from a simulation of the drying process which was carried out using the same drying schedule. There is a relatively good level of agreement between the drying experiment and the simulation results of TORKSIM v5.11 simulation program in the case of the simulated and experimentally determined drying curves. The magnitude of numerical values for the DC agrees with this finding, as do the wood’s moisture profile in the final phase of the drying experiment at 142 hours, the simulated and measured wood surface temperatures from the beginning of drying to a point at 60 hours into the process, and the simulated wood stresses when compared with the maximum values for the electrical surface-core ratio (ESCR) graph, as determined by the experiment. It was found that the DC’s numerical value decreases sharply by about 1.5 times after transitioning from the first drying phase to the second drying phase.

Key words: critical diffusion coefficient, moistening impulse, optimization, wood drying.

Authors' addresses: Institute of Forestry and Rural Engineering, Estonian University of Life Sciences, Kreutzwaldi 5, 51006 Tartu, Estonia; *e-mail: hannes.tamme@student.emu.ee

Introduction

In order to add value to wood as a renewable resource, the process of convective drying for sawn timber is one of the key steps in the further use of wood in the construction trade and in the furniture industry, as well as in the production of thermowood (Kask *et al.*, 2021). The purpose behind the wood drying process is to reduce the aver-

age moisture content in the wood (with a final moisture content level of up to 7–12% MC). The accompanying goal is to disinfect the wood material at temperatures between 50–70°C, without causing discoloration (Tamme *et al.*, 2021). The main measurable quantity to have been monitored in the industrial wood drying process is the wood average moisture content (MC), the changing over time of which provides what is

DOI: 10.2478/fsmu-2021-0017



© 2021 by the authors. Licensee Estonian University of Life Sciences, Tartu, Estonia. This article is an open access article distributed under the terms and conditions of the Creative Commons Attribution (CC BY) license (<http://creativecommons.org/licenses/by/4.0/>).

known as the wood drying curve (Tamme *et al.*, 2011; Tronstad *et al.*, 2001; Tamme, 2016; Mändoja, 2015; Poljakov, 2013). The validity of the stress readings, which have been found in the industrial drying simulation, has also been checked by means of a case-hardening test (Mändoja, 2015; Poljakov, 2013). Unfortunately, it is not possible to decide on the basis of the drying curve and the case-hardening test alone whether or not the wood drying process is optimal in terms of the desired quality and energy consumption levels. In fact, the standard equipment being used for wood dryers (in the form of kilns) does not include specific surface MC and deformation sensors, both of which are important when it comes to solving the optimization task, but which would also be unlikely to withstand the extreme climatic conditions which prevail inside the drying chamber. An attempt has also been made to resolve the problem of optimizing the wood drying process with the help of the wood drying simulation program, TORKSIM (Salin, 1990; Salin, 2007). The TORKSIM program provides an upper limit when it comes to the allowable tensile stresses, which should not exceed one third (0.33) of the maximum stress point which will produce a rupture in the tangential direction of the wood fibre. This program has been selected as the main criterion for optimizing the drying process (Salin, 2007). The commercial process optimization program, StatEase Design-Expert, includes what is known as the desirability function as an optimization criterion. The wood drying simulation program, TORKSIM v5.11, and the optimization program, StatEase Design Expert (DE) v9 and v11, were both used to resolve the problem of optimizing wood drying times in Sova *et al.* (2016), and in Tamme *et al.* (2021). DE requires for its drying tensions the use of time-constant drying modes as an input for the optimization process, which unfortunately causes drying stresses which are higher than 0.33 for material which is thicker than 20 mm, thereby creating a substantial contradiction

between the TORKSIM and DE optimization criteria (Tamme *et al.*, 2021).

The aim of this paper is to investigate the possibilities involved in the process of being able to optimize drying stresses and drying time during the convective drying of wood, by experimentally determining the optimum water vapour diffusion coefficients in the drying process and using a timed moistening impulse. To this end, novel sensors were developed for wood surface moisture content and wood surface deformation, and these were calibrated for use in the harsh climatic conditions of a wood kiln.

Material and Methods

Theoretical background

The local diffusion coefficient can be experimentally determined according to Fick's first law (Fick, 1855; Crank, 1956; Salin, 1990; Tamme, 2016):

$$F = -D \frac{\partial u}{\partial x} \quad (1)$$

where F - mass flux, ($\text{kg}/\text{m}^2\text{s}$); D - diffusion coefficient, (m^2/s); u - mass concentration, (kg/m^3); x - coordinate, (m).

During the convective drying of wood, heat is transferred from the surrounding air through the surface to the interior of the wood and, at the expense of the heat energy being transferred to it, the moisture evaporates from the wood, i.e., the wood is dried. The main equations for describing the heat flow of dry air which is transferred to wood and the heat flow of moist air which leaves the wood are as follows (Salin, 1990):

$$\Theta_1 = \alpha S(T_0 - T) \quad (2)$$

$$\Theta_2 = \beta c_p S(T_0 - T) \quad (3)$$

where Θ_1 and Θ_2 - heat flow (W); α - heat

transfer coefficient ($W/m^2 \text{ } ^\circ C$); β – mass transfer coefficient (m^2/s); c_p – the specific heat of humid air in equilibrium with the wood’s surface ($J/^\circ C \text{ } m^3$); S – the surface area of the specimen (m^2); T_0 – surrounding air temperature ($^\circ C$); T – wood surface temperature ($^\circ C$).

Materials and cross-sections of wood specimens used in the study

As part of the laboratory drying experiment, three pine sapwood specimens were used which had been cut from the same board with a cross-section of 35 mm (thickness) \times 150 mm (width) and a length of 100 mm along the wood fibres. Sensors were attached to specimen a) to monitor the drying process; and with specimen b) being the reference specimen for determining the drying curve by weighing; while specimen c) was used to determine the moisture content of the wood at different depths by the slicing method (Tremblay *et al.*, 2000; Tamme *et al.*, 2021).

Description of the methodology used in the investigation

For a wood drying optimization system, it is first necessary to develop reliable and accurate sensors to be able to record the average moisture, local moisture, and surface moisture levels in the wood, as well as including a sensor to record the deformation of the wood’s surface. These sensors must simultaneously withstand temperatures of 50–80 $^\circ C$ and high relative humidity levels of 95–100% RH which are characteristic of a convective kiln (Tamme *et al.*, 2021). In addition to the laboratory drying experiment, it is necessary to carry out various simulations using the commercial program, TORCSIM v5.11 for the optimization process. As there are no specified sensors in the standard equipment of any industrial wood dryers as supplied which would allow any optimization, it makes sense under laboratory conditions to optimize a specific drying recipe (i.e., create a drying plan) which is to be used in an industrial

dryer, and then to incorporate the laboratory-optimized method into standard industry practices once it has been proved to be the right choice.

The methodology for the experiment is described in more detail, together with photos, in the final report for the EIC contract No 16200 (Tamme *et al.*, 2021). The basic scheme for the experiment is shown in Figure 1(a) and Figure 1(b) in the photograph.

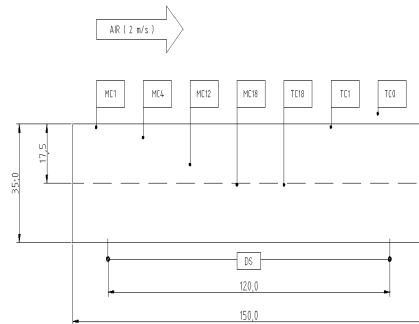


Figure 1. (a) Schematic diagram of the drying experiment and some insight into the Feutron working space of the climatic chamber (Feutron Klimasimulation GmbH, 2021).



Figure 1. (b) Three specimens were used in the experiment being shown here. Sensors were attached to specimen a) to monitor the drying process; specimen b) was a reference specimen which was being used to determine the drying curve by means of weighing; and specimen c) was used to determine the moisture content of the wood at different depths by means of slicing.

For monitoring the drying process, the 9-channel data logger Almemo 2890-9 manufactured by Ahlborn (Ahlborn, 2021) as well as the 8-channel data loggers Thermofox and Gigamodule produced by Scanntronik (Scanntronik, 2021) were used. Drying simulation was done with the program TORKSIM v5.11. For entering the simulation results and experiment log files in the data processing aggregate table, the so-called robot laboratory assistant was used to reduce manual processes and avoid human error in data entry (Tamme, 2013; Romann *et al.*, 2014). For data processing and figure formatting, the spreadsheet program Excel and freeware program MatPlotLib v. 3.4.3. were applied.

Results and Discussion

The calibration of electrical resistance sensors for wood MC detection sensors

When calibrating electrical resistance sensors for wood MC monitoring sensors, a cross-section linear calibration function was used, an example of which is shown in Figure 2 at depth levels of 1 mm and 4

mm below the wood’s surface. The points A, B, C, and D which are shown in Figure 2 are known as calibration points with corresponding coordinates ($x = 10\text{LogR}$; $y = \text{MC}\%$). For sections AB, BC, and CD, the calibration function was presented in a generalised form (Tamme *et al.*, 2021):

$$\frac{y - y_1}{y_2 - y_1} = \frac{x - x_1}{x_2 - x_1} \tag{4}$$

From Formula (4), one calibration function was derived for each section at a particular depth level. Corresponding calibration functions are shown in Table 1. To calibrate the electrodes being used in the experiment at depths of 1 mm, 4 mm, 8 mm, 12 mm, and 18 mm into the wood’s MC sensors, three calibration functions are required for each depth level, so that a total of fifteen calibration functions were derived in order to be able to monitor the wood’s MC through five depth electrodes. Six of them are presented in Table 1. The feasibility of using the cross-section linear calibration function was proven by means of modelling for two papers (Tamme *et al.*, 2014; Tamme, 2016).

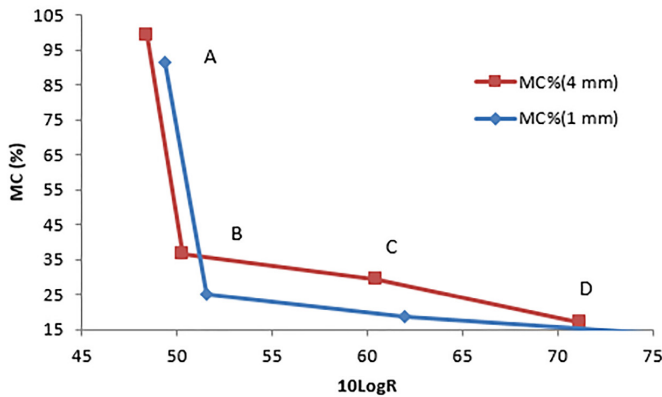


Figure 2. A cross-section linear calibration function for the calibration of resistance-type sensors into the wood’s MC sensors. Points A, B, C and D are the endpoints of the line segment.

Table 1. Calibration functions were derived from Formula (4) for electrical resistance sensors at depths of 1 mm and 4 mm from the surface of the wood in sections AB, BC, and CD.

Depth (mm)	AB	BC	CD
1 mm	$y = -30.277x + 1584.9$	$y = -0.6058x + 56.458$	$y = -0.3867x + 42.873$
4 mm	$y = -32.895x + 1691.4$	$y = -0.7255x + 73.292$	$y = -1.1495x + 98.947$

A determination of the optimal diffusion coefficient, experimentally and through simulations

In the laboratory drying experiment and the drying simulation, an industrial drying schedule was used for pine wood specifically, which is presented in Table 2.

Table 2. Industrial 35 mm pine wood drying schedule used in the experiment and the simulation section.

Time (h)	Air temp. (°C)	Air RH (%)
0	20	93
1	47	93
12	47	93
36	50	90
60	52	85
84	52	80
108	52	69
132	52	59
156	52	49
180	52	39
204	52	39

The diffusion coefficient was determined from Fick's first law according to Formula (1) (Tamme *et al.*, 2011). Fick's first law, in the form of a partial derivative differential equation Formula (1), is not directly suitable for processing experimental data or the simulation data. Firstly, in Formula (1) the partial derivatives must be adjusted for finite increments in order to process the experimental and simulation data. Secondly, the experiment and simulation data are dimensionless with relative units (MC %). In order for the diffusion coefficient (DC) which is found in finite

increments to acquire the correct dimensions (m^2/s), a constant which contains the dimensions of the units of measurement must be introduced into the formula for practical use. Thirdly, both the experimental data and the simulation data contain random errors, which must be carefully filtered out prior to calculating the DC. In principle, the diffusion coefficient DC can be given according to Formula (1) as the ratio of the mass flux to the gradient:

$$D = -\frac{\text{Massflux}}{\text{Gradient}} \quad (5)$$

$$\text{Massflux} = -\Delta(\text{MC}\%) \frac{m_{\text{dry}}}{\Delta t * S} \quad (6)$$

$$\text{Gradient} = \Delta(\text{MC}\%) \frac{\rho_{\text{wood, dry}}}{\Delta x} \quad (7)$$

where D - diffusion coefficient (DC) (m^2/s); $\Delta(\text{MC}\%)$ - the finite increment of the wood's MC% on the time axis for the mass flux and in the material thickness (x-axis) for the gradient (MC%); m_{dry} - the wood's dry mass (kg); S - the specimen's surface area (m^2); Δt - the time increment (s); $\rho_{\text{wood, dry}}$ - the wood's dry density (kg/m^3); Δx - the x coordinate's increment (m).

After filtering out the random errors, the DC calculation is presented schematically using the four-point method shown in Figure 3. The coordinates of the points which have been marked with the 'diamond' marker in Figure 3 are presented in Table 3. The principle of the four-point method is that, initially, two mass flux val-

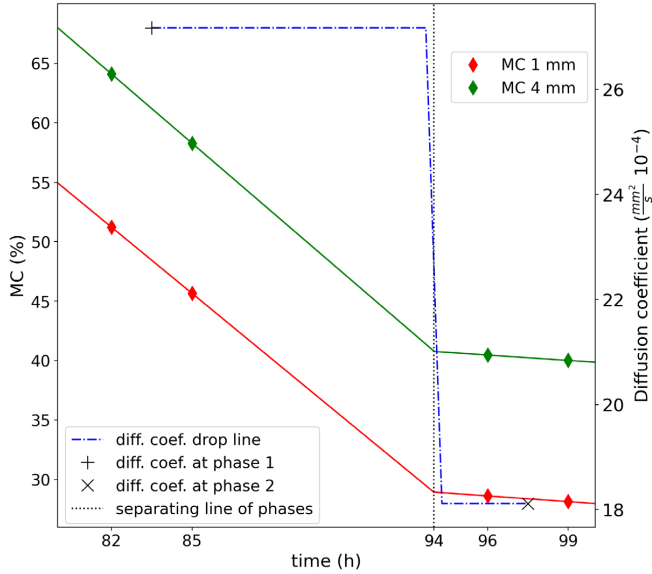


Figure 3. A schematic for calculating the diffusion coefficients in the first and second drying phases, using the four-point method based on experimental data.

ues were obtained at depths of 1 mm and 4 mm, from which the arithmetic mean mass flux was obtained following averaging. Two gradients were also obtained at two different time points, which were then arithmetically averaged. Finally, the average DC at the average depth, i.e., $(1 + 4) / 2 = 2.5$ mm deep from the wood's surface, was calculated according to Formula (5).

After carrying out these calculations, the values of the experimental DC were following: $DC_{1ph.} = 27 \cdot 10^{-4} \text{ mm}^2/\text{s}$ in the first drying phase and $DC_{2ph.} = 18 \cdot 10^{-4} \text{ mm}^2/\text{s}$ in the second drying phase (Tamme *et al.*, 2021). At the end of the first drying phase and at the beginning of the second drying phase, the simulated DC has an almost equal value (i.e., $11.8 \cdot 10^{-4} \text{ mm}^2/\text{s}$).

As the drying process passes from the first drying phase to the second drying phase, a sharp decrease in the numerical value of DC occurs at 94 hours. From Figure 3 it can be concluded that there is a sharp decrease in mass flux in the second drying

phase when compared with the first drying phase. The gradient is approximately constant in the first drying phase, and there is a minimal decrease in the average gradient in the second drying phase. Consequently, the sharp decrease in DC is due to the sharp decrease in mass flux in the second drying phase. Consequently, in order to optimize the drying process, the first drying phase should remain within the region of the maximum mass flux for as long as possible. This fact should be taken into account when optimizing the drying schedule. The maximum value of the diffusion coefficient immediately before entering into the second drying phase was named the *critical diffusion coefficient*. Mass flux, gradient, and critical DC are values which are difficult to determine under industrial wood drying conditions. Therefore, based on the separating line of the first and second drying phase, it makes more sense to determine the critical relative humidity (RH) of the drying air on the basis of the

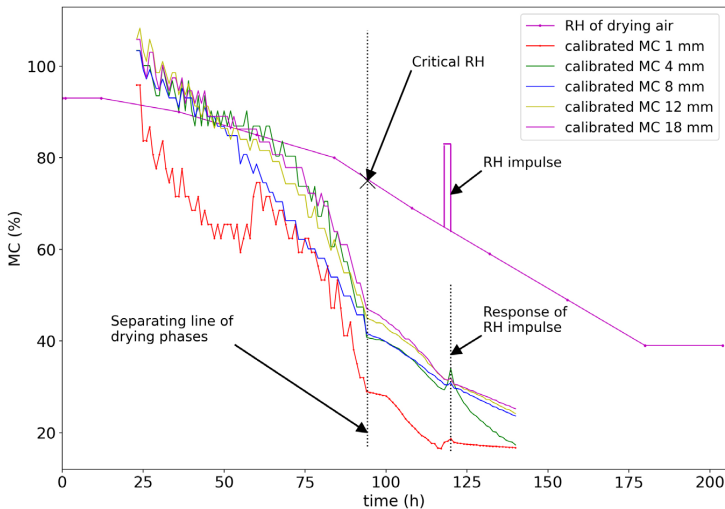


Figure 4. Identification of the critical RH of the drying air according to the separating line of the first and second drying phase.

laboratory test, below which the drying process enters the second drying phase. Monitoring the critical RH value is not a problem in industrial conditions, as wood dryers are usually standard-equipped with a corresponding sensor and a logging option. The determination of critical RH is shown schematically in Figure 4.

Options involved in terms of distinguishing between the first and second drying phases on the basis of sensor readings and log files

The ability to be able to determine the critical RH on the basis of sensor readings alone would be of great practical value under industrial conditions, as the somewhat complex procedure for calibrating the sensors and the equally complex procedure for determining the critical DC would both be eliminated.

The distinction between the first and second drying phase based on the log file of an electrical resistance sensor (i.e., before calibrating into a sensor for the wood's MC) is illustrated in Figure 5. Figure 5

shows that, at 1 mm and 4 mm, electrical resistance starts to increase systematically from 94 hours (i.e., at the transition point to the second drying phase), when compared to the linear trend line for the average electrical resistance in the first drying phase.

The distinction between the first and the second drying phases is illustrated in Figure 6, based on the log files of three sets of temperature sensors and the displacement sensor. It can be seen from Figure 6 that, at the beginning of the second drying phase, the thermocouple readings from the wood's surface and from the centre part begin to diverge. At the same time, the readings from the displacement sensor, which registers the shrinkage of the wood surface, begin to decrease. Both changes in the sensor readings start at 94 hours of drying. Therefore, the first and second drying phase can experimentally be distinguished in four independent ways: according to (a) uncalibrated and (b) calibrated electrical resistance sensors, (c) a displacement sensor, and (d) log files of three temperature sensors.

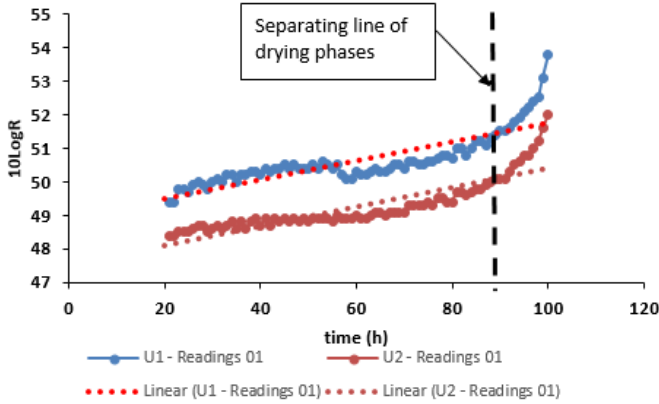


Figure 5. The response for uncalibrated electrical resistance sensors (at depths of 1 mm and 4 mm) upon transition from the first drying phase to the second drying phase.

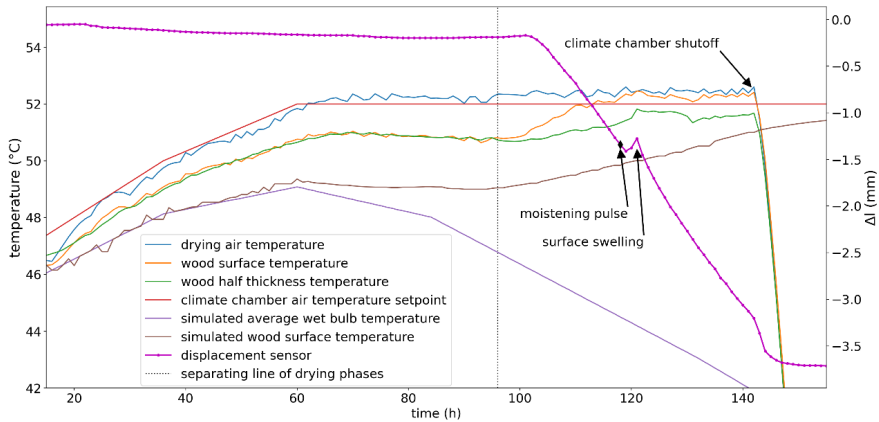


Figure 6. A distinction between the first and the second drying phases based on the log files of three Ahlborn thermocouples and an Ahlborn displacement sensor.

Sensor responses to a short-term increase in the RH of the drying air, i.e., the so-called moistening impulse

A short three-hour moistening impulse was generated during the experiment, in the second phase of drying, starting at 116 hours, in order to verify the response of, and delay inherent in the sensors. From the initial level of RH = 65.1% at 116 hours, the relative humidity RH of the climate cham-

ber air was increased to 95% by opening the valve with a manually operated humidifier, and was maintained at this level for three hours. The humidifier valve was then closed, and the climate chamber's automation quickly restored the RH value of the air in the chamber as prescribed by the drying program. The effect of the moistening impulse on the electrical resistance sensors is shown in an enlarged format

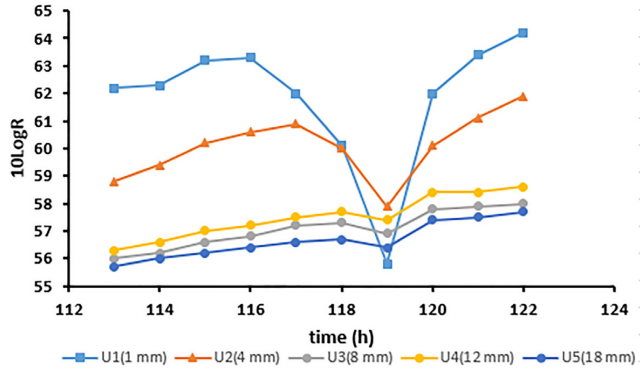


Figure 7. Effect of moistening impulse on the electrical resistance sensors.

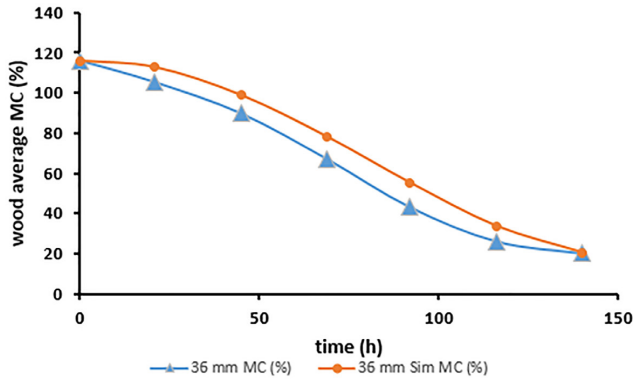


Figure 8. A comparison of drying curves under simulation and during experimentation as determined on the basis of the industrial drying schedule.

in Figure 7. The real effect of the moistening impulse on the displacement sensor is shown in Figure 6. Figure 6 shows that the moistening impulse essentially has no effect on the temperature sensors (thermocouples).

The expansion of the wood's surface layer which was identified in Figure 6 counteracts the tensile stresses in the surface layer which are caused by drying. Consequently, a precisely timed moistening impulse based on a simulation could in practice be used to alleviate the maximum tensile stresses to a safe limit (0.33) in the

surface layer, thereby reducing the risk of drying cracks appearing due to tensile stresses.

The results from optimizing the industrial pine wood drying schedule

The industrial drying schedule (see Table 2) shows that the drying schedule satisfies the main optimization conditions which were set in the TORKSIM program, i.e., the maximum relative tensile stresses in the surface layer are less than the maximum allowable value of 0.33 (Salin 2007; Tamme *et al.*, 2021). Whether the industrial

drying schedule being used in the experiment is also the optimum one in terms of drying time is something which still needs to be confirmed. To this end a new drying schedule was drawn up, based on the definitions of critical DC and its associated critical RH. A corresponding optimized drying schedule (Tamme *et al.*, 2021) is presented in Table 3, and the drying results which were simulated with the optimized drying schedule are shown in Figure 8.

Table 3. Optimized industrial pine wood drying schedule based on the definition of critical DC and critical RH.

Time (h)	Air temp. (°C)	Air RH (%)
0	20	60
1	47	83
113	52	81
132	52	59
156	52	49
180	52	39
204	52	39

Figure 9 shows that an optimized drying schedule can provide an MC in the wood which is up to 30.9 % lower with the same drying time when compared to an unop-

timized drying schedule at virtually the same relative stress levels (0.25) (Tamme *et al.*, 2021).

Another way to shorten the drying time is to force the drying process (Tamme *et al.*, 2011). The drying time in the initial drying schedule was reduced by using as a basis the consideration that the relative humidity of the drying air would decrease by 16% RH per day (Tamme *et al.*, 2011). Forced drying of this type would reduce the overall drying time by about 3.5 days when compared to the original industrial drying regime (see Table 5). In principle, the same thing was done using the StatEase Design Expert program, when the drying time was randomly varied within a predetermined range (Sova *et al.*, 2016, Tamme *et al.*, 2021). Usually, an arbitrary shortening of the drying time in the drying schedule, i.e., forcing the drying process, leads to an increase in the drying stresses above the dangerous level (0.33). According to the results which were obtained previously, dangerous stresses can be neutralised by means of a precisely timed moistening impulse in the second drying phase. The forced drying schedule is presented in Table 4. The corresponding simulation results for the forced drying schedule are presented in Figure 10.

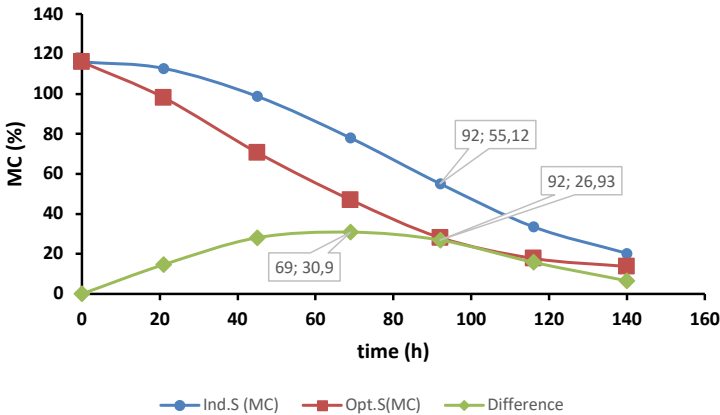


Figure 9. The results of simulations regarding optimized and unoptimized drying schedules.

Table 4. A forced drying schedule for pine wood. Data regarding the stages of the moistening impulse are given in parenthesis in the table.

Time (h)	Air temp. (°C)	Air RH (%)
0	20	93
1	47	93
24	47	77
48	50	61
72	52	45
(90)	(52)	(40)
96	52	29
120	52	13

Figure 10 and Table 4 indicate that, due to the forcing of the drying schedule, the total drying time decreased by 84 hours but, due to the moistening impulse which was added to the drying schedule, the drying time increased by ca 1 h, and the simulated stress decreased by 0.30. Therefore the savings in the drying time at safe stresses (0.30) in order to achieve the same final moisture content of 12% MC was set at 83 hours.

The statistical processing of experimental data

The statistical processing phase should at least broadly reflect the causal rela-

tionships between the physical processes which take place during the drying of the wood. From this general point of view, it would be interesting to be able to study the compatibility of the ‘electric fingerprint’ of wood drying, i.e., the log files regarding the wood’s electrical resistance levels, and the relative stresses in simulated wood, in two cases shown in detail below: a) by examining on a non-statistical basis the coincidence of the maximum point of the electrical indicator on the drying time scale; and b) by compiling a linear model of the relationship between the electrical indicators of the behaviour of the wood’s surface layer and its central part.

The electrical surface-core ratio (ESCR) was chosen as an electrical indicator of the behaviour of the wood’s surface layer and inner layer, defined as follows:

$$(ESCR) = (10\text{Log}R_{1\text{mm}} + 10\text{Log}R_{4\text{mm}}) / (10\text{Log}R_{8\text{mm}} + 10\text{Log}R_{12\text{mm}} + 10\text{Log}R_{18\text{mm}}) \quad (8)$$

Using the Scantronik Gigamodule measurement channel designations in the electrical resistance log file, the formula can be shortened:

$$ESCR = (U1 + U2) / (U3 + U4 + U5) \quad (9)$$

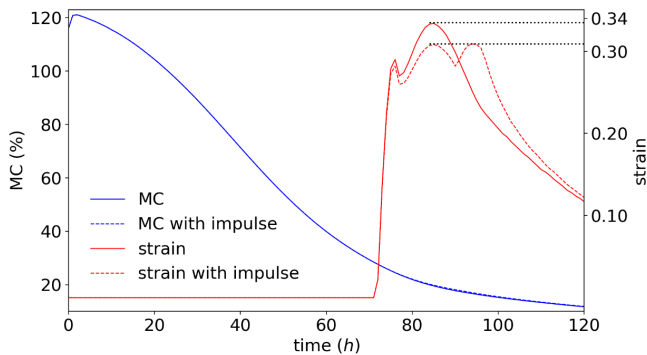


Figure 10. The forced drying schedules simulation graphs without the moistening impulse, and with the moistening impulse.

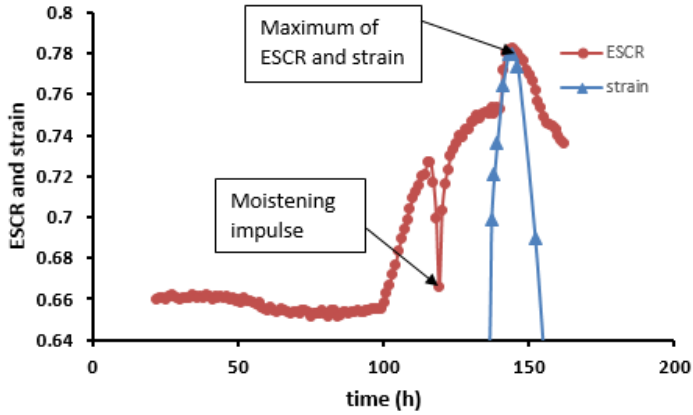


Figure 11. Dependencies of the ESCR value and the TORKSIM v5.11 simulated relative drying stresses on drying time. For a better visual comparison, the simulated relative stresses are multiplied by a factor of 3.12.

In Figure 11, the drying time scale on the ESCR graph shows three clearly distinguishable elements of the laboratory drying experiment, with the correct turnout time: firstly, the transition from the first drying phase to the second drying phase at 92 hours. (Note: the transition of the drying phases begins at 94 hours, with a slow rise, and only becomes noticeable at 100 hours in Figure 11); secondly: the start of the moistening impulse at 116 hours; third:

the full coincidence of the maximum ESCR and the maximum simulated relative stress at 143 hours.

In the linear model of electrical indicators for the wood's surface layer and inner layer in Figure 12, the determination coefficient is $R^2 = 0.9838$, which indicates the existence of a strong causal relationship between the wood's surface layer and inner layer in the drying test. Based on the model, it can be assumed that the moisture

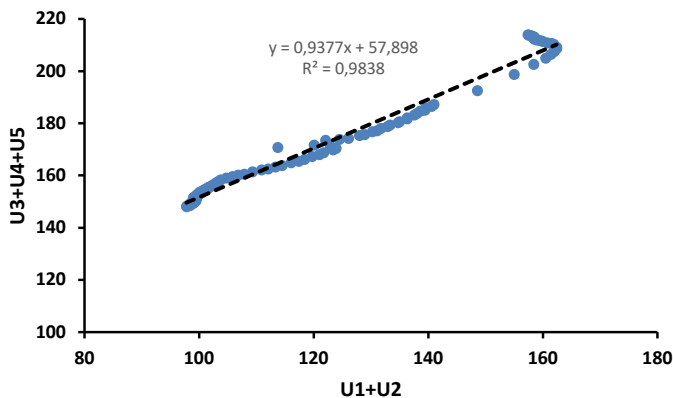


Figure 12. A linear model of the relationship between the electrical indicator for the surface layer and the electrical indicator for the inner layer.

content of the wood's surface layer controls the moisture content of its inner layer.

The potential advantages of the wood tension indicator which is presented in Figure 11 over an indicator which is based on acoustic emission (AE) (Tiitta *et al.*, 2010) include a simpler technical implementation, better reliability in the harsh climatic conditions of a wood dryer, and higher sensitivity levels. However, the advantages and disadvantages of both indicators would be identified by the use of a benchmark.

An analysis of coincidences and differences in the results of the experiment and the TORCSIM v5.11 simulation programs

There is relatively good agreement between the drying experiment and the simulation results in the simulated and experimentally determined drying curves (see Figure 8), the wood's moisture profile before the end of the second phase of the drying experiment at 142 hours (see Figure 13 (b)), the wood's surface simulated and measured in terms of temperature from

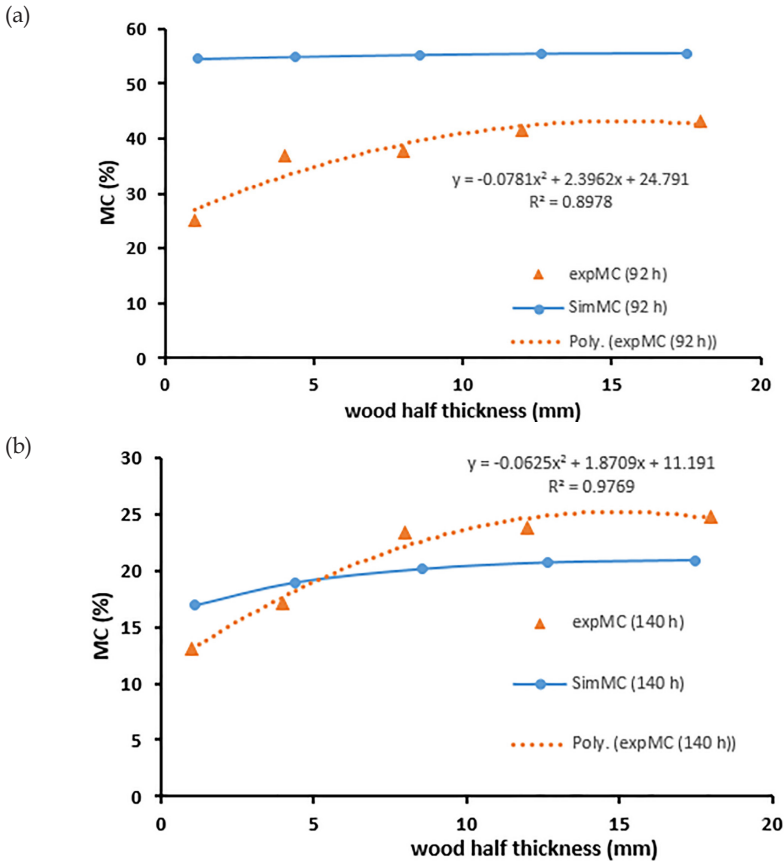


Figure 13. Comparison of experimental and simulated moisture profiles in pine wood: a) after 92 hours b) after 142 hours. Figure 13. Comparison of experimental and simulated moisture profiles in pine wood: a) after 92 hours b) after 142 hours.

the start of drying to 60 hours into the process (see Figure 6), and at simulated wood stresses at the maximum level of the ESCR graph as determined through the experiment (Figure 11).

The critical DC, which is something that is characteristic of the experiment (see Figure 3), is very weakly expressed based on the simulation results. At the end of the first drying phase and at the beginning of the second drying phase, the simulated DC (diffusion coefficient) has an almost equal value (i.e., $11.8 \cdot 10^{-4} \text{ mm}^2/\text{s}$).

The DC's numerical values as determined and simulated through the experiment also differ significantly both ten hours before and ten hours after the 94-hour mark, which is when the transition from the first drying phase to the second drying phase takes place (accordingly: $DC_{1ph.} = 27 \cdot 10^{-4} \text{ mm}^2/\text{s}$, $DC_{2ph.} = 18 \cdot 10^{-4} \text{ mm}^2/\text{s}$, and $DC_{sim.} = 11.8 \cdot 10^{-4} \text{ mm}^2/\text{s}$). There is also no agreement between the wood MC profiles which have been simulated and determined from the experiment at 92 hours (Figure 13 (a)), at the measured and simulated wood surface temperatures after 60 hours until the end of the drying experiment (Figure 6). From the significant difference between the simulated and measured wood surface temperatures it can be concluded that the heat transfer coefficient and mass transfer coefficient in theoretical background Formulas (2) and (3) are no longer constant after 60 hours, but instead depend upon the wood moisture content.

Conclusions

When processing the data from the drying experiment, both coincidences and significant differences were found when comparing this experiment with the results from the simulation run on the basis of the same drying schedule. It was shown that it is possible to optimize the wood drying process in two independent ways, i.e., using a critical DC and/or using a moistening im-

pulse for the drying air in the second drying phase. From the point of view of monitoring the drying experiment, it seems expedient that the minimum number of resistance-type wood moisture sensors is five, and the optimum number of temperature sensors (thermocouples) is three. There should be at least one displacement sensor placed in the drying experiment. Based on the raw files of the electrical resistance measuring channels, a rather expressive drying tensile stress indicator can be constructed in graphical form.

Acknowledgements. This work was supported by the Environmental Investment Centre of Estonia (Grant No. 16200).

References

- Ahlborn. [WWW document]. - URL <http://www.ahlborn.com>. [Accessed 22 October 2021].
- Crank, J. 1956. *The Mathematics of Diffusion*. Oxford, Clarendon Press. 347 pp.
- Feutron Klimasimulation GmbH. [WWW document]. - URL <https://www.feutron.de/en/weathering-chamber/>. [Accessed 22 October 2021].
- Fick, A. 1855. Ueber Diffusion. - Pogendorff, J.C. (ed.). *Annalen der Physik und Chemie*, Vol. 94, 59–86. (In German).
- Kask, R., Mitt, R. 2021. Increasing the potential for the use of red cored gray alder, black alder and birch wood by heat treatment. (Punasüdamikuga halli lepa-, sanglepa-, ja kasepuidu kasutusvõimaluste suurendamine termilise töötlemise abil.) - KIK metsanduse programmi projekti nr. 16531 lõpparuanne, 33 pp. [WWW document]. - URL <https://mi.emu.ee/teadusinfo/projektide-aruanded/kik-projektid/> [Accessed 22 October 2021]. (In Estonian).
- Mändoja, M. 2015. Wood drying simulation "TORKSIM" adjusting to actual industrial drying curve in order to improve the reliability of tension calculations and electrical humidity sensors. (Puidu kuivatuse simulatsiooniprogrammi "TORKSIM" sobitamise reaalsete tööstusliku kuivatuskõvera, eesmärgiga tõsta pinge arvutuste ja elektriliste niiskusandurite usaldusväärsust). - Bachelor thesis. Tartu, Estonian University of Life Sciences. 51 pp. (In Estonian with English summary).

- Poljakov, A. 2013. Wood material comparison of actual moisture content monitoring data in wood dryer "Mühlböck" and "Hekotek". (Puitmaterjali tegeliku niiskussalduse võrdlus monitooringu andmetega puidu kuivatites "Mühlböck" ja "Hekotek") - Master thesis. Tartu. Estonian University of Life Sciences. 125 pp. (In Estonian).
- Romann, T., Oll, O., Pikma, P., Tamme, H., Lust, E. 2014. Surface chemistry of carbon electrodes in 1-ethyl-3-methylimidazolium tetrafluoroborate ionic liquid - an in situ infrared study. - *Electrochimica Acta*, 125, 183-190.
- Salin, J.G. 1990. Simulation of the timber drying process. Prediction of moisture and quality changes. - Doctoral thesis. Helsinki, EKONO Oy. 103 pp.
- Salin, J.G. 2007. Lectures. Riga, 2007. [WWW document]. - URL <http://www.coste53.net/downloads/WG2/WG2-Riga/Lectures/Riga2007-Salin.pdf>. [Accessed 22 October 2021].
- Scantronik Mugrauer GmbH. [WWW document]. - URL www.scantronik.de/. [Accessed 22 October 2021].
- Sova, D., Bedeleian, B., Sandu, V. 2016. Application of Response Surface Methodology to optimization of wood drying conditions in a pilot-scale kiln. - *Baltic Forestry*, 22(2), 348-356.
- Tamme, H. 2013. Process management framework on the example of convective drying of wood and spectroelectrochemistry. - MSc. thesis. Tartu, University of Tartu. 25 pp.
- Tamme, V. 2016. Development of resistance-type control methods for wood drying. - PhD thesis. Tartu, Estonian University of Life Sciences. 135 pp.
- Tamme, V., Muiste, P., Mitt, R., Tamme, H. 2011. Determination of effective diffusion coefficient and mechanical stress of pine wood during convective drying. - *Baltic Forestry*, 17(1), 110-117.
- Tamme, V., Muiste, P., Padari, A., Tamme, H. 2014. Modelling of resistance-type wood moisture meters for three deciduous tree species (black alder, birch, aspen) in moisture contents above fibre saturation point. - *Baltic Forestry*, 20(1), 157-166.
- Tamme, V., Tamme, H., Muiste, P. 2021. Development of experimental and theoretical methodology for optimization of quality and energy consumption of convective drying of wood (chamber drying and tunnel drying. (Puidu konvektiivkuivatuse (kamberkuivatuse ja tunnelkuivatuse) kvaliteedi ja energiakulu optimeerimise eksperimentaalse ja teoreetilise meetodika välja töötamine.) - KIK metsanduse programmi projekti nr. 16200 lõpparuanne, 44 pp. [WWW document]. - URL <https://mi.emu.ee/userfiles/instituudid/mi/MI/Projektid/Projekt1620.pdf>. [Accessed 22 October 2021]. (In Estonian).
- Tiitta, M., Tomppo, L., Lappalainen, R. 2010. Combined method for monitoring wood drying process. - Proceedings of 11th International IUFRO Wood Drying Conference, Sweden, 18-22 January. Skellefteå. 76-80.
- Tremblay, C., Cloutier, A., Fortin, Y. 2000. Experimental determination of the convective heat and mass transfer coefficients for wood drying. - *Wood Science and Technology*, 34(3), 253-276. <https://doi.org/10.1007/s002260000045>.
- Tronstad, S., Sandland, K.M., Toverød, H. 2001. Drying quality of softwood based on 140 industrial tests in Norwegian sawmills and actions to improve the quality. - Proceedings of the 3rd workshop of COST Action E15 on softwood drying to specific end-uses. Advances in the drying of wood (1999-2003). Finland, 11-13 June, Helsinki, 13 pp.

Männipuidu kuivatuse protsessi optimeerimine, kasutades kriitilist difusiooni konstanti ja ajastatud niisutusimpulssi

Hannes Tamme, Peeter Muiste ja Valdek Tamme

Kokkuvõte

Selles artiklis näidati, et männipuidu kuivatuse protsessi optimeerimine on võimalik kahel teineteisest sõltumatu viisil, st kasutades eksperimendist määratud kriitilist difusioonikonstanti DK (DC) ja/või kuivatuse õhu niisutusimpulssi teises kuivatusefaasis. Männipuidu kuivatamise eksperimendi andmete töötlemisel leiti nii kokkulangevusi kui ka erinevusi võrreldes sama kuivatuse plaani (*drying schedule*) alusel simulatsiooniprogrammiga TORK-SIM v. 5.11 läbi viidud kuivatuse protsessi simulatsiooni tulemustega.

Suhteliselt hea kokkulangevus kuivatuseksperimendi ja simulatsiooni tulemuste vahel on simuleeritud ja eksperimendist määratud kuivamiskõveratel (*drying curve*), DK arvuliste väärtuste suurusjärgul, puidu niiskusprofiilil kuivatuseksperimendi lõppfaasis 142. tunnil, puidu pinna simuleeritud ja mõõdetud temperatuuridel kuivatuse algusest kuni 60. tunnini, ja simuleeritud puidu tõmbepingetel (*stress*) eksperimendist määratud *electrical sur-*

face-core ratio (ESCR) graafiku maksimumiga.

Leiti, et eksperimendist määratud DK arvuline väärtus väheneb hüppeliselt ca 1,5 korda pärast üleminekut esimesest kuivatusefaasist teise kuivatusefaasi. Artiklis kirjeldati originaalset elektritakistuse logifailidel põhinevat puidu pinnakihi tõmbepingete elektrilist (ESCR) indikaatorit, mis võimaldab kuivatuse protsessis reaajas monitorida kuivamispingete (*drying stress*) evolutsiooni. Artiklis saadud tulemused on männipuidu tööstusliku kuivatamise optimeerimisel koheselt praktikasse rakendatavad. Samuti on artiklis kirjeldatud eksperimendi meetodika rakendatav lehtpuude kuivatuse uurimisel. Artiklis kirjeldatud eksperimendi meetodika ei eelda ega välista katsetatava puuliigi jaoks kuivatuse simulatsiooni programmi kasutamist, st kuivatuse optimeerimise ülesanne on praktikas edukalt lahendatav ainuüksi eksperimendi tulemustest lähtuvalt.

Received November 17, 2021, accepted December 31, 2021

CURRICULUM VITAE

First name: Hannes
Surname: Tamme
Citizenship: Estonian
Date of birth: 25.11.1982
Address: Institute of Forestry and Engineering, Estonian
University of Life Sciences, Kreutzwaldi 5, 51006 Tartu,
Estonia
E-mail: htamme@emu.ee

Education:
2017 – 2023 Doctoral studies in forestry, Institute of Forestry and
Engineering, Estonian University of Life Sciences
2008–2013 Master of Science in Computer Engineering, University
of Tartu
2002–2007 Aircraft maintenance, Estonian Aviation Academy,
1998–2002 Forestry technician, Luua Forestry School

Foreign Languages: English, Russian

Professional employment:

Since 2022 Estonian University of Life Sciences, Institute of
Forestry and Engineering, Chair of Forest and Land
Management and Wood Processing Technologies, Junior
Researcher
Since 2016 University of Tartu, Faculty of Science and Technology,
Institute of Computer Science, System Administrator

Research interests: Physical and mechanical properties of wood and
wood material

Projects and cooperation:

1.01.2023–31.12.2025 MLTAT23131 (101101903) “National
Competence Centres in the framework of
EuroHPC Phase 2”
1.01.2021–31.12.2024 TT12 “Estonian Scientific Computing
Infrastructure”

- 8.08.2022–11.03.2024 T220055MIMP (RE.4.08.22-0049) “Development of an experimental methodology for optimizing the quality and energy consumption of convective drying of deciduous trees of industrial importance in Estonia (birch, aspen, alder)”
- 1.01.2018–28.02.2023 MOBTT75 “Holistic Big Data Analytics-as-a-Service Framework”. Research staff.
- 1.09.2020–31.08.2022 MLTAT20472R (951732) “National Competence Centres in the framework of EuroHPC”
- 1.12.2020–31.12.2021 COVSG21 “Vacuum deposition of SARS-CoV-2 virus disintegrating metal nanolayers (Cu, alloys, compounds) onto adhesive coatings and face masks”
- 1.01.2020–31.12.2021 RITA1/02-102-02 (RITA1/02-102-02) “Cyber defence simulation of Internet of Things and Mobile Networks in the Cyber Range”

ELULOOKIRJELDUS

Eesnimi: Hannes
Perekonnanimi: Tamme
Kodakondsus: Eesti
Sünniaeg: 25.11.1982
Aadress: Metsanduse ja inseneeria instituut, Eesti Maaülikool,
Kreutzwaldi 5 Tartu 51014, Eesti
E-post: htamme@emu.ee

Haridus:

2017 – 2023 Doktoriõpe, metsanduse õppekava, Metsanduse ja inseneeria instituut, Eesti Maaülikool
2008–2013 Tartu Ülikool, arvutitehnika magistriõpe
2002–2007 Eesti Lennuakadeemia, õhusõiduki hooldus
1998–2002 Luua Metsanduskool, metsandustehnik

Võõrkeelte oskus: Inglise keel, vene keel

Teenistuskäik:

Alates 2022 Eesti Maaülikool, Metsanduse ja inseneeria instituut, Metsa- ja maakorralduse ning metsatööstuse õppetool, nooremteadur
Alates 2016 Tartu Ülikool, Loodus- ja täppisteaduste valdkond, arvutiteaduse instituut, süsteemihaldur

Teadustöö suunad: Puidu ja puitmaterjali füüsikalised ja mehaanilised omadused

Projektid:

1.01.2023–31.12.2025 MLTAT23131 (101101903) ”EuroHPC kompetentsikeskus 2”
1.01.2021–31.12.2024 TT12 ”Eesti Teadusarvutuste Infrastruktuur”
8.08.2022–11.03.2024 T220055MIMP (RE.4.08.22-0049) ”Eestis tööstuslikku tähtsust omavate lehtpuude (kask, haab, lepp) konvektiivkuivatuse kvaliteedi ja energiakulu optimeerimise eksperimentaalse meetodika välja töötamine”

- 1.01.2018–28.02.2023 MOBTT75 ”Terviklik Suurandmete Analüütika-Teenusena Raamistik”
- 1.09.2020–31.08.2022 MLTAT20472R (951732) „EuroHPC kompetentsikeskus”
- 1.12.2020–31.12.2021 COVSG21 „SARS-CoV-2 viirust hävitavate nanokihtide (vask, sulamid, ühendid) tekitamine vaakumsadestusmeetoditega kleebitavatele pinnakatetele ja näomaskidele”
- 1.01.2020–31.12.2021 RITA1/02-102-02 (RITA1/02-102-02) „Eseme- ja mobiilsidevõrgu kaitse simuleerimine küberharjutusväljal”

LIST OF PUBLICATIONS

Publications in journals indexed in the Thomson Reuters Web of Science and SCOPUS database.

Tamme, V., Jänes, A., Romann, T., Tamme, H., Muiste, P., Kangur, A. 2022. Investigation and modelling of the electrical charging effect in birch wood above the fibre saturation point (FSP). *Forestry Studies / Metsanduslikud Uurimused*, 77, 21–37. DOI: 10.2478/ismu-2022-0010.

Tamme, V., Tamme, H., Müidla, P., Muiste, P. 2021. Novel polarization-type moisture meter for determining moisture content of wood above fibre saturation point. *European Journal of Wood and Wood Products*, 1–11. DOI: 10.1007/s00107-021-01682-6.

Tamme, H., Kask, R., Muiste, P., Tamme, V. 2021. Comparative testing of two alternating current methods for determining wood moisture content in kiln conditions. *Forestry Studies / Metsanduslikud Uurimused*, 74 (1), 72–87. DOI: 10.2478/fsmu-2021-0005.

Tamme, H., Muiste, P., Tamme, V. 2021. Optimizing the pine wood drying process using a critical diffusion coefficient and a timed moistening impulse. *Forestry Studies*, 75, 150–165. DOI: 10.2478/fsmu-2021-0017.

Romann, T., Anderson, E., Pikma, P., Tamme, H., Möller, P., Lust, E. 2017. Reactions at graphene | tetracyanoborate ionic liquid interface – New safety mechanisms for supercapacitors and batteries. *Electrochemistry Communications*, 74, 38–41. DOI: 10.1016/j.elecom.2016.11.016.

Tamme, V., Muiste, P., Padari, A., Tamme, H. 2014. Modelling of Resistance-Type Wood Moisture Meters for Three Deciduous Tree Species (Black Alder, Birch, Aspen) in Moisture Contents Above Fibre Saturation Point. *BALTIC FORESTRY*, 20 (1), 157–166.

Tamme, V., Muiste, P., Tamme, H. 2014. Experimental study of resistance type wood moisture sensors for monitoring wood drying process above fibre saturation point. *Forestry Studies / Metsanduslikud Uurimused*, 59, 28–44.

Romann, T., Oll, O., Pikma, P., Tamme, H., Lust, E. 2014. Surface chemistry of carbon electrodes in 1-ethyl-3-methylimidazolium tetrafluoroborate ionic liquid – an in situ infrared study. *Electrochimica Acta*, 125, 183–190. DOI: 10.1016/j.electacta.2014.01.077.

Tamme, V., Muiste, P., Kask, R., Padari, A., Tamme, H. 2012. Experimental study of electrode effects of resistance type electrodes for monitoring wood drying process above fibre saturation point. *Forestry Studies / Metsanduslikud Uurimused*, 56, 42–55. DOI: 10.2478/v10132-012-0004-6.

Tamme, V., Muiste, P., Mitt, R., Tamme, H. 2011. Determination of Effective Diffusion Coefficient and Mechanical Stress of Pine Wood during Convective Drying. *BALTIC FORESTRY*, 17, 110–117.

Industrial property

Tamme, V., Tamme, H., Bernotas, T., Muiste, P., Olt, J. 2020. Moisture meter and method for measuring the moisture content of wood above the fibre saturation point of wood with the electric charging effect. <https://sise.etis.ee/File/DownloadPublic/1f3d01f6-a44d-4224-a702-f0f6e6281226?name=EE05822B1.pdf&type=application%2Fpdf>

Conference proceedings and presentations

Tamme, H., Tamme, V., Kask, R., Muiste, P. 2019. Non-destructive dielectric method for determining the moisture content of newly sawn timber for moisture content above FSP. *Proceedings: 21st International Nondestructive Testing and Evaluation of Wood Symposium.: 21st International Nondestructive Testing and Evaluation of Wood Symposium, Freiburg, Germany, 2019*. Ed. Wang, X., Sauter, U. H., Ross, R. J. Forest Research Institute Baden-Württemberg, 213–224.

Tamme, H., Tamme, V., Kask, R., Muiste, P. 2019. Modelling of wood resistance+type moisture meters in wood moisture contents above the fibre saturation point. *Proceedings of the 14th annual meeting of the Northern European Network for Wood Science and Engineering*

(WSE2018), Tallinn, Estonia, 2018. Ed. Heikko, K. Tallinn University of Technology, 19–21.

Tamme, V., Muiste, P., Kask, R., Padari, A., Tamme, H. 2012. The research of electrode effects on wood drying above fiber saturation point. Proceedings of the 12th International IUFRO Wood Drying Conference: 12th International IUFRO Wood Drying Conference, 30.07-03.08, 2012 - BELÉM, PARA, BRAZIL. Belém, Para, Brazil: Instituto de Pesquisas e estudos Florestais, 47–47.

Tamme, V., Muiste, P., Polyachenko, R., Tamme, H. 2010. Determination of Dynamics of Moisture Content, Temperature and Mechanical Stress of Pine Wood During Convective Drying. Recent Advances in the Field of Wood Drying: 11th International IUFRO Wood Drying Conference Skelleftea Sweden, January 18- 22, 2010. Ed. Tom, M., Lena A., Margot, S., 147–154.

Other scientific publications

Tamme, V., Kask, R., Muiste, P., Tamme, H. 2012. Puidu niiskusmõõtjate võrdlus laiendatud mõõtepiirkonnas. TEUK XIV TAASTUVATE ENERGIAALLIKATE UURIMINE JA KASUTAMINE NELJATEISTKÜMNENDA KONVERENTSI KOGUMIK: TEUK XIV Tartu, 08.11.2012. Toim. Normak, A., Suitso, I., Jõgi, E., Vollmer, E. OÜ Paar, 98–108.

VIIS VIIMAST KAITSMIST

MARII RASVA

PÕLLUMAJANDUSMAA KASUTUSE MUUTUSED EESTIS: TASAKAALUSTATUD
MAAKASUTUSE TAGAMISE VÕIMALUSED
CHANGES IN AGRICULTURAL LAND USE IN ESTONIA: OPPORTUNITIES FOR
STABLE LAND USE

Kaasprofessor Evelin Jürgenson ja kaasprofessor Aive Liibusk

9. märts 2023

VELJO RAIDE

VEDELKÜTUSTEST MOODUSTATUD KÜTTESEGU TÖÖTLEMISE SÜSTEEM
SÄDESÜÜTEGA MOOTORGENERAATORITES KASUTAMISEKS KRIISI
OLUKORRAS

LIQUID FUELS AIR-FUEL MIXTURE PROCESSING SYSTEM WITH SPARK
IGNITION ENGINE FOR USE IN GENERATORS IN A CRISIS SITUATION

Professor Jüri Olt, kaasprofessor Risto Ilves

14. aprill 2023

MARGE LANNO

BIOJÄÄTMETE KOMPOSTIMINE RINGMAJANDUSE TINGIMUSTES
BIO-WASTE COMPOSTING IN THE FRAMEWORK OF CIRCULAR ECONOMY

Kaasprofessor Merrit Shanskiy, professor Mait Kriipsalu, teadur Anu Kisand

28. aprill 2023

KEYVAN ESMAEILZADEH SALESTANI

MULLA MIKROBIOOM JA ODRA TRANSKRIPTOOM ERI VIJELUSVIISIDES
IMPACT OF CROPPING SYSTEMS ON SOIL MICROBIOME AND BARLEY
TRANSCRIPTOME

Dotsent Evelin Loit

16. juuni 2023

MERLE VALDMANN

TSÜTOLOOGILINE ENDOMETRIIT PIIMALEHMADEL: DIAGNOOSIMINE, MÕJU
SIGIVUSELE JA PRAAKIMISELE NING SEOSSED METABOOLSE STRESSIGA
CYTOLOGICAL ENDOMETRITIS IN DAIRY COWS: DIAGNOSTICS, EFFECTS ON
FERTILITY AND CULLING, AND ASSOCIATIONS WITH METABOLIC STRESS

Professor Andres Valdmann

22. august 2023

ISSN 2382-7076

ISBN 978-9916-719-18-3 (trükis)

ISBN 978-9916-719-19-0 (pdf)